Highly Efficient Planar Antenna System Based on the Planar Waveguide Technology for Low Cost Millimeter-Wave Applications

by

Wael Mahmoud Abdel Wahab

A thesis
presented to the University of Waterloo
in fulfillment of the
thesis requirement for the degree of
Doctor of Philosophy
in
Electrical and Computer Engineering

Waterloo, Ontario, Canada, 2011

AUTHOR'S DECLARATION

I hereby declare that I am the sole author of this thesis. This is a true copy of the thesis, including any required final revisions, as accepted by my examiners.

I understand that my thesis may be made electronically available to the public.

Wael Mahmoud Abdel Wahab

Abstract

This thesis investigates the integration of planar antennas, such as Dielectric Resonator Antennas (DRAs) to the planar waveguide structure, specifically the Substrate Integrated Waveguide (SIW) for high radiation efficiency millimeter-wave (mm-wave) applications. The SIW is a low cost and low loss technology, since it almost keeps the guided wave inside the structure. Therefore, it is an excellent candidate feeding scheme compared to traditional planar (multi-conductor) structures, such as the Microstrip Line (MSL) and Co-planar Waveguide (CPW) for many planar antennas. It enhances the antenna's overall radiation efficiency by minimizing the conduction loss, which dominates at the mm-wave frequency band.

For this thesis, two different SIW-integrated DRA configurations operating at mm-wave frequency band are presented. The rectangular DRA is excited in its fundamental mode $TE_{\delta 11}$ for radiation through a narrow slot cut on the SIW broad wall. However, the coupling slot itself is excited by the SIW TE_{10} fundamental mode. In addition, the design guidelines, and a parametric study is also conducted on the proposed antenna parameters to investigate their impact on the antenna's overall performance including the reflection coefficient and radiation pattern (gain). The results are provided within this thesis. The antenna is made of low cost and low loss materials that are available commercially. It is fabricated by using a novel and simple technique, which is compatible with the Printed Circuit Board (PCB) technology. The board is treated as multi-layers composed of the SIW-layer, and DRA element(s) layer, respectively. The fabricated antenna prototypes are tested to demonstrate their validity for real microwave/mm-wave applications. Their reflection coefficients and radiation patterns are measured, and the antenna shows a boresight gain of *5.51 dB* and a radiation efficiency of more than *90 %* over the operating frequency band of *33-40 GHz*.

Antenna arrays based on the SIW integrated DRA are investigated for high gain/radiation efficiency applications. Different array configurations such as, linear (series-fed and corporate-fed) and two-dimensional (2D) arrays are presented. The series-fed DRA array is characterized by a single SIW line loaded by DRA-slot pairs, whereas the SIW-power splitter is used to form the corporate-fed DRA array, when loaded by DRA-slot pairs. While the SIW hybrid-feeding scheme (series-feed combined with corporate-feed) is used to form 2D DRA arrays. In this design, the SIW-power splitter is used to split the power equally and in-phase among the sets (rows) of SIW series fed-DRA elements (columns). A simple and generic Transmission Line (T.L.) circuit model is proposed to simplify and expedite the antenna array design process. It is used to calculate the antenna reflection coefficient and radiation pattern (gain). The T.L. model does not take the mutual coupling between the DRA elements into account, since our study shows that its less than *-20 dB* over the operating bandwidth. However, it is useful and faster than full-wave solvers, such as HFSS, which consumes time and memory due to the huge generated mesh. The developed T.L. circuit model is used to design the antenna array and study the impact of its main designed parameters on the antenna performance. The developed antenna array T.L. model leads to a general design methodology (guidelines). It also allows for optimum array designs for a given set of performance requirements and to have more physical insight into the SIW technology based antenna systems for mm-wave bands.

The designed antenna array samples are fabricated and tested within the operating frequency band *33-40 GHz*. The series-fed antenna array shows a measured boresight gain of *11.70 dB*, and high radiation efficiency, which is more than *90 %* over an operating frequency band of *4%*. Furthermore,

the measured results are compared to these calculated by the proposed T.L. circuit model and full-wave solver. A good agreement between the measured and the HFSS results are observed, especially near the frequency at which the reflection coefficient is minimum. However, some deviation is noticed between the proposed circuit model and the measured results. This deviation is attributed to the discrete nature of the SIW structure that affects the Short Circuit (SC) performance (magnitude and phase), the T.L. lengths, and the mutual coupling between any two adjacent antenna elements. All these issues are handled efficiently and are taken into account by the full-wave solver. Therefore, the measured reflection coefficient agrees with that of the HFSS, except for a very small deviation, caused by the fabrication tolerances and measurement errors. However, the proposed T.L. circuit model is still valid and can easily predict and estimate the resonance behavior and the impedance bandwidth of the proposed antenna arrays in a very short time compared with the full-wave solver.

Acknowledgements

I would like to express my sincere thanks to my supervisor, Professor Safieddin Safavi-Naeini of the University of Waterloo for his invaluable guidance, advice and support throughout my postgraduate program. I thank him for his kindness, understanding and support during this period.

I am thankful to the committee members, Prof. Yahia Antar, Prof. Chaudhuri, Prof. Mansour, and Prof. Abdel-Rahman, for spending their time to review my thesis and give me valuable comments.

Also, I would like to acknowledge my dear parents. Give my thanks to them for their endless support, sacrifice, and patience. My warmest thanks to my beloved wife, Marwa, for her great emotional and physical support in the recent months when I was busy in writing my thesis. Having her is the greatest fortune in my life. I also need to appreciate my beloved son Mahmoud and little angel Haajar, for their understanding the nature of my carreer as a researcher that keeps me busy most of the time.

During the course of this study I enjoyed being a member of an active and friendly research group. Thanks to all the EM/ RF group members at University of Waterloo for their useful discussions.

Dedication

This thesis is dedicated to my home beloved country, Egypt, and all the people around the world who are fighting for their freedom, liberty, and human rights.

Table of Contents

List of Figures

List of Tables

Chapter 1

Introduction

1.1 Antenna Features Requirements for Wireless Communications Overview

The wireless communication industry was commercially born in 1970 with the introduction of reliable, miniaturized, solid-state Radio Frequency (RF) components. The proliferation of wireless communication systems in the recent years has dramatically changed the way people exchange information [1]. As the demand for wireless communications increases, cheaper and more reliable systems have to be developed. At the same time, constraints placed on the systems by spectrum allocation issues increase. Current research is being devoted to the development of systems designed to work in the millimeter-wave (mm-wave) frequency range. This frequency band designated as *30-300 GHz* [2,3] is vastly unused compared to lower frequency bands which are heavily populated.

Developing communication systems at the mm-wave band allows compact system components, which are critical for mobile and portable systems. Furthermore, mm-wave frequency bands provide a greater bandwidth, meaning that large amounts of data can be transmitted at higher speeds with better reliability. In addition, Wireless Local Area Networks (WLANs) and other high-speed multi-media delivery services require large amounts of bandwidth to operate effectively. Many useful applications have been assigned for this band, such as passive imaging applications (*91 GHz*) [4], collision avoidance radar sensors (*77 GHz*) [5]. Also, an important application for this frequency band is satellite communications. A portable system with a fixed beam of around *20/30 GHz* to receive and transmit respectively has been investigated in [6]. The conclusion from the above discussion is that the development of the mm-wave band systems is important to the future of wireless communication systems.

Antennas as a part of a wireless communication system have to be developed to satisfy most of the high frequency application requirements. Owing to their small size and low profile, planar antenna systems are suitable for mm-wave wireless communication applications. In addition, they are compatible with the Monolithic Millimeter Wave Integrated Circuits (MMIC).

As most of the wireless systems are being designed for mobile and portable applications, antennas designed for wireless communications at mm-wave frequencies should fulfill some requirements such as having profile, high low efficiency, light weight and low fabrication cost. Traditional waveguide and reflector antennas are unsuitable, because they are bulky and high cost. Furthermore, as the frequency increases the performance of some of these antennas degrades, since surface roughness and conductor loss become significant for metallic components. The microstrip and printed antenna technology on the other hand, have low profile, low cost, lightweight, conformity and easy to fabricate for wireless applications operating at mm-wave. A microstrip printed dipoles array antenna was proposed by [6], where a low and medium power amplifier has been distributed and integrated within the array.

The Microstrip Patch Antenna (MPA) element and arrays architectures have been presented in some literature [6, 7] at mm-wave frequencies for wireless communication systems. They have been

placed inside a metallic cavity to form an array of high gain [6] at *30 GHz* or integrated with a low noise amplifier to form an active antenna array at *42 GHz*. The feeding microstrip lines can be printed on the same layer of metallization for a patch array configuration using the same photolithographic technique. However, it has been found that their conductor and dielectric loss are significant, especially for large arrays, the microstrip antenna has a narrow bandwidth of *4%*, which makes it unsuitable for mm-wave wide band applications.

Dielectric Resonator Antennas (DRAs) have been shown to radiate efficiently at high frequencies [8], making them more attractive for wireless applications operating at mm-wave frequencies. They exhibit no conductor loss (high radiation efficiency), a larger bandwidth than MPAs, and have a lower profile than reflector and the horn antennas. In addition, they are easier to fabricate at this frequency range and can be excited in many different ways, as we will discuss later in Chapter 2.

Relatively few studies using DRA at mm-wave frequencies have been reported. Existing work includes a single element fed by a CPW at *60 GHz* [9] and arrays fed by an aperture [10], and a dielectric waveguide [11] at *40 GHz* and *32.5 GHz* respectively. The antenna feeding systems at mm-wave frequencies usually utilize some type of planar transmission line and apertures or radiating slots. There are several types of planar transmission lines including the strip line, the coplanar waveguide, the slot line, the coplanar strip, and the MSL. The planar transmission lines are easy to fabricate in small dimensions. They are also compatible with MMIC technology. MSL and CPW are the most commonly used types of feeding systems for both MPAs and DRAs. However, they become very susceptible to conductor loss at high frequencies, which degrades the radiation efficiency of the antenna system. Consequently, another high Q-factor feeding structure with low complexity has to be developed.

1.2 Motivations

Recently, there is a growing interest in antenna systems, which operate in the mm-wave region. The conventional metallic antennas suffer problems with regards to power loss, which degrades radiation efficiency, and radiated power capabilities. There are also fabrication difficulties when reduced to the sizes necessary to operate in this band. The DRA meets these requirements. It has been shown that DRA is an attractive element for use in the microwave and mm-wave frequency bands [9], [12-18]. DRAs are made of low-loss and high dielectric constant materials that have higher radiation efficiency than printed antennas at higher frequencies due to the absence of the ohmic loss and surface wave. Also, they are compact in size, lightweight, and low cost.

Many different traditional feeding schemes can be used for the DRA such as a coaxial-probe feed, an aperture-coupling feed, a direct microstrip-line feed, a coplanar waveguide feed or a waveguide slot feed to name a few. Among these excitation schemes, the microstrip line feeding technique is often used for the DRA because of easy fabrication and compatibility with MMICs. However, when microstrip-lines and open slots are used to excite the DRA, they will produce undesirable backside radiation, and the DRA's radiation pattern is also affected by the parasitic radiation of the feeding MSLs. Additionally, the conventional microstrip-like feeding systems suffer from significant tradeoff between the cost, size and performance at the microwave and mm-wave frequency band. Finally, it suffers from conduction loss, which degrades the overall efficiency of the whole antenna system.

A novel planar feeding mechanism based on the planar waveguide technology called the Substrate Integrated Waveguide (SIW) technique is used for planar antennas, such as Dielectric Resonator Antennas (DRAs) designed at the mm-wave band. The SIW is a closed guiding structure that keeps the excitation fields inside. It has an excellent shield between the exterior and interior, thus minimizing losses and avoiding radiation loss, and consequently, the overall antenna radiation efficiency is enhanced.

Recently, the SIW has proven to be useful for many RF circuits/antennas designed for microwave/mm-wave applications [19-25]. The SIW is constructed entirely by copper- plating through vias, and it is fabricated by a standard Printed Circuit Board (PCB) technique. Both the SIW and the DRA are low cost/loss structures (high Q-factors); therefore they are an excellent candidate for mm-wave applications when combined together. The primary objective of this research is to explore, analyze, and design a low cost substrate integrated waveguide integrated planar antennas, such as SIW Integrated DRA (SIW-DRA) for microwave and mm-wave applications.

1.3 Proposed Work and Thesis Outline

The objective of this thesis is to investigate the characterization, modeling, and design aspects of low cost high gain/radiation efficiency DRA arrays based on the planar waveguide technology. A prime focus in this research is implementing new planar antenna technology using an integrated low cost DRA technology. By utilizing this novel technology, other high Q-factor RF circuits in the front ends such as phase shifters can be integrated easily in the same antenna substrates. This antenna system can be used for emerging mm-wave communication systems such as a *60 GHz* high data rate wireless network, automotive radar and proximity sensor applications at *24 GHz*, *35 GHz*, and *77 GHz*. More specifically, the main objective of this research is to explore the concept of low cost technology SIW-based DRA system with enhanced radiation efficiency. The proposed research is focused on the following two inter-related topics:

a. Millimeter-Wave High Radiation Efficiency SIW Technology-Based Dielectric Resonator Antenna (DRA) single element: Analysis, Design, and Fabrication

The SIW is utilized as a novel low loss feeding mechanism for the Dielectric Resonator Antenna (DRA) made of low cost materials that are available commercially. The DRA is designed to resonate in its fundamental mode for radiation at the mm-wave frequency band.

In the proposed antenna design, a Rectangular Dielectric Resonator Antenna (RDRA) is excited by the SIW fundamental mode, TE_{10}, through a narrow transverse/longitudinal slot. The initial design parameters are based on the waveguide theory; however, due to the RDRA loading effect, and the SIW's periodic nature, these values deviate from the more accurate ones obtained from rigorous computational simulations. Therefore, a parametric study has been conducted to study the impact of these parameters on the coupling between DRA and the coupling slot. The proposed antennas have been fabricated by using a novel fabrication technique, which is compatible with the multi-layer PCB low cost technology. The board is treated as a multi-layer PCB with two dielectric layers compromising the SIW layer, and the RDRA elements, respectively. The fabricated prototypes are

tested to demonstrate their validity for real high radiation efficiency needed for mm-wave applications. Ultimately, the SIW technology can be combined with other planar antennas such as MPAs to enhance their overall radiation efficiency which is often degraded by traditional planar feeding schemes.

b. High Gain/Radiation Efficiency Millimeter-Wave SIW Technology-Based DRA Array: Modeling, Design, and Fabrication

In addition to the proposed design concept for the RDRA fed by a SIW single element, general design layouts for Standing Wave (SW) antenna arrays, SIW series-fed DRA, SIW corporate-fed DRA, and SIW hybrid-fed DRA configurations, with two different slot orientations, have been presented. Numerical full-wave solvers, such as HFSS have been used to analyze, optimized, and design these complicated antenna structures. However, they are time and memory consuming due to the huge generated mesh required to simulate these large structures. Therefore, a fast and efficient T.L. model based method has been developed for analysis and design optimization. This method is fast and efficient compared to the full-wave EM numerical solvers that have been used to study and design these antennas.

In conclusion, this research comprises both theoretical and experimental investigations. The theoretical work addresses the theoretical aspects of the antenna (single element and arrays) modeling/design problem, which ultimately leads to a general methodology for optimal antenna designs in the mm-wave band. The developed antenna array T.L. model would allow antenna designers to optimize the antenna array structures for a given set of performance requirements and to have more physical insight into the SIW technology based antenna systems. This technology would contribute to the advancement of the mm-wave research and technology development by providing low cost, compact, and efficient RF-circuit and antenna systems in the range of the mm-wave band.

The thesis includes five-chapters. In Chapter 2, the SIW based mm-wave state-of-art applications are introduced. Necessary background information on the DRs and how they can be useful as antennas, especially at mm-wave frequency band is introduced. Different types of shapes, and excitations including recent research work of the SIW integrated DRA are presented. Moreover, the SIW technology, its applications, modeling, and recent studies are outlined to emphasize the importance of using this structure at mm-wave frequencies. Finally, the SIW main propagation characteristics including the propagating modes, equivalent rectangular waveguide, losses, and band gap are provided. Moreover, the SIW design considerations are also presented. In Chapter 3, the SIW-fed RDRA at the mm-wave frequency band is presented using two different configurations. In addition, the full-wave simulations and the experimental verification are presented. An extension for the SIW-fed RDRA to the array applications is presented in Chapter 4 including the modeling, design and fabrication. Finally, Chapter 5 provides the conclusion and future research.

1.4 Publications

The research work publications for this thesis are listed as follows:

A. Patents:

1) ***Wael M. Abdel Wahab***, Safieddin Safavi-Naeini, Dan Busuoic, "Multi-layer Fabrication Process for Millimeter-Wave Antennas", US Patent (*File No. 61/344,234*).

B. Refereed Journal:

1) ***Wael M. Abdel-Wahab***, Safieddin Safavi-Naeini,"Wide Bandwidth 60 GHz Aperature-Coupled Microstrip Patch Antennas (MPAs) Fed by Substrate Integrated Wavegudie(SIW)", *IEEE Antennas and Wireless Propagation Letters," IEEE Antennas and Wireless Propagation Letters,* vol. 10, 2011.

2) ***Wael M. Abdel-Wahab***, Safieddin Safavi-Naeini, Dan Busuoic,"Millimeter-Wave High Radiation Efficiency Planar Waveguide Series-Fed Dielectric Resonator Antenna(DRA) Array: Analysis, Design, and Measurements," *IEEE Transactions on Antennas and Propagation, Vol. 59,No. 8, pp. 2834-2843, August 2011*.

3) ***Wael M. Abdel-Wahab***, Safieddin Safavi-Naeini, Dan Busuoic, "High Millimeter-Wave Q-Factor Parallel Feeding Scheme for Dielectric Resonator Antenna Arrays," *IEEE Antennas and Wireless Propagation Letters,* vol. 10, pp. 53-55, 2011.

4) ***Wael M. Abdel-Wahab***, Safieddin Safavi-Naeini, Dan Busuoic,"Low Cost Planar Waveguide Technology Based Dielectric Resonator Antenna (DRA) for Millimeter-Wave Applications: Analysis, Design, and Fabrication," *IEEE Transaction on Antennas and Propagations, Vol. 58,No. 8, pp. 2499-2507, August 2010*.

C. Refereed Conference Proceedings:

1) ***Wael M. Abdel-Wahab***, Safieddin Safavi-Naeini,"Transmission Line Circuit Model for RF-Circuits Based on Planar Waveguide Techololgy Used for Millimeter-Wave Applications,", *the 10th International Conference for Upcoming Engineering(IEEE ICUE), Reyerson University , Tornoto, Ontarion, Canada, May 2011.*

2) ***Wael M. Abdel-Wahab***, Safieddin Safavi-Naeini,"Mutual Coupling Investigation Between Dielectric Resonator Antennas(DRAs) Excited by Substrate Integrated Waveguide,", *the 10th International Conference for Upcoming Engineering, Reyerson University , Tornoto, Ontarion, Canada, May 2011.*

3) ***Wael M. Abdel-Wahab***, Safieddin Safavi- Naeini, Dan Busuoic,"High Gain/Efficiency 2D-Dielectric Resonator Antenna Array for Low Cost mm-Wave Systems,", *Antenna and Propagation Society International Symposium, 2011, AP-S 2011, IEEE, Spokane, WA, USA, July 2011.*

4) ***Wael M. Abdel-Wahab***, Safieddin Safavi-Naeini, Dan Busuoic," Low Cost 60 GHz Millimeter-Wave Microstrip Patch Antenna Arrays Using Low-Loss Planar Feeding Scheme," *Antenna and Propagation Society International Symposium, 2011, AP-S 2011, IEEE , , Spokane, WA, USA, July 2011.*

5) ***Wael M. Abdel-Wahab***, Safieddin Safavi-Naeini, Dan Busuoic,"Low Loss Double-Layer Substrate Integrated Waveguide-Hybrid Branch Line Coupler for mm-Wave Antenna Arrays,", *IEEE Antenna and Propagation Society International Symposium, 2011, AP-S 2011 Spokane, WA, USA, July 2011.*

6) ***Wael M. Abdel-Wahab***, Safieddin Safavi-Naeini,"A Simple Circuit Model for Planar Waveguide Power Splitters Used for Millimeter-Wave Beam Forming Network", *IEEE*

Antenna and Propagation Society International Symposium, 2011, AP-S 2011, Spokane, WA, USA, July, 2011.

7) ***Wael M. Abdel-Wahab***, Safieddin Safavi-Naeini, Dan Busuoic,"A Substrate Integrates Waveguide (SIW) Quadrature Hybrid- Junction for Low Cost Millimeter-Wave Planar Antenna Array" *in the Procedding of Antenna and Propagation Society International Symposium, 2010, AP-S 2010, IEEE, Toronto,ON, Canada, July 2010.*

8) ***Wael M. Abdel-Wahab***, Safieddin Safavi- Naeini, Dan Busuoic," A Convienient Circuit Model for Millimeter-Wave Substrate Integrated Waveguide(SIW) Corporate Feed for Dielectric Resonator Antenna Arrays" *in the Proceeding of IEEE Antenna and Propagation Society International Symposium, 2010, AP-S 2010, Toronto, ON., Canada, July 2010.*

9) ***Wael M. Abdel-Wahab***, Safieddin Safavi- Naeini, Dan Busuoic," Low Cost Microstrip Patch Antenna Array Using Planar Waveguide Technology for Emerging Milimeter-Wave Wirless Communications" *in the Proceeding of the 14th International Symposium on Antenna Technology and Applied Electronagnetics (ANTEM),OTTAWA, ON, July 2010.*

10) ***Wael M. Abdel-Wahab***, Safieddin Safavi-Naeini, Dan Busuoic, " Low Profile and Low Cost Efficient Linear Array Antenna Based Substrate Integrted Waveguide Technology for Millimeter-Wave Applications", *Progress In Electromagnetics Research Symposium (PIERS 2010) , Cambridge, USA(Abstract).*

11) ***Wael M. Abdel-Wahab***, Safieddin Safavi-Naeini, Dan Busuoic, "A Novel Feeding Scheme for Microstrip Patch Antenna (MPA) Array for Millimeter-Wave Band Applications ", *Progress In Electromagnetics Research Symposium (PIERS 2010), Cambridge, USA.(Abstract)*

12) ***Wael M. Abdel-Wahab*** , Safieddin Safavi-Naeini, Dan Busuoic "Mutual Coupling Mitigation Using New Feeding Scheme Suitable for 2D Planar Antenna Array at Millimeter-Wave Band", *Progress In Electromagnetics Research Symposium (PIERS 2010) , Cambridge, USA.(Abstract)*

13) ***Wael M. Abdel-Wahab***, Safieddin Safavi-Naeini, Dan Busuoic,"A Simple Circuit Model for Milliemeter-Wave Substrate Integrated Waveguide (SIW) Series-Fed Dielectric Resonator Antenna Arrays", *in the Proceeding of IEEE Antenna and Propagation Society International Symposium, 2010, AP-S 2009,Charleston, SC, USA, June 2009.*

14) ***Wael M. Abdel-Wahab***, Safieddin Safavi- Naeini, Dan Busuoic,"High efficiency Milliemeter-Wave Planar Waveguide Fed Dielectric Resonator Antenna (DRA)", *in the proceeding of IEEE Antenna and Propagation Society International Symposium, 2010, AP-S 2009,Charleston, SC, USA June 2009.*

15) ***Wael M. Abdel-Wahab***, Safieddin Safavi-Naeini, Dan Busuoic,"SIW-Series Fed RDRA Array System for Millimeter-Wave Applications", *in the Proceeding of the 3rd European Conference on Antenna and Propagation, March,Berlin, Germany 2009.*

16) ***Wael M. Abdel -Wahab***, Safieddin Safavi-Naeini, Dan Busuoic,"Low Cost Low Profile Dielectric Resonator Antenna (DRA) Fed Planar Waveguide Technology for Millimeter-Wave Frequency Applications", *in the Proceeding of the 4th International Conference on Radio and Wirless,San Diego,USA, Jan, 2009.*

Chapter 2

Substrate Integrated Waveguide (SIW)-Based Microwave/Millimeter-Wave Technologies: Review of State-of-Art

2.1 Introduction

Dielectric Resonator Antennas (DRAs) are resonant antennas, made of low-loss microwave dielectric material. They offer several attractive features such as a small size, and high radiation efficiency [8]. They are also compatible with Microwave Integrated Circuits (MIC), have an intrinsic mechanical simplicity and the ability to obtain different radiation patterns using different modes. Research interest on the DRAs, in the early 1990s, began to grow due to the potential of the DRAs to show several advantages over the traditional Microstrip Patch Antenna (MPA) [26]. As the system frequency increases, the inherent loss of the DRAs is kept at minimum level due to the absence of ohmic loss and surface wave compared to printed antennas.

Different feeding schemes have been used for the DRA including the traditional planar feeding structures, such as microstrip line [27] and coplanar waveguide [28], but they become lossy due to conduction loss that dominates at mm-wave frequency band. Recently, Substrate Integrated Waveguide (SIW) [29] technology has provided many low cost and low loss RF-circuit and antenna components operating at mm-wave applications. Therefore, it is an excellent candidate feeding scheme for the DRA that minimizes conduction loss at mm-wave frequency band.

In this chapter, a thorough investigation on the DRA and SIW technologies and their recent state of the art is presented, including the DRA shapes, traditional excitation schemes, and DRAs microwave/mm-wave recent applications. Furthermore, the SIW based RF-circuits and antennas applications, modeling, and design are introduced in this chapter to show the usefulness of the SIW technology, especially in mm-wave frequency band.

2.1.1 DRAs Shapes

The most common Dielectric Resonator Antenna (DRA) shapes are: cylindrical, rectangular, triangular, and hemispherical dielectric resonators, which made of low dielectric material permittivity ε_{rd}. The DRA resonant frequencies inside the DRA are affected by its material prosperities, shape, and size.

The Cylindrical DRAs (CDRAs) are the most common known shape, because it has been extensively used in microwave circuits [30], and the analysis of their structures are well known. Due to its rotational symmetry, it lends itself to a Body of Revolution analysis (BOR) [31]. The CDRA's resonant frequency depends only on the radius to its height ratio for a chosen dielectric permittivity ε_{rd}. This means that this ratio cannot be arbitrary, since the pattern shape depends on this value. This leaves one degree of freedom in the design. Furthermore, mode degeneracy in the cylindrical DRAs is present and can result in high cross-polarization levels [32]. The natural resonant frequencies of the circular dielectric disc as well as the near field distributions shows that the first four modes that have

low radiation quality factor (Q-factor) are TE_{01}, TM_{01}, HEM_{11}, *and* HEM_{12} [33, 34]. Accordingly, they are the most radiating modes.

The Rectangular DRA (RDRA) is an attractive shape for many applications, because it is simple and easy to fabricate. Also, it has two degrees of freedom for the frequency design and no degenerate modes. However, it is more difficult to analyze and design than the CDRA, because of its edge-sharp boundaries. Therefore, it has no closed form solution for Green's Function. An approximate solution based on the Dielectric Waveguide (DWG) model is used to predict the resonance frequency inside the resonator [35]. The RDRA's fundamental radiating mode is TE_{111} (also known as $TE_{\delta 11}$), which radiates like a magnetic dipole. A more detailed analysis about this model will be covered in Chapter 3.

The Triangular Dielectric Resonator Antenna (TDRA) is considered to be the smallest for specific dielectric constant and the same operating frequency is compared to both the rectangular and cylindrical resonators [36]. However, it is advantageous in the DRA array design, since a large range for the spacing between elements is allowed.

The hemispherical dielectric resonator antenna is easy to analyze, and it has a closed form for Green's Function [37]. However, it is not attractive to antenna applications compared to cylindrical and rectangular shapes, because it has no degree of freedom and is difficult to fabricate in mm-wave frequency band.

2.1.2 DRA Excitation Schemes

The DRA is characterized among the other planar antennas in its compatibility with most of the planar/non-planar feeding schemes for different applications. Many different excitation methods have been used to couple energy to the DRA. The coaxial probe feed is an efficient and popular [31, 38] schemes. However, it adds large reactive components at high frequency, which degrades its efficiency. It is also sometimes difficult to drill the DRAs to make a hole.

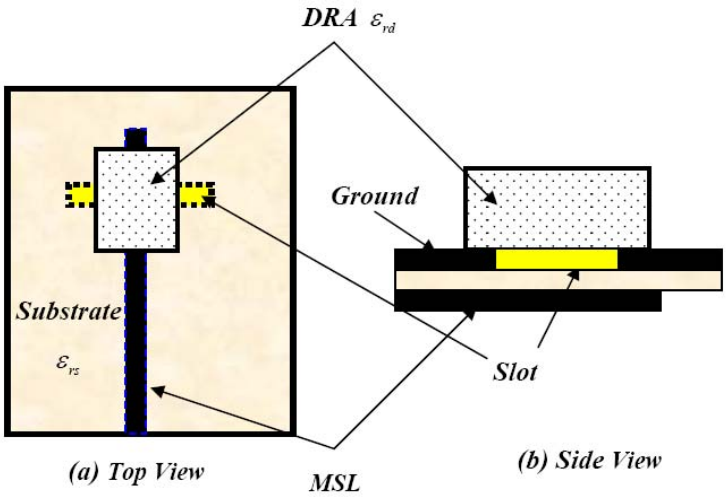

Figure 2.1 Layout of MSL aperture- coupled DRA.

The Microstrip Line (MSL) is popular in microwave circuits, and it has been used in a number of ways to feed the DRA [27, 39-43]. The MSL aperture coupled DRA in Figure 2.1 is a more compatible feeding scheme for the DRAs because the radiating element is isolated from the feeding circuit by the ground plane. This prevents any coupled radiation from the antenna to the MSL circuit causes unwanted reflection.

The DRAs can also be easily tuned. However, this requires an accurate alignment between the slot and the DRAs, especially at high frequencies. The cross aperture and rectangular aperture slots have been used for the DRAs coupling. Cross aperture and rectangular aperture slots. The cross-slots shapes have been used to produce a Circular Polarized (CP) DRA [44]. Also, the MSL has been used as a conformal strip to excite the DRAs. The conformal strip feed method is relatively new and has been used to feed both cylindrical [47], and hemispherical [48] shaped DRAs. The feeding strip is cut from an adhesive conducting tape, which is attached directly to the surface of DRA such that it excites the desired mode. Two conducting strips can be used to excite DRA differentially, as shown in Figure 2.2, and for common mode interference suppression [16] to increase the signal- to- noise ratio.

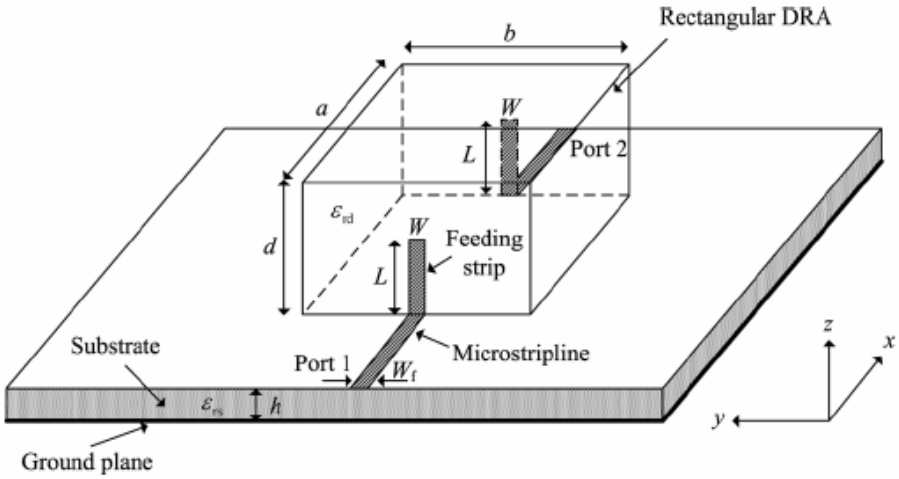

Figure 2.2 DRA fed differentially using two conformal strip lines [16].

Another example of a planar circuit fed DRA is the Coplanar Waveguide (CPW) [28, 45, and 46]. The CPW is currently used in microwave circuits for ease of fabrication and compatibility with solid state devices. Moreover, due to the low loss and less dipressive nature of CPW line, the CPW has emerged as an attractive feeding structure compared to traditional feeding structures. In addition, the CPW feed is particularly suitable for mm-wave applications due to its reduced surface wave excitation in the electrically thick substrate, compared to microstrip feed.

The four common CPW fed RDRA configurations as shown in Figure 2.3, are the open ended CPW, the CPW with inductive coupling slot [47], the CPW capacitive and the square feed configurations. The offset distance from the RDRA center to the open-ended slot center was used to detune the input impedance [48]. A square loop feed configuration showed particular attractive over other that were attractive configurations[46] because of its considerably small area that can be

designed on a low permittivity substrate and is completely enclosed within the DRA area for effective coupling. A Conductor Backed Coplanar Waveguide (CB-CPW) was experimentally studied as a new proposed structure to excite the RDRA. It has offered a high gain, broadband, better cross polarization performance [49], and it could be a possible solution to the antenna integration for System in Package (SIP) [50]. A CPW-fed Dielectric Resonator Above Patch (DRAP) [9] fabricated by micromachining technology was proposed to align and bond a small DRA with a feed slot at mm-wave frequency of 60 GHz for broadband wireless applications.

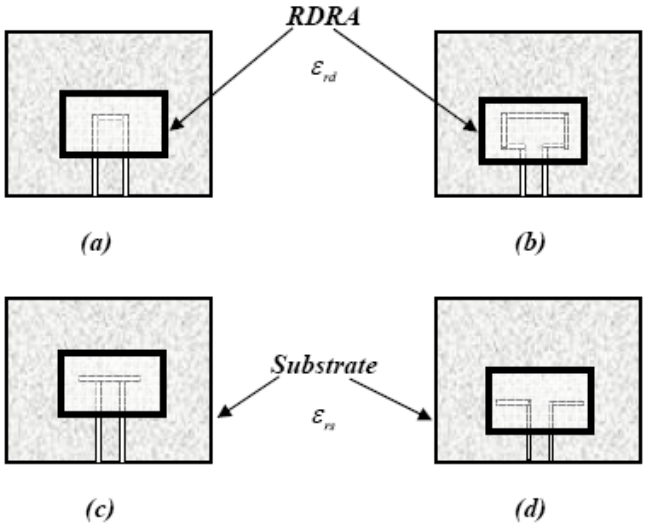

Figure 2.3 CPW fed RDRA configurations [46]: (a) open ended CPW, (b) square CPW, (c) capacitive coupling CPW, and (d) Inductive coupling CPW.

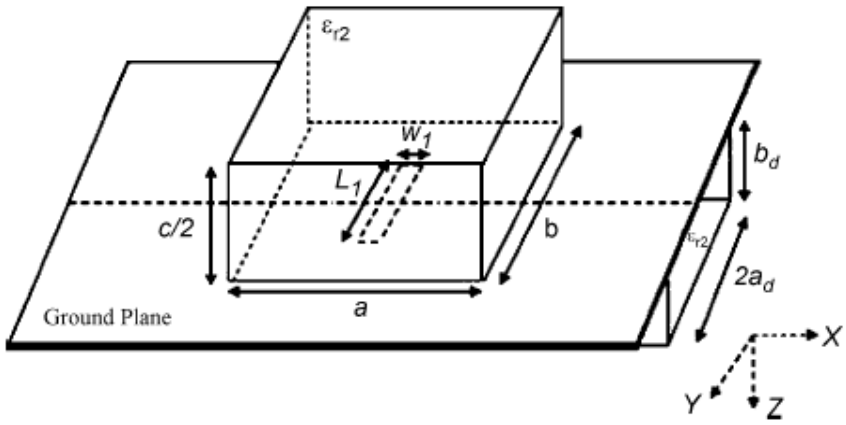

Figure 2.4 DIG fed RDRA configuration [53].

The aforementioned planar feeding schemes losses become considerable at microwave and mm-wave frequencies due to the metallic loss. The Dielectric Image Guide (DIG) is a relatively low loss feeding structure, and it eliminates the conductor losses, when used to feed the DRA [51-53]. In this

case, the DRA has to be positioned properly as shown in Figure 2.4, in order to couple with the DIG excited mode. However, the DIG suffers from radiation losses, since the excitation fields are not confined within the guiding structure causing radiation efficiency degradation. Also, a transition to the Rectangular Waveguide (RWG) is needed to couple the power to the DIG which adds more loss to the antenna system.

Lastly, RWG is another attractive and low loss feeding structure for the DRA [54-58]. The DRA's radiating mode was excited by the RWG through a narrow slot cut in the ground plane [54, 55], or probe feed [59, 60], as shown in Figure 2.5. Both the slot and the probe are excited by the RWG fundamental TE10 mode. A proper choice of the slot/probe's length and position with respect to the waveguide and DRA can achieve a wide impedance bandwidth.

The RWG is an excellent shielding facility as a guiding structure between the exterior and interior, which avoids feeding line radiation loss due to its metallic walls, but it is expensive to fabricate, and not compatible with planar circuits. Furthermore, the transitions from the RWG to the planar circuits are lossy at the mm-wave frequency band.

Recently, a novel-feeding scheme, based on the Substrate Integrated Waveguide (SIW) technique, attracts lots of attention for its advantages such as high Q-factor, high integration, and low cost [61]. The SIW is a synthetic RWG in the planar form that is formed by using copper-plating through vias to mimic the RWG side walls. The SIW can be connected to another planar circuit, such as the MSL and the CPW within the same circuit by using very low loss planar transitions[62, 63], as we will discuss later, owing to these advantages the SIW is a good feeding structure candidate for the DRA. A Few research papers have been published on that subject, as described in Section 2.3.4.

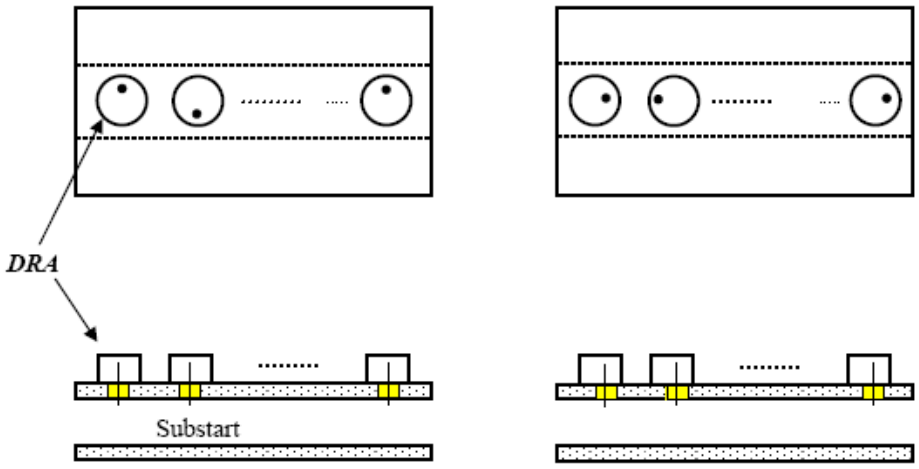

Figure 2.5 RWG fed-DRA using probe feed [60](a) H-plane arrangement, (b) E-plane arrangement.

2.1.3 DRAs for Microwave/Millimeter-Wave Applications and Recent Work

The DRA have higher radiation efficiency than the printed antenna at a high frequency due to the absence of ohmic loss and surface waves. They are also compact size, light weight, and low cost.

Significant progress has been made in various DRA technology aspects over the last three decades as evidenced by the more than 800 publications as shown in Figure 2.6, and over two dozen issued patents [64].

The practical range of frequencies over which the DRA operates is determined by various factors. At low frequencies, the physical properties of antenna are often the limiting factors, meanwhile at higher frequencies; it is the mechanical tolerance and electrical losses that normally dominate the antenna design. The DRA is characterized by its maximum dimension (L) that is related to the free-space resonant wavelength λ_o by the approximate relation $L \propto \frac{\lambda_o}{\sqrt{\varepsilon_{rd}}}$, where ε_{rd} is the dielectric constant of the DRA. The radiation efficiency of the DRA is not significantly affected by ε_{rd}. Therefore, a wide range of values can be used ($2 < \varepsilon_{rd} < 140$) [64]. However, the bandwidth of the DRA is inversely related to ε_{rd} , and it may limit the DRA material choice. There are many published designs of DRAs operating from *1-40 GHz*, with dimensions ranging from a few centimeters down to a few millimeters, and dielectric constants ranging approximately from $2 < \varepsilon_{rd} < 100$.

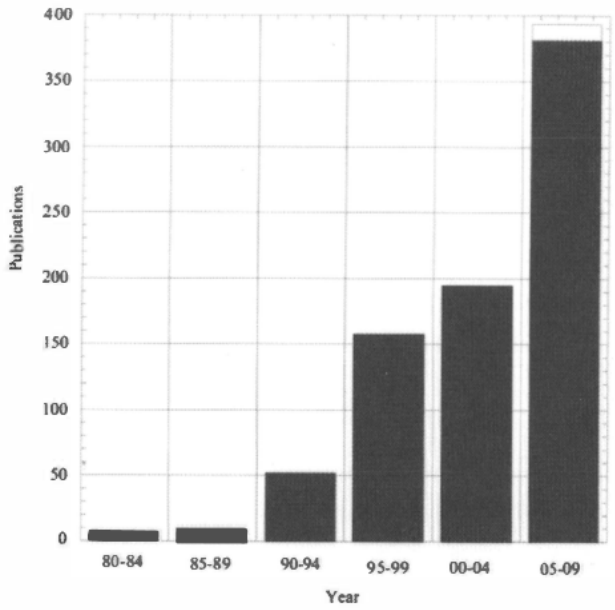

Figure 2.6 DRA publications [64].

These publications involved designing the DRA for specific applications, including the integration into mobile handsets for PCS, IMT-2000, and WLAN applications, and the use in cellular base-station antennas. UWB applications, radar, and breast cancer imaging, and the use in all dielectric wireless receivers have been reported. Research in the DRA within the microwave/mm-wave frequency band involves the following: low profile and compact designs [36, 65-67], wideband designs [68-73], ultra-wide band designs [68-70], circular-polarization [44, 71-74], gain enhancement [75-80], reconfigurable designs [81-85], arrays [40, 86-89], and micro-machined DRAs [9, 90]. Most of the DRA designs for mm-wave applications presented are based on traditional multi-conductor

feeding structures, such as the MSL and the CPW, which suffer from conduction loss, degrading the overall DRA efficiency.

2.1.4 SIW for Microwave/Millimeter-Wave Applications and Recent Work

2.1.4.1 Substrate Integrated Circuits (SICs) Technology

The classical waveguide technology, such as the metallic RWG is still the mainstream for designing high-performance mm-wave systems. However, this technology is not suitable for low-cost mass-production. Furthermore, the integration with the planar circuits becomes a real problem for manufactures. These challenging problems are usually encountered in the design low loss ICs, for example the high Q-filters and duplexers.

Subsequently, the concept of a new generation of high-frequency integrated circuits called Substrate Integrated Circuits (SIC) has been developed [61]. This technology allows the integration of the planar and non-planar circuits to be integrated in single substrate and/or multi-layer platform. The non-planar waveguides are synthesized in planar forms. Therefore, almost of all the kinds of dielectric-based waveguides can be synthesized by simply using air-filled and metalized-holes with SIC technology. The resulting structure on the substrate will be a planar waveguide, which has much better loss characteristics than their planar counterparts. Furthermore, efficient planar wideband transitions [63, 91] can be used to connect the embedded waveguide to other planar RF-circuits. Figure 2.7 shows different non-planar waveguide that can be synthesized using SICs technology. The recently developed SIC platforms are Substrate Integrated Waveguide (SIW) [92], the Substrate Integrated Slab Waveguide (SISW) [93], the Substrate Integrated NRD (SINRD) guide [94-96], and Substrate Integrated Image Guide (SIIG) [97]. The SIW is considered to be the most popular as it is easy to model using its equivalent RWG, and easy to fabricate.

The Substrate Integrated Waveguide (SIW), also called post wall or laminated waveguide, is a promising candidate for mm-wave and terahertz applications [98]. The SIW is a periodic guiding structure, as shown in Figure 2.8, and is composed of two rows of conducting cylinders (vias) separated by W. Each via has a diameter D_{via} and a guiding periodic length b embedded in the dielectric substrate ε_{rs} with thickness of h that connects two parallel metal plates. The SIW is a synthetic metallic RWG of equivalent width w_{eff} filled with dielectric material in planar form. More details about the SIW modeling, design rules, and loss mechanisms to minimize the loss inside this guide will be presented in Chapter 3. The SIW is considered to be a low loss and low cost technology for mm-wave applications. Therefore, many applications including interconnects, filters, diplexers, couplers, oscillators, phase shifters, and antennas have been presented for front mm-wave systems. A modified compact SIW structure called the Half Mode SIW (HMSIW), which has a better attenuation loss performance has been presented in [99] for mm-wave applications. Its size is nearly half of the SIW, as shown in Figure 2.9, and it allows for many RF-circuits and antennas [100-102] to be built in compact designs.

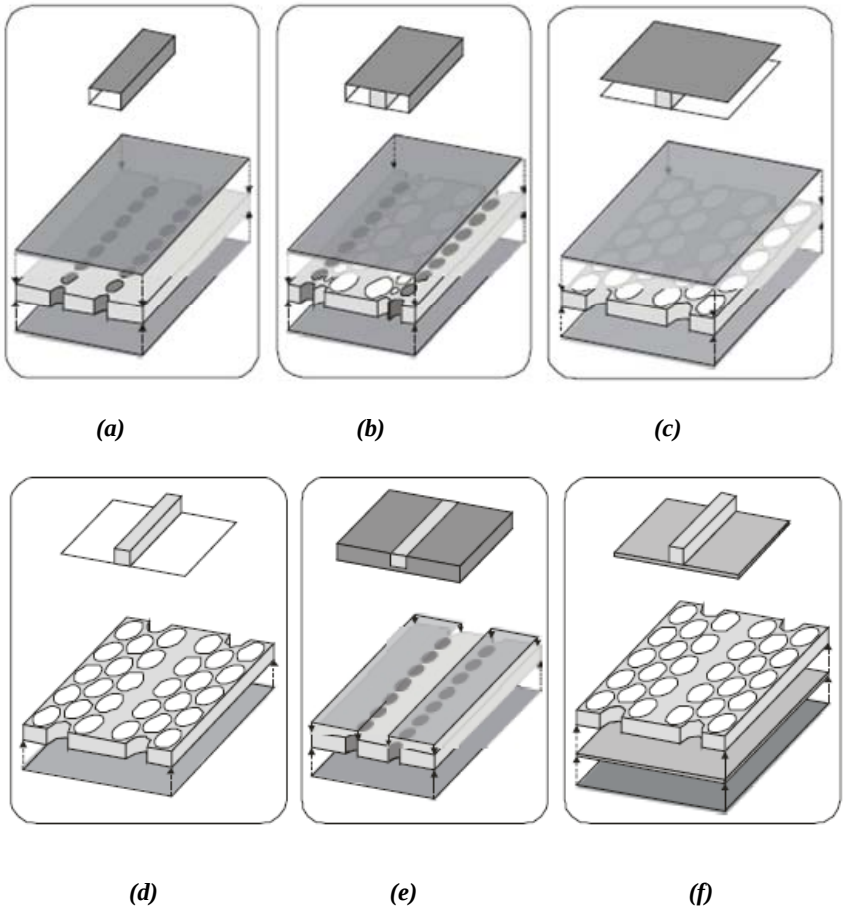

Figure 2.7 Topologies of different non-planar SIC structures[61],(a) Substrate Integrated wave guide (SIW),(b)Substrate Integrated Slab Waveguide (SISW),(c)Substrate Integrated Non-Radiating Dielectric (SINRD) Guide,(d)Substrate Integrated Image Dielectric Guide (SIID),(e)Substrate Integrated Inset Dielectric Guide (SIINDG),(f) Substrate Integrated Insular Guide (SIIG).

2.1.4.2 Interconnects, Couplers, Power Splitters Based on SIW Technology

As the frequency continues to rise in the microwave/mm-wave above *3 GHz*, the problem with signal integrity, cross coupling and radiation become increasingly difficult to overcome. The experimental and computational study reported by [103] showed that the SIW interconnects can achieve *100%* bandwidth via optimal excitation of the dominant mode TE_{10} and avoidance of the excitation of the TE_{20} mode. Also, it maintains the same relative bandwidth while transmitting around *45°* and *90° dB* bends, and achieves measured cross talk of better than *-30 dB* over the entire pass band. Furthermore, the SIW interconnects can handle medium average power with an extremely high peak power over the microwave/mm-wave frequency band [104]. To increase the channel capacity of the SIW interconnects based systems, the multi-mode signal transmission concept has been proposed in [105]. Two orthogonal excited modes, TE_{10}, and TE_{20}, of the SIW have been used to form two uncoupled channels, which showed an excellent data transmission rate of *1-Gb/s*/channel.

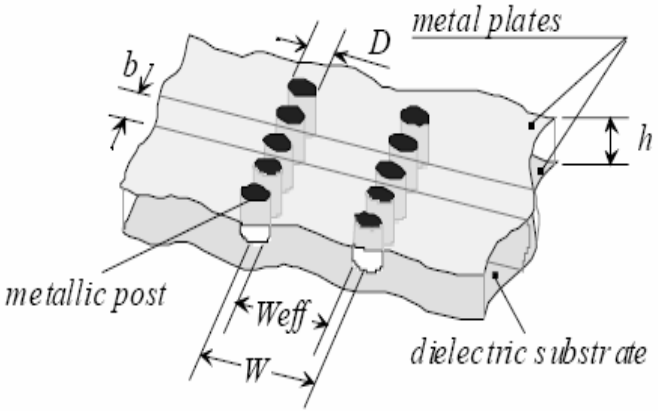

Figure 2.8 Substrate integrated waveguide (SIW) configuration and its modeled parameters [61].

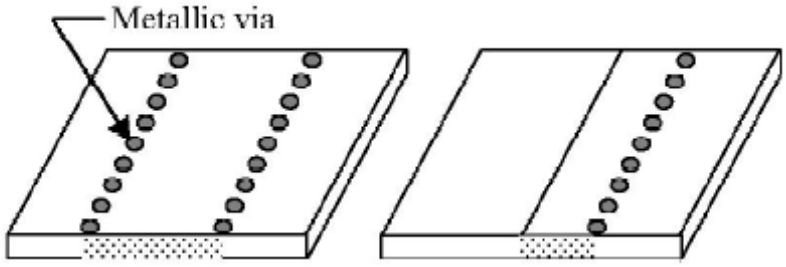

(a) (b)

Figure 2.9 The structure of (a) SIW, (b) HMSIW [99].

Due to the similarity between the SIW and metallic RWG structures in their propagation characteristics, the SIW couplers[106, 107] and power splitters[108, 109] have been integrated and designed by the equivalent RWG concept, and fabricated in a planar form by a standard low cost PCB technique.

2.1.4.3 Resonators and Filters Based on SIW Technology

The analysis of the SIW cavity has been studied numerically by using FDFD [110], and it has been proven that the leakage from the via gaps can be neglected and the SIW cavity with a high Q can be obtained easily. A low cost and high Q- factor resonator, which is an essential part in microwave and mm-wave SIW filters and oscillators, has been reported in[111, 112]. Different coupling methods between the SIW cavity and the planar circuit have been proposed in [111], such as the MSL, the CPW, or voltage probe. A cylindrical SIW resonator has been designed using LTCC technology [113] to enhance the resonator's Q-factor. The resonator is implemented by replacing the vertical metallic walls by closely spaced via posts.

Recently, the SIW filters attracted much more attention due to its low cost, low loss and easy fabrication; therefore a variety of filter topologies has been proposed. A simple SIW- filter with an inductive-post operating at *28 GHz* has been presented [114]. The measured insertion loss of the three poles in the Chebyshev filter was *1dB* and the return loss better than *17 dB*. A band pass filter with an

iris operating at *60 GHz* [115] was designed and fabricated. It was integrated in an alumina substrate with a measured insertion loss was *3 dB*. Also, cavity filters with circular [116] and rectangular shapes [117] have been developed. They allow a better design flexibility and show higher selectivity. Elliptical filters with four cavities operating in the C-band have been implemented [118] in a two-layer substrate. In this design, the coupling between the cavities in the same layer was controlled by metallic vias. The coupling between cavities in different layers is controlled by the aperture sizes integrated on the layer interface. The SIW integrated electromagnetic band-gap structure in the ground plane allows for super-wide band-pass filters as presented in [119] covering the frequency range of *8.5-16.50 GHz*.

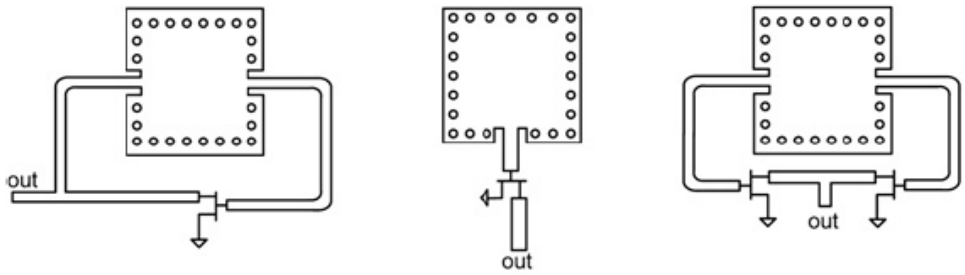

(a) (b) (c)

Figure 2.10 Oscillator circuits in SIW technology [120] (a) Feedback oscillator, (b) Reflection oscillator, and (c) Push-push reflection oscillator.

2.1.4.4 Active Circuits Based on SIW Technology

Compared to the reported development in the SIW-based passive circuits, the implementation of active circuits has received less attention [120]. Most of the active circuits, such as the oscillator, the amplifier circuits, and the mixers consist of embedding active devices in passive SIW circuits and interconnects for low fabrication cost, low loss and high isolation applications. In the microwave/mm-wave frequency range, the SIW cavity resonator is used in the oscillator in three different configurations as shown in Figure 2.10. The first reported SIW-oscillator used a rectangular SIW cavity placed in the feedback path between the input and output of an amplifier circuit at *12 GHz* [121]. Utilizing the SIW technology improves the oscillator phase noise due to its high unloaded Q-factor, and providing good tuning bandwidths, while maintaining a high Q-factor.

Also, frequency conversion circuits, and mixers, have been integrated by coupling active devices to passive circuits implemented using the SIW technology. A X-band single balanced mixer using a 90o hybrid has been proposed [122] in *24 GHz* automotive radar system-on-package. The mixer showed a *6.70 dB* conversion loss at a RF signal of a *24.1 GHz*, when the Local Oscillator (LO) signal was applied at *22.60 GHz*. The mixer return loss was better than *-10 dB* over the frequency band of *23-26 GHz* band, and the radio Intermediate Frequency (IF) isolation was better than *17 dB* within the *24-24.25 G*Hz Industrial Scientific and Medical band of interest for continuous wave radar applications.

The first amplifier integrated in the SIW in X-band was presented in [123] demonstrating a *9dB* gain and less than a *2 dB* ripple over the entire band. The active device was coupled directly to the

input and output eliminating the use of the SIW to MSL transition, as shown in Figure 2.11. Also, the SIW structures have also been proposed in designing a bias network for a power amplifier [124], and that would replace the typical bias network based on MSL technology, which may not be able to support DC currents. Alternatively, the SIW supports very large DC currents and suppresses the second and third harmonic components.

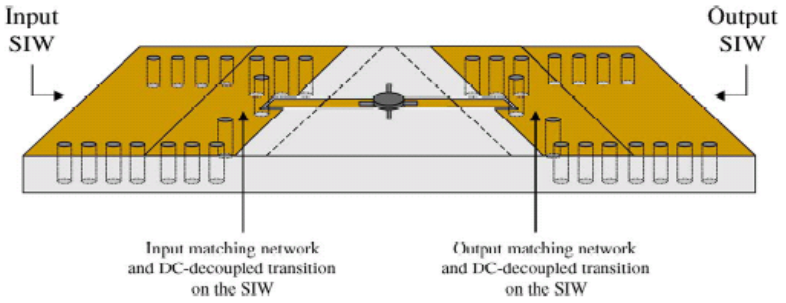

Figure 2.11 Configuration of amplifier embedded SIW [123].

2.1.4.5 Phase Shifters Based on SIW Technology

Phase shifters are extremely useful microwave components and have been used in many applications, such as wireless communication systems, and radar systems, measurements. However, the most important application of the phase shifter is phased arrays. Less work has been done on implementing phase shifters using SIW technology, especially at the mm-wave frequency band.

The proposed research work that has been conducted on the SIW phase shifter can be classified into different categories: fixed devices and variable devices. In fixed devices, the desired phase variation is obtained by employing SIWs of different widths [125, 126], inductive posts [127], or inserting a ferrite toroid into the SIW substrate [128]. As an alternative, a broadband compensating phase shifter using delay lines and equal-length and unequal-width in Figure 2.12 has been presented in [129]. The features of this phase shifter have been experimentally demonstrated by providing design examples. The *90°* phase shifter design showed an amplitude and phase imbalance of *0.2 dB* and ± *2.5°*, respectively, within the frequency band of *25.11- 39.79 GHz*.

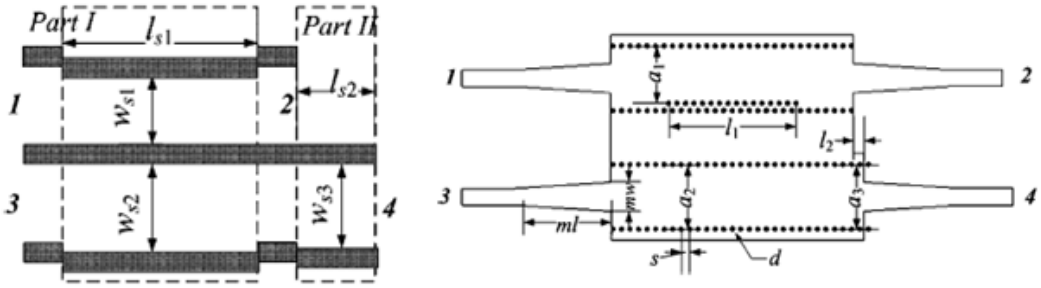

(a) (b)

Figure 2.12 Configuration compensating phase shifter [129], (a) Solid wall model, (b) Real SIW model.

However, in variable devices, the phase variation is obtained by variable/switching RF-components controlled by biasing circuits. A SIW reflective-type phase shifter operating in Ku-band [130] allows a controlled continuous phase shift by using reactive variable loads to a SIW quadrature hybrid junction. The load in Figure 2.13 is a transverse slot, cut on the SIW broad wall loaded by a varactor diode. A two-cascaded loaded slot reflective load was fabricated and measured. This had a nearly *360°* differential phase shift was achieved, within the biasing control voltage range of *0-20 volts*. Also, the reported measured losses were in the order of *6dB*.

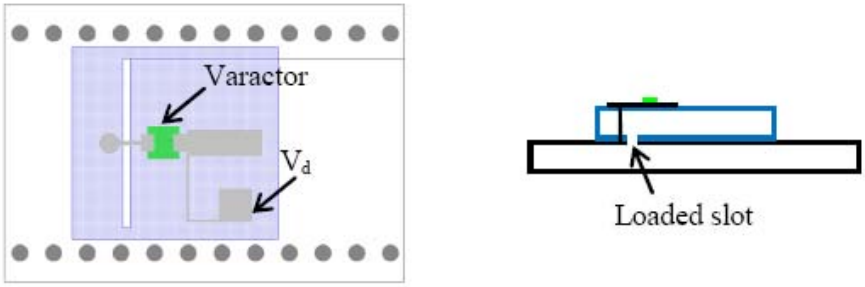

(a) (b)

Figure 2.13 Varactor loaded slot layout [130]: (a) top view, (b) cross-section view.

2.1.4.6 Antennas, and Subsystems Based on SIW Technology

Recently, there has been a growing interest in SIW-based antennas where the SIW has been either used as the main feeding scheme [131, 132], or as a backed cavity to the radiator [133, 134]. The classical SIW antenna [135] known as a slotted-waveguide antenna, is formed by etching longitudinal slot in the top metal surface of the SIW. The SIW-leaky-wave [131] antenna generates radiation leakage when the longitudinal spacing between the vias is sufficiently large. In a different topology, the SIW-Vivaldi radiator has been presented in [132]. It consists of dual V-type linearly tapered slot antenna, with center frequency at *36 GHz*. The antenna was fabricated by using PCB technology, and the measured gain was *10.6 dB*. Cavity-Backed SIW (CB-SIW) antennas have been developed and tested, and the simplest design structure is presented in [134]. It consists of a slotted waveguide cavity fed by a coplanar waveguide. Another design that uses SIW-cavities for a *2×2* metal patch antenna array at Ku-band has been presented in [133]. The cavities are formed by using metal vias, and the patches are excited by using MSLs that are centrally fed by a coaxial probe.

An extensive effort has been devoted in the development of multi-beam and scanned antennas using SIW technology, which in sequence required a beam forming network to achieve the desired distribution of amplitude and phase coefficients among the network outputs. A SIW multi-beam antenna based on the parabolic reflector principle has been implemented at *37.50 GHz* [136].

The parabolic antenna was realized in planar form as shown in Figure 2.14, using metallic vias, and a beam forming network has seven input ports to generate the corresponding number of output beams. Another attractive and common solution is to implement a beam forming network is the Rotman lens. It was implemented in the SIW [25] at *28 GHz* with seven inputs, which generated the same number of beams for a nine SIW linear slot array. Furthermore, the 2D solid angle with multiple beams was generated by grouping several antennas together in different ways. There is also the Butler matrix [137], which has been implemented in many planar technologies. It is an attractive solution for

a beam forming network implemented using SIW technology, since it can be built on a standard single-layer printed circuit board. The components needed in the feeding network are a *90°* hybrid coupler, cross coupler, phase shifter, and a power splitter implemented in SIW form. The measured results for an 8-port network present an insertion and reflection loss below *2.5 dB*, and *-25 dB*, respectively over an operating frequency of *58-62 GHz*.

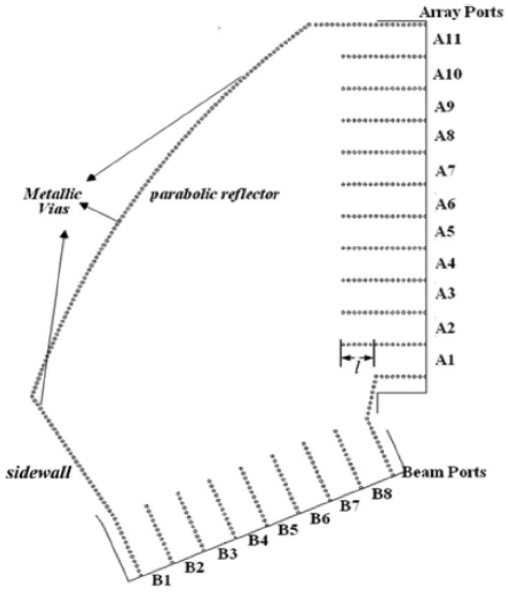

Figure 2.14 The geometry of the printed SIW parabolic reflector [136].

2.1.5 SIW to Planar RF-Circuit Transitions

The transition between the SIW and the planar circuits, such as MSL, CPW, or SL circuits can be built on the same substrate. The MSL and CPW transitions are used to excite the TE_{10} waveguide mode, while the TE_{01} is excited by the SL. The first transition that has been presented involved a MSL [92]. A taper MSL transition as shown in Figure 2.15 a, is used to gradually match the quasi-TEM mode to the waveguide mode. Design equations for the MSL to SIW transition has been derived using curve fitting technique and presented in [138]. These equations relate the optimum MSL width to the SIW width showing low loss and wide bandwidth performance. However, the low thickness substrate causes noticeable conduction loss in the waveguide section. To minimize conduction loss, the waveguide substrate must be increased. Accordingly, the radiation loss increases in the MSL that is not recommended for the integrations of active devices at mm-wave frequencies.

The simplest form of the SIW to CPW transition [139] is shown in Figure 2.15b. It consists of a CPW with a *90°* bend on each slot. A stub was on the CPW to match the transition. This transition has a limited bandwidth a *7%* at *a 15 dB* return loss and an insertion loss of better than *3.20* dB at *25 GHz*. Different transition designs have been proposed to match the structure's two modes, to enhance operating bandwidth, and to minimize the insertion loss. In [140], a current probe (inductive post) is used to couple the power between the CPW and the SIW. The experimental results showed a wider bandwidth of *10%* and insertion loss less than *0.73 dB* over the bandwidth of interest. An Ultra-wideband SIW to CPW transitions have been achieved within the entire Ka-band by gradual mode

matching as presented in [62], and by using linear taper transition as presented in [91] with a minimum insertion loss of *0.7 dB*, and a wideband width of *70 %* at *10 dB* return loss.

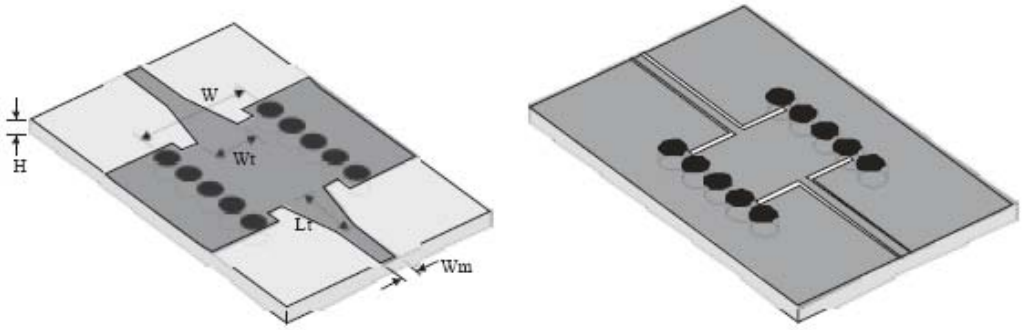

(a) (b)

Figure 2.15 Integrated transitions from planar circuits to SIW guiding structure [61] (a) MSL, (b) CPW.

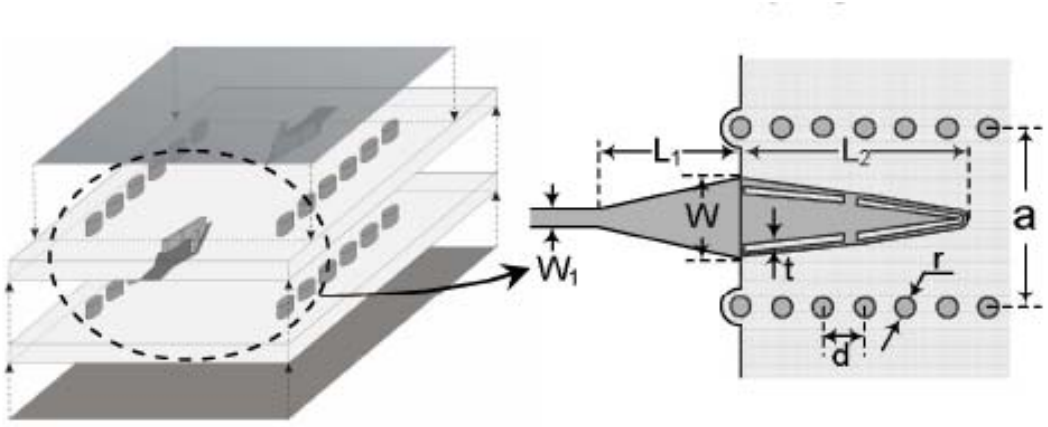

Figure 2.16 Configuration of a 2-layer SIW to CPW back-to back transition [63].

Alternatively, the SIW to MSL transition in a multi-layer substrate [63] has been proposed to achieve a broadband response and minimize the radiation and conduction losses. It makes the use of tapered ridged SIW and the tapered MSL to provide both the impedance and field matching, as shown in Figure 2.16. The proposed transition showed an effective bandwidth of *14.50 %* at a *15 dB* return loss, and an insertion loss of *1.50 dB* within the operating mm-wave band.

Several types of transitions between the coaxial (COAX) line and the RWG have been reported in [143-145] including their analysis and designs. However, the manufacturing reliability and the frequency characterization are not discussed for the mm-wave frequency band. A developed transition between the COAX and the SIW has been presented in [141]. Figure 2.17 shows the proposed transition with different configurations. An open ended structure in Figure 2.17a [143, 145] is characterized by its inner conductor suspended in the middle of the dielectric substrate. A wide bandwidth input impedance can be is controlled by changing the distance h and the short circuit position. Figure 2.17b shows the conventional short-ended structure [144], which is easy in

metallization. However, it presents a high input impedance, causing a narrow bandwidth even the though addition posts may be used to suppress reflections. The wide bandwidth transitions are obtained by either the stepped structure [146] in Figure 2.17c, or the taper-stepped structure [141] in Figure 2.17d. They lower the input impedance and widen the matching bandwidth to the COAX. Precise manufacturing and metallization of the inner conductor is needed though. The experimental results show that the transitions in Figure 2.17c, 2.17d provide impedance bandwidths of *14.7%* and *13.2 %*, respectively for a reflection coefficient less than *-15 dB*.

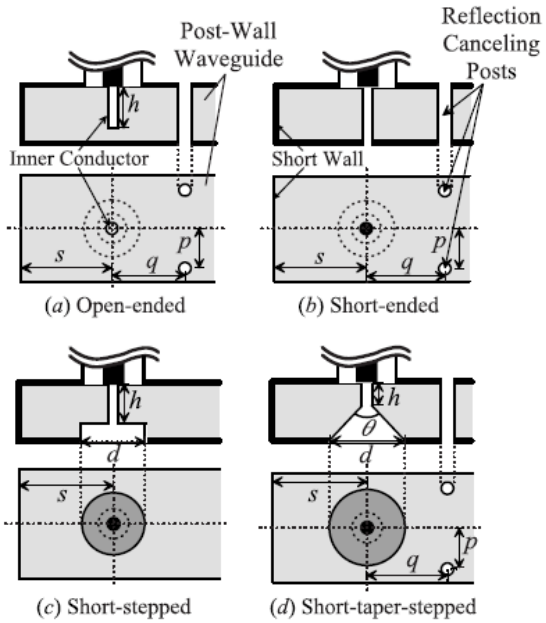

Figure 2.17 Transition between coaxial line (COAX) and SIW (posted vias are replaced with conducting walls)[141].

2.1.6 DRA Based on SIW Technology (SIW-Fed DRA)

The SIW has been presented as a feeding scheme for the CDRA in [102, 142] through a narrow slot cut on the SIW broad-wall. The slot was used to couple the power from the SIW to the CDRA. In [142], the CDRA TM_{110} mode is excited by the SIW-full structure at *18 GHz* as shown in Figure 2.18a. Extensive full-wave simulations have been performed to optimize the antenna performance, and the designed antenna showed a linear polarized radiation pattern (simulated) with a boresight gain of *6 dB* over an operating bandwidth (measured) of *17.90-18.20 GHz*. However, neither the measured radiation pattern nor the radiation efficiency was reported.

A Similar design has been presented in [102] for *60 GHz* applications, except that the $HEM_{11\delta}$ mode is excited by a Half-Mode SIW (HMSIW) structure to have the compact design as shown in Figure 2.18b. The measured gain was *5.5 dB* at *60 GHz* and the radiation efficiency was between *80 %-90%* over an operating frequency band of *24.2 %*. However, the gain showed by a single CDRA element is quite low (less than *6 dB*). Therefore the antenna arrays based SIW technology are an excellent candidate for high gain/radiation efficiency mm-wave applications. In this thesis, the design,

modeling, and experimental aspects of DRA arrays were based on the SIW technology, which to our knowledge have not been addressed before.

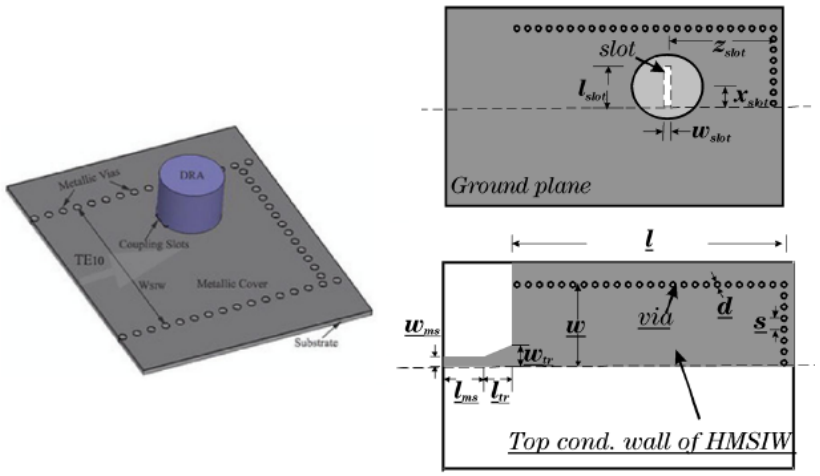

(a) (b)

Figure 2.18 SIW-fed CDRA, (a) using full SIW structure [142], (b) using HMSIW structure [102].

2.1.7 SIW-based components: Full-wave Simulations, and Fabrication Technologies

Currently, the tools for antenna designers are available for designing specific components such as the antenna element, very small sub-arrays or very small feed network. There is commercial software based on the Method of Moment (MOM), such as the Agilent Advanced Design System (ADS)[148], which can be used for the planar element or feed design of the sub-array with a few elements. There is also the software based on the Finite Element Method (FEM), such as Ansoft High Frequency Software Simulator (HFSS) [149], which can be used for a variety of designs. However, such full-wave solvers might fail in many cases (designs) due to the limited computational resources (CPU time and memory), especially when the periodic structures and large arrays including their feeds need to be simulated.

Only small subsections of the overall structure (arrays) can be simulated, and the antenna designers need to rely on his knowledge and experience to determine the configuration of the overall system.

Sometimes, full-wave solvers fail to give physical insight into the important design parameters effect, and they do not help RF/antenna designers in obtaining the optimal configuration for a set of physical requirements. Figure 2.19 shows the typical process needed by RF/antenna designers for RF front-end system development [147]. This process ignores the mutual coupling between the antenna elements, especially for non-planar antennas. Moreover, optimizing the overall antenna system using this process is considered to be time and memory consuming. Therefore, developing a coarse model that would expedite the design process and helps the designers to have more physical insight about the antenna system parameters, and their effect on the overall performance is important.

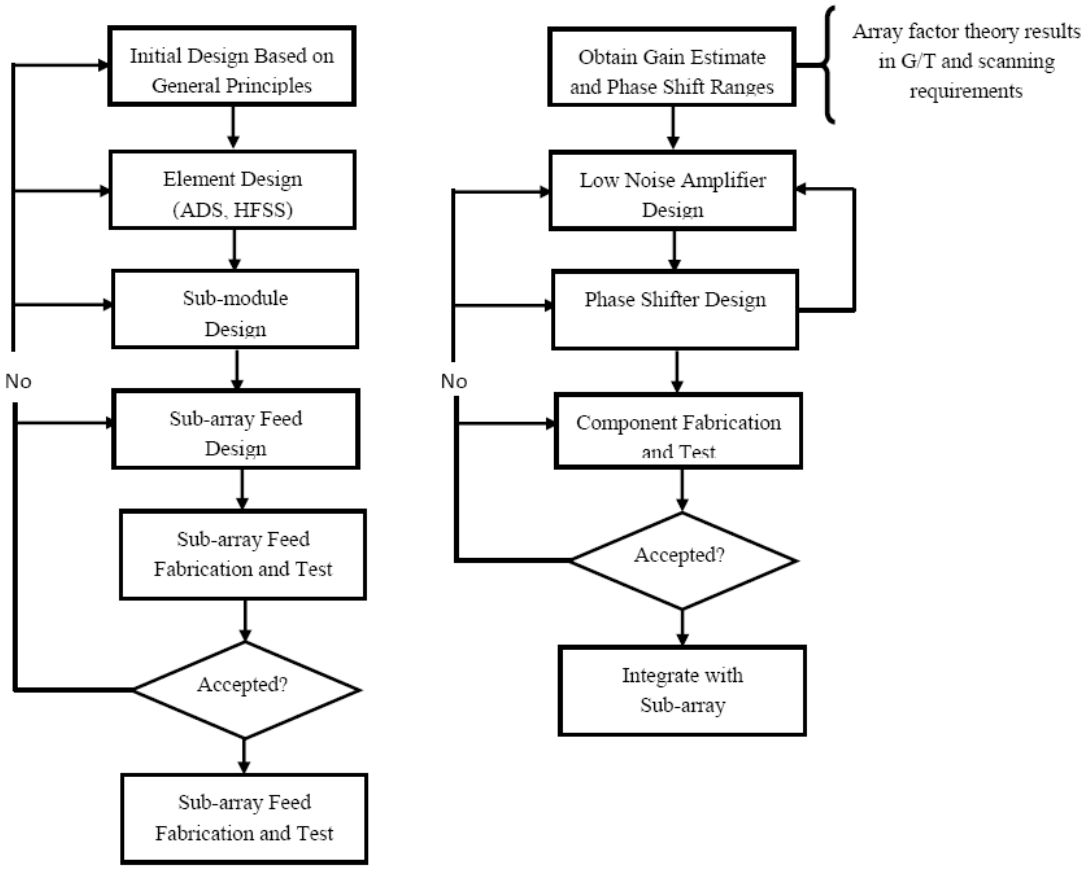

Figure 2.19 Typical design process using full-wave solver, (a) Sub-array design technique, (b) Front-end design [147].

The implementation and the development of the SIW structures are limited by the fabrication technologies available, especially in the mm-wave frequency band higher than *60 GHz* [120]. Due to the low fabrication cost and high design flexibility, PCB techniques have been widely used to implement the SIW structures. It also allows the integration of a planar passive circuit as well as an active circuit to the same substrate. In this case, metal holes are created either by micro-drilling or by laser cutting. The metallization is performed by using a conductive paste or metal plating [114].

As the frequency increases, some technological limitations arise that prevent the separation between the vias from going below a certain value. However, a solution has been proposed in [150], where the vias are replaced by metalized slots in a SIW circuit operating at *94 GHz* as shown in Figure 2.20. The LTCC technology allows for extremely compact SIW components, such as filters to be integrated [151, 152]. In these structures, several SIW resonator layers are vertically stacked with the help of a tiny dimension of via holes.

The SIW components operating above *100 GHz* were fabricated using photo-imageable thick film materials that have an excellent tolerance and dielectric loss [153]. The fabrication process is summarized as follows: first, a uniform metal layer is printed on an alumina substrate, to form the bottom wall of the waveguide. Then, a *10 μm* dielectric layer is printed and photo-imaged, forming

the trenches required for the waveguide side walls. This step is repeated to achieve the required thickness of the SIW structure. Finally, a conductor layer is printed and photo-imaged to form the upper wall of the waveguides. After printing and imaging, each layer is dried and fired prior to the subsequent layers. The SIW filter operating at *180 GHz* is fabricated by using this technology, and was designed, and experimentally verified [153].

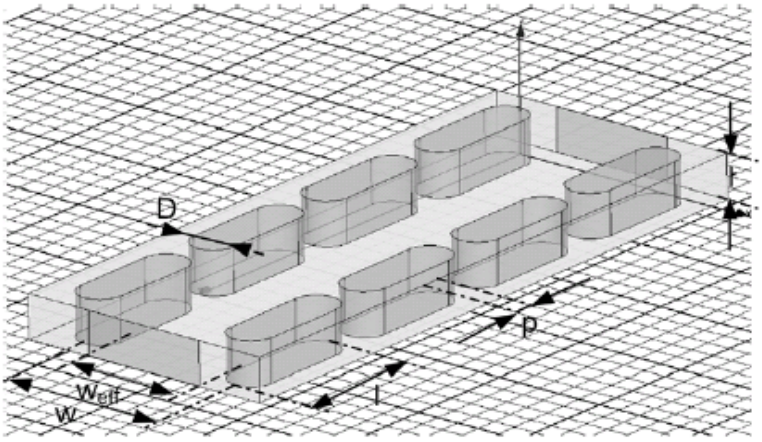

Figure 2.20 Geometrical view and description of the proposed W-band SIW transmission line [150].

2.1.8 Substrate Integrated Waveguide (SIW), Analysis and Modeling

2.1.8.1 Proposed Analysis Methods and models for Substrate Integrated Waveguide (SIW)

The SIW modeling and characterization has been presented using different analysis techniques, which are classified by reference [19] into three groups. The first group used the solution of the transcendental equations $det[F(\gamma)]=0$ generated from the Method of Moments (MOM) [154, 155] to calculate the unknown currents on the conducting cylinders. The Floquet-Bloch theorem is used to restrict the computational domain to such currents within one period. These techniques are versatile and simple to implement. However, their convergence is slow.

The second group used the classical eigenvalue formulations $[F]x=\gamma x$, derived from a full-wave analysis [20, 21, and 156]. These numerical methods are used to calculate the transmission matrix of one period. Then, the modes propagation constants in the waveguide are obtained by applying the Floquet-Bloch theorem. The main disadvantage of such method is the difficulty in calculating the attenuation constant due to leakage.

The third group used the surface impedance concept in their analysis [157, 158] to model the rows of vias by two complex impedance walls. In this method, the transverse resonance method [157], or an iterative technique [158] are used to calculate the SIW propagation constant. Modeling the SIW using the surface impedance is simple; however, it is limited to certain regular geometries. In [19], the surface impedance's concept has been developed to provide a fast and accurate method to calculate

the complex propagation constant in the SIW. The plane wave scattering from the rows of vias is calculated numerically by MOM, and is used to calculate the SIW surface impedance. Also, useful design rules have been proposed.

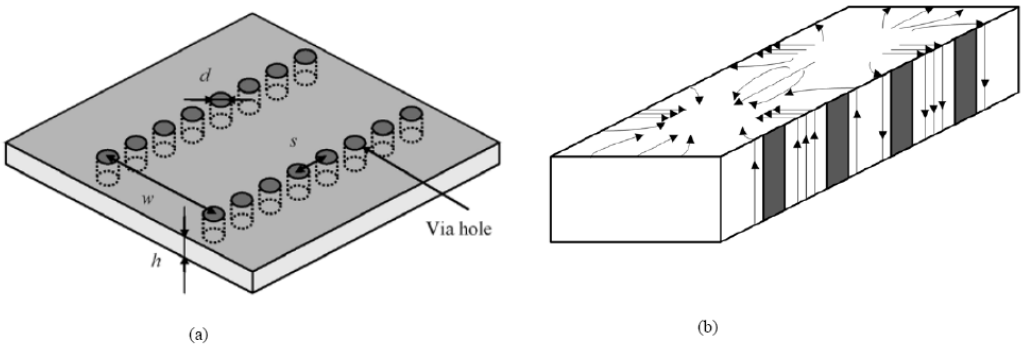

Figure 2.21 Wave guide structures (a) SIW 3D view, (b) TE_{10} Surface currents distribution of the Rectangular Waveguide with slot in narrow walls [29].

2.1.8.2 SIW characterizations

Figure 2.21a shows a typical SIW structure that is synthesized with a linear array of metallic via-holes with diameter d, a periodic length s on a low loss material substrate of permittivity ε_{rs} and the effective SIW width w. Although the SIW structure has similar properties as the conventional rectangular waveguides, it has different characteristics. The SIW is a periodic guided wave structure; therefore; it may lead to the electromagnetic band gap phenomenon. Also, the SIW structures are subjected to a potential leakage problem due to the periodic gaps. Therefore, the wave traveling in SIW structure has different characteristics from those of the conventional rectangular waveguide.

2.1.8.3 Propagating Modes in SIW structure

The SIW characteristics have been studied numerically by using Finite Difference Frequency Domain (FDFD) [29]. It has been found that the TM modes cannot be formed inside the SIW structure. Moreover, only the TE_{n0} modes can exist in the SIW structure. Hence, the SIW can be considered to be a rectangular waveguide with a series of slots on the narrow walls as shown in Figure 2.21b. These slots form physical discontinuities, which prevent the z-directed currents to circulate. All of those modes having a y-directed magnetic field, TE_{0n}, TE_{mn}, and TM_{mn} present significant leakage loss if excited, whereas in the TE_{n0} modes the slots do not cut the surface currents on the narrow walls as shown in Figure 2.21b for the TE_{10} case. Consequently, the mode exists inside the waveguide. This means that the vias not only play a role in shielding the electromagnetic waves, but also are responsible for connecting the surface currents in order to preserve the guided wave propagation.

2.1.8.4 Substrate Integrated Waveguide (SIW) and its Equivalent Rectangular Waveguide (RWG)

As the propagation characteristics of the SIW and the conventional RWG are similar, the SIW can be completely analyzed as a RWG with a modified width provided that the spacing between the posts is sufficiently small. Namely, as $\frac{w}{s}$ become larger or $\frac{s}{d}$ become smaller, the leaky wave radiating wave from gapes between metallic vias decreases and the SIW guiding wave property appears to be more similar to the equivalent waveguide. A correspondence between the cutoff frequencies of TE_{10}-like and TE_{20} -like modes of SIW, with respect to the diameter d and the width w are evaluated by using Boundary Integral-Resonant Mode Expansion (BI-RME) method[156], and the cutoff frequencies of both TE_{10} and TE_{20} modes of the SIW are represented by:

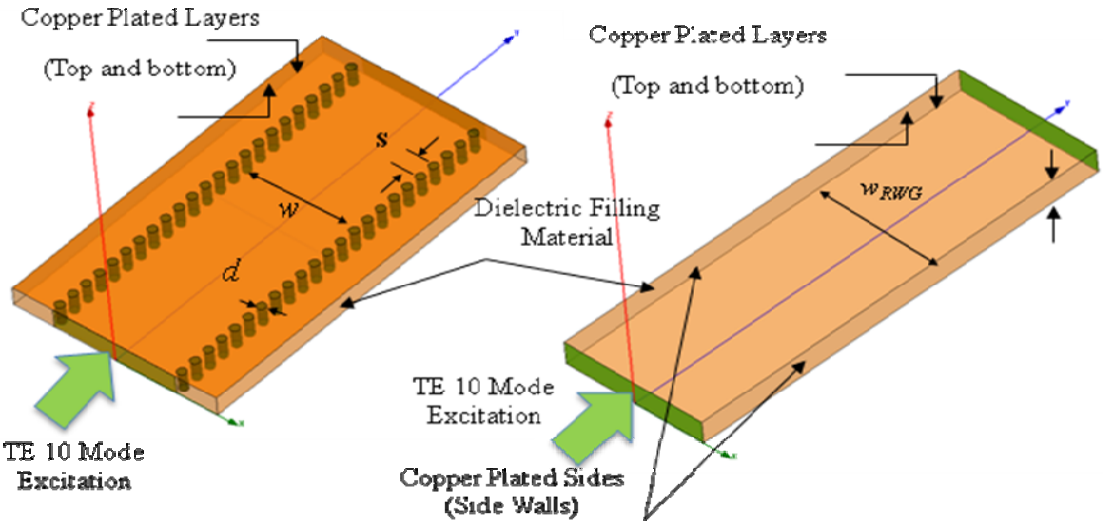

Figure 2.22 SIW and its equivalent Rectangular Waveguide (RWG).

$$f_{C(TE_{10})} = \frac{c_o}{2\sqrt{\varepsilon_{rs}}}\left(w - \frac{d^2}{0.95s}\right)^{-1} \tag{2.1}$$

$$f_{C(TE_{20})} = \frac{c_o}{\sqrt{\varepsilon_{rs}}}\left(w - \frac{d^2}{1.1s} - \frac{d^3}{6.6s^2}\right)^{-1} \tag{2.2}$$

A precision better than $\pm 4\% / \pm 9\%$ for these equations is possible, when $s \le \frac{\lambda_o \sqrt{\varepsilon_{rs}}}{2}$, and $s \le 4d$. Experiments and simulations results based on measuring the phase difference of the two guided wave length and comparing the first two modes of the SIW with those of an equivalent RWG filled with the same dielectric material as shown in Figure 2.22, have proven that the dispersion characteristics of the SIW are the same as those of its equivalent RWG whose equivalent width, is given by:

$$w_{RWG} = w - \frac{d^2}{0.95s} \tag{2.3}$$

Provided that the separation, *s*, is sufficiently small, a more accurate empirical equation was proposed to take the $\frac{d}{w}$ ratio into account [29]:

$$w_{RWG} = w - 1.08\frac{d^2}{s} + 0.1\frac{d^2}{w} \tag{2.4}$$

More detailed analyses have been carried out in [159] using the 3D Finite Element Method (FEM) package at nearly all microwave and mm-wave bands. The simulated results showed that the SIW insertion loss and its equivalent rectangular waveguide agreed well. However, some discrepancies between the characteristics of the SIW and those of the rectangular waveguide with the same effective width of the SIW have been observed. A derived empirical equation has been introduced using the Method of Lines (MOL) to calculate the SIW's equivalent RWG whose effective width is give by [20]:

$$w_{RWG} = \xi_1 + \frac{\xi_2}{\frac{s}{d} + \frac{(\xi_1 + \xi_2 - \xi_3)}{\xi_3 - \xi_1}} \tag{2.5}$$

$$\xi_1 = 1.0198 + \frac{0.3465}{\frac{w}{s} - 1.0684}$$

$$\xi_2 = -0.1183 - \frac{1.2729}{\frac{w}{s} - 1.2010}$$

$$\xi_3 = 1.0082 - \frac{0.3465}{\frac{w}{s} + 0.2152}$$

The dispersion characteristics of the SIW higher order modes are also similar to its equivalent RWG counterpart. However, there is a small difference in the equivalent width w_{RWG} between the higher-order modes and the fundamental mode [21,141].

2.1.8.5 Loss in Substrate Integrated Waveguide (SIW)

The overall performance of the SIW structure is affected by three types of losses, metallic loss (α_l), dielectric loss (α_d), and leakage loss (α_l). The overall losses are described by the following relation:

$$\alpha = \alpha_l + \alpha_d + \alpha_c \tag{2.6}$$

The loss performance of the SIW has been analyzed in [160] at *30 GHz* for different via diameter, *d (mm)*, and via spacing, *s (mm)* combinations. Figure 2.23a shows the attenuation constant due to the

radiation losses α_l, and it indicates that the losses increase when the vias become smaller and father apart. If the period length, *s*, increases, part of the EM energy may propagate outside the two arrays of cylinders; thus resulting in leakage loss (radiation). This loss arises in the form of coupling between the waveguide TE_{10} mode and the parallel-plate modes [19]. In particular, it was noticed that the attenuation constant α_l is smaller than *1dB/m* if the ratio $\frac{s}{d} \leq 2.5$ [160].

Assuming *w* is chosen for a given cutoff frequency of the TE_{10} mode, the dielectric and conduction losses in the SIW can be estimated using the formulation for the dielectric loss in a filled metallic waveguide [161]:

$$\alpha_d = \frac{k_o^2 \tan\delta}{2\beta} \tag{2.7}$$

$$\alpha_c = \frac{R_m}{a_e \eta \sqrt{1 - \frac{k_c^2}{k_o^2}}} \left[\frac{w}{b} + 2\frac{k_c^2}{k_o^2} \right] \tag{2.8}$$

Where $k_o = \omega\sqrt{\mu\varepsilon} = \frac{2\pi}{\lambda}$ is the wave number of the material filing the waveguide, and β is the propagation constant of the waveguide, $k_c = \frac{2\pi}{\lambda_c}$ is the cut off wave number, $\tan\delta$ represents the dielectric loss factor , $R_m = \sqrt{\frac{w\mu_o}{2\sigma}}$, $\eta = \sqrt{\frac{\mu_o}{\varepsilon_o \varepsilon_{rs}}}$, λ_c is the TE_{10} cut off wave length , and σ is the conductivity of the metal . It has been shown by [19] that the dielectric substrates which have a relative permittivity between *2* and *13* can be used in the design of the SIW components within the frequency range of *10-300 GHz*, with a dielectric loss factor of 10^{-3} - 10^{-4} . The conductor loss is determined by the total loss in SIW via walls, which includes the top / bottom solid metallic conductor and periodic via walls. SIW circuits are usually covered with copper having conductivity $\sigma = 5 \times 10^7$ with magnitude of the dielectric and the conducting losses range is 10^{-4} - 10^{-3} Np/m . Therefore, this feature makes the SIW structure an interesting practical low cost structure for this frequency range if its dimensions are chosen properly to minimize the losses.

Also, the conduction losses due to the finite conductivity of the metal, and the dielectric losses versus the via diameter and spacing is shown in Figure 2.23b, and 2.23c, respectively. It is noticed that the former decreases when the metal vias are large and closely spaced, and the latter is slightly affected by the vias diameter and spacing. In general, to keep the overall losses at minimum level, more restrictive conditions are presented in [29]:

$$\frac{s}{d} \leq 2.5 \quad \text{and} \quad , \frac{d}{w} < \frac{1}{8} \tag{2.9}$$

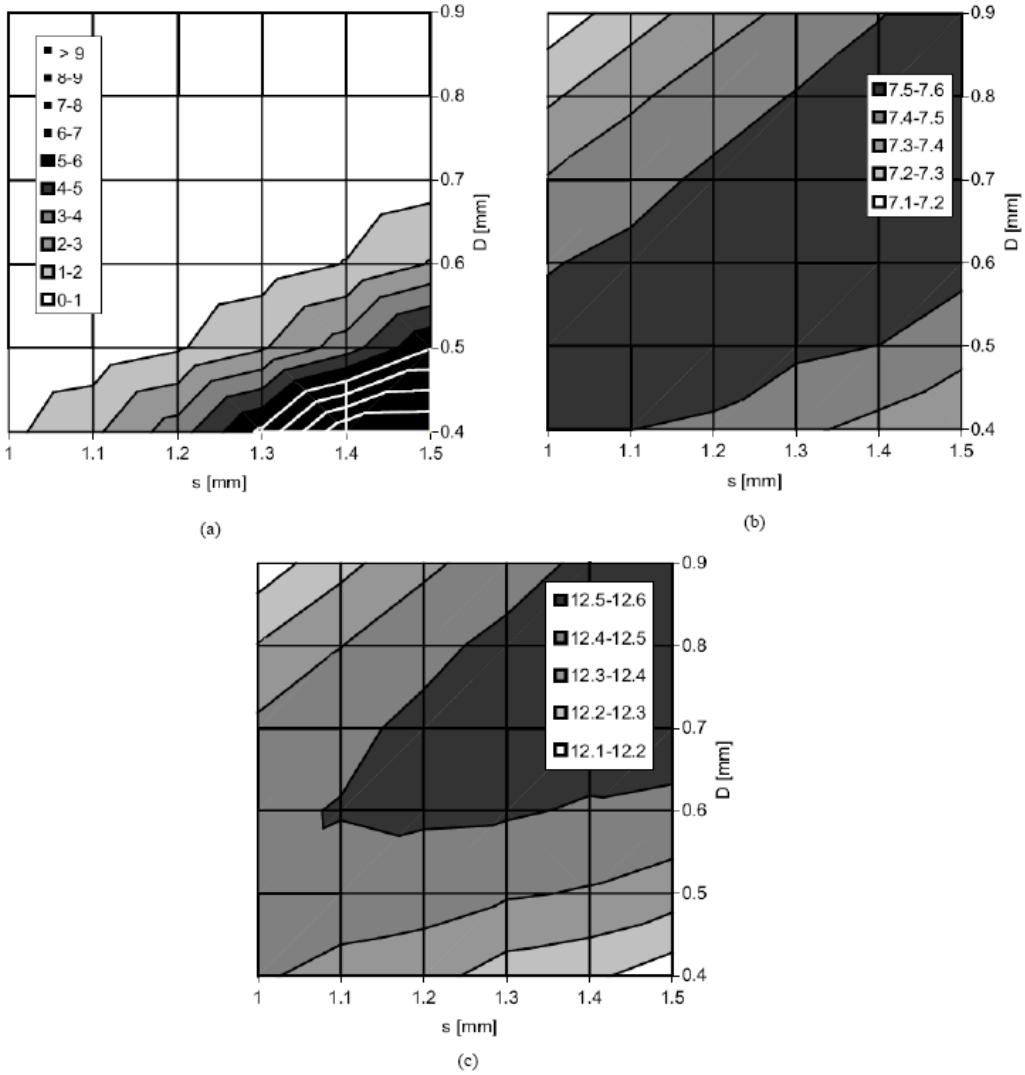

Figure 2.23 Attenuation constant (dB/m) of the SIW excited by TE_{10} mode versus the via diameter *D(mm)* and via spacing *S (mm)*[160] (a) due to leakage (radiation), α_l, (b) due to ohmic losses, α_c, (c) due to dielectric losses, α_d.

The losses in the SIW structure were compared to these of traditional multi-conductor structures, such as the MSL and the CPW were reported in [162]. These structures were built using the same substrate. Both the MSL and the CPW as designed to exhibit $50\,\Omega$ characteristic impedances, as shown in Figures 2.24a, 2.24b. Figure 2.24c shows the calculated attenuation constant of the three planar interconnect structures. The losses in the MSL and the CPW increase with the frequency. Conversely, the SIW, like in the RWG have losses that are high near the cutoff frequency which decreases as the frequency increases. Therefore, the SIW can replace these traditional planar structures in low loss mm-wave applications.

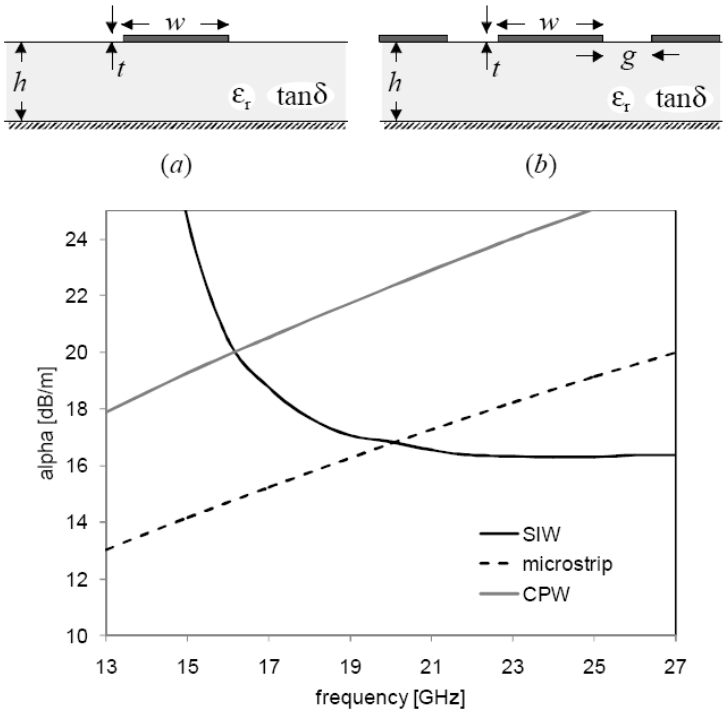

Figure 2.24 Comparison of the attenuation constant in SIW, microstrip and CPW, (a) MSL, (b) CPW, (c) attenuation constants of the three structures [162].

2.1.8.6 Bandgap Effects

The SIW is a periodic guided wave structure, and it may be subjected to the band-stop phenomenon if not designed properly. In the design of the SIW components, one must ensure that there is no bandgap over the operating waveguide bandwidth. Therefore, to avoid the bandgap appearance, the SIW period *s* should not exceeded a certain critical value, $s_{critical} = \frac{\lambda_c}{2\sqrt{3}}$ [19]. A more restrictive condition $\frac{s_{critical}}{\lambda_c} < 0.25$ should be used to avoid any band-gap effect in the operating bandwidth. The FDFD has been used to study the bandgap phenomenon [29], it was found that, the frequency at which the band-stop appears is very high if $\frac{s}{d}$, and $\frac{d}{w}$ are small. Also, the band-stop width and magnitude are very small. However, if $\frac{s}{d}$ or $\frac{d}{w}$ increases, the width and the magnitude of band-stop becomes significantly large, and the frequency point at which the band-stop appears, move to the lower frequency [29].

2.1.8.7 SIW Design Considerations and Strategy

There are certain values for both $\frac{d}{\lambda_c}$ and $\frac{s}{\lambda_c}$ at which the SIW is equivalent to a conventional waveguide that has negligible leakage losses, and it does not present any band-gap in the operating bandwidth. Design rules have been presented in [19] to satisfy all these requirements. Also, the authors in [163] have proposed two design rules as $\frac{s}{\lambda_c} < 0.35$ and $s \le 2d$ within the operating bandwidth. However, a sufficient condition to ensure negligible leakage losses in the SIW is to have the cylindrical via diameter to be at least one-half of the periodic length [19]. The design of the SIW is based on the fundamental TE_{10} mode propagation in the frequency of interest. It means that the waveguide width should be selected properly to excite this mode. Since the first two modes to propagate in waveguide are TE_{10} and TE_{20}, with $f_c(TE_{20}) = 2 f_c(TE_{10})$, a reasonable choice is to choose a TE_{10} cutoff frequency $f_c(TE_{10}) = \frac{f_o(SIW)}{1.5}$, where $f_o(SIW)$ is the center frequency of the operation for the SIW. The ratios $\frac{s}{d}$ and $\frac{d}{w}$ are chosen to be small using condition (2.9) based on the aforementioned analysis and from the manufacturing cost point of view. Then, the SIW rectangular waveguide equivalent's effective width w_{RWG} is calculated by:

$$w_{RWG} = \frac{1}{2 f_c(TE_{10}) \sqrt{\mu \varepsilon_{rs}}} \tag{2.10}$$

By using this equation along with equation (2.5), the following equation is used to calculate the SIW effective width (the distance between the centers of the via walls)

$$w = \frac{3}{4 f_o(SIW) \sqrt{\mu \varepsilon_{rs}}} + 1.08 \frac{d^2}{s} - 0.1 \frac{d^2}{w} \tag{2.11}$$

Chapter 3

Planar Waveguide Based Dielectric Resonator Antennas: Analysis, Design, and Fabrication

3.1 Introduction

In this chapter, the planar waveguide, the Substrate Integrated Waveguide (SIW), based Dielectric Resonator Antenna (DRA) is investigated. The Rectangular Dielectric Resonator Antenna (RDRA) is designed to radiate in millimeter-wave (mm-wave) frequency band. Modal analysis using the Dielectric Waveguide (DWG) model described in Appendix A along with the Eigen Model Full-Wave Solver, HFSS, are used to calculate the isolated RDRA fundamental mode resonance frequency. The SIW fed-RDRA made of low cost materials is proposed in this chapter to enhance the antenna's overall radiation efficiency.

The design SIW fed-RDRA is fabricated by a simple process, which would minimize the tolerance and fabrication errors. This fabrication technique is also compatible with the Printed Circuit Board (PCB) low cost technology. The antenna prototypes are tested to verify their validity to real high radiation efficiency mm-wave applications. Their measured reflection coefficients and radiation patterns are compared to these calculated by full-wave solver.

3.2 Substrate Integrated Waveguide (SIW) Fed Dielectric Resonator Antenna: Material and Parameters Characterization

The RDRA is characterized by its simplicity, mode purity, and ease of fabrication. It provides more flexibility in terms of bandwidth control. Therefore, it is preferred over other DRA shapes in this work. As discussed in Appendix A, for the DRA to be an effective radiator, its material dielectric constant has to be chosen low as $5 \leq \varepsilon_{rd} \leq 20$. Otherwise, the RDRA would be a highly efficient Q-factor (low bandwidth) energy storage element rather than a radiator. In addition, a RDRA with a higher dielectric constant has smaller dimensions that would make the fabrication difficult. In this work, a low loss/cost material, *RT/Duriod 6010 LM* ($\varepsilon_{rd}=10.20$, and $\tan\delta = 0.002$), is chosen to design the RDRA. Since the RDRA dimension affects the resonant modes and their internal field pattern, it has to be chosen properly to excite the correct mode for radiation and have a strong coupling between that mode the excitation source.

Figure 3.1 shows the isolated model of the RDRA which is designed to resonate for radiation at a mm-wave frequency band. A theoretical model and a numerical analysis of the RDRA modes by using HFSS Eigen Mode Solver were utilized to characterize and design this RDRA. Afterwards, the RDRA excited model that consists of the RDRA element fed by a narrow slot cut on the broad wall of the SIW is proposed. A parametric analysis is also conducted to investigate the impact of the designed parameters on the antenna performance. The resonant frequency of the RDRA fundamental mode, TE_{111}, can be determined by using the Dielectric Waveguide (DWG) model as described in Appendix A. Based on the solutions of the equations (A8)-(A10), different possible RDRA dimensions can be

obtained for the same resonant frequency at f_o=*30 GHz*. Table 3.1 lists some of the possible RDRA dimensions that can be fabricated on a commercially available low cost material with standard thicknesses h_{sd}=*b* for dielectric constant ε_{rd}=*10.20*. The full-wave Eigen Mode Solver, HFSS, was used to verify the natural resonance behavior of the RDRA. The modal analysis was carried out for different RDRA dimensions. The model consists of a RDRA, which resides on an infinite ground plane as shown in Figure 4.1.

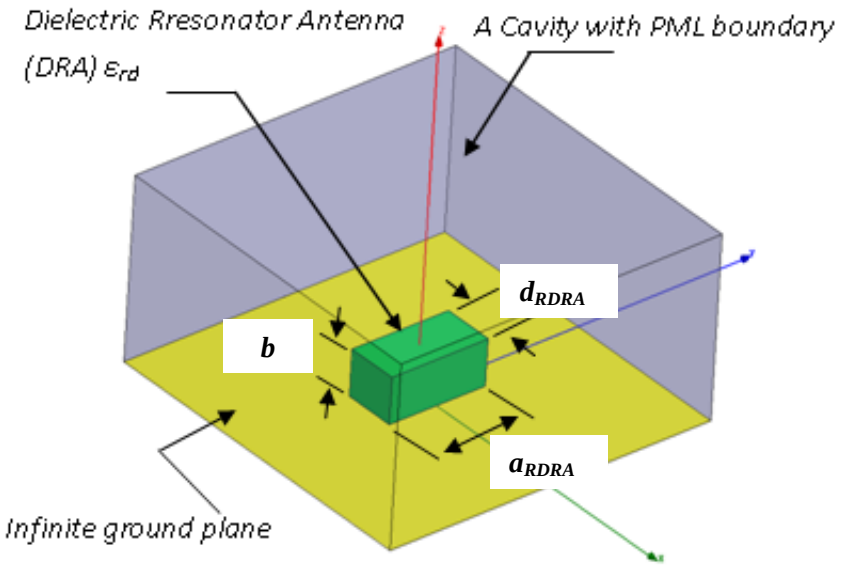

Figure 3.1Rectangular dielectric resonator antenna (RDRA) resides on infinite ground plane [164].

Table 3.1RDRA possible dimensions (mm) for ε_{rd} =*10.20 at 30 GHz [164]*.

h_{sd}	2b	a_{RDRA}	d_{RDRA}	f_o (GHz) (DWGM)	f_o (GHz) (HFSS)	% ERROR
2.50	*5.0*	2.0	2.0	29.57	29.15	0.7
		3.0	0.80	30.29	29.78	0.8
		2.50	1.0	30.22	30.54	0.5
1.90	*3.80*	3.80	0.76	30.33	29.62	1.2
		4.20	0.70	30.10	29.46	1.1
		2.10	1.90	30.41	30.05	0.6
1.27	*2.54*	3.0	1.50	30.40	30.75	0.6
0.64	*1.28*	*Too thin to be used at this frequency*				
0.25	*0.50*	*Too thin to be used at this frequency*				

As shown in Table 3.1, there is a good agreement between the DWG model result and that of the HFSS Eigen Mode Solver solution with the PML boundary condition in predicting the TE^{x}_{111} mode resonance frequency. For our reference, Figure 3.2 shows the field's vector plots of this mode. In order to strongly excite this mode, a source (slot) should be located at a strong field (magnetic) to ensure a good coupling [35]. A narrow slot cut on the SIW broad wall is used to excite the RDRA. Two different slot configurations are proposed, horizontal polarized (transverse), and vertical polarized (longitudinal) slot as shown in Figures 3.3a and 3.3b, respectively. The proposed SIW structure consists of two integrated rows of metalized vias with a diameter of d_{via} separated by a_{SIW} (SIW width), and each two neighboring vias are s_{via} apart (center to center). The top and bottom planes are copper plated with thickness of h_c , as in Figure 3.3c. The SIW is integrated on a dielectric substrate with constant of ε_{rs} and a thickness of h_{sb}. The SIW substrate thickness and the dielectric constant are selected to minimize the conduction loss and provide a compact design. Also, the SIW parameters are chosen to minimize the losses.

The SIW width a_{SIW} is chosen for a single fundamental TE_{10} mode operation, and it is calculated by using the SIW equivalent RWG concept presented in [29]. For completeness, the SIW to MSL taper transition shown in Figure 3.3 is needed to connect the proposed antenna to other RF-planar circuits, such as filters. As discussed in Chapter 2, the SIW-MSL transition is used to match the MSL Quasi-TEM mode to the SIW TE_{10} mode. It is designed and optimized following the criteria presented in [138]. For simplicity, the following antenna analysis and design will be conducted without the SIW-MSL transition. However, this transition will be used for experimental verification.

In Figure 3.3, the slot's dimensions, L_{Slot}, W_{Slot}, and the position, X_{SC}, is optimized in order to efficiently couple the energy from the SIW to the RDRA. Initially, X_{SC}, is chosen to be $\frac{\lambda_g(inside\ SIW)}{2}$ for Figure 3.3a, and $\frac{\lambda_g(inside\ SIW)}{4}$ for Figure 3.3b, which corresponds to a maximum standing wave field intensity (maximum coupling). The *Rogers RT5870* ($\varepsilon_{rs}=2.33$, $tan\delta=0.0013$) dielectric substrate with standard thickness of $h_{sb}=31\ mil$ is used to implement the SIW. It has a width of $a_{SIW}=4.80\ mm$. The metallic vias have a diameter of $d_{via}=0.3302\ mm$ and are separated by $S_{via}=0.60\ mm$. The RDRA element is made of Rogers RT6010 ($\varepsilon_{rs}=10.20,\ tan\delta=0.0031$) with a thickness of $h_{sd}=50\ mil$. The RDRA has a length of $a_{RDRA}=3.0\ mm$, and a width of $d_{RDRA}=1.50\ mm$, respectively and symmetrically is centered with respect to the coupling slot (zero offset).

3.3 SIW-Fed-RDRA Characterization and Parametric Study

Some design parameters may affect the coupling between the slot and the RDRA [42, 64]. Therefore, a detailed parametric study is then useful to study the effect of the antenna parameters. The antenna parameters are slot position X_{SC}, slot length l_{Slot}, slot width w_{Slot} and the RDRA's relative position to slot. The impact of these parameters on the antenna performance has to be investigated. Then, they should be optimized to obtain maximum energy coupling between both the slot and the RDRA [18]. For brevity, the impact of these parameters has been conducted for the antenna in Figure 3.3a, whereas, the optimized antenna parameters in Figure 3.3b are implicitly included in the final design.

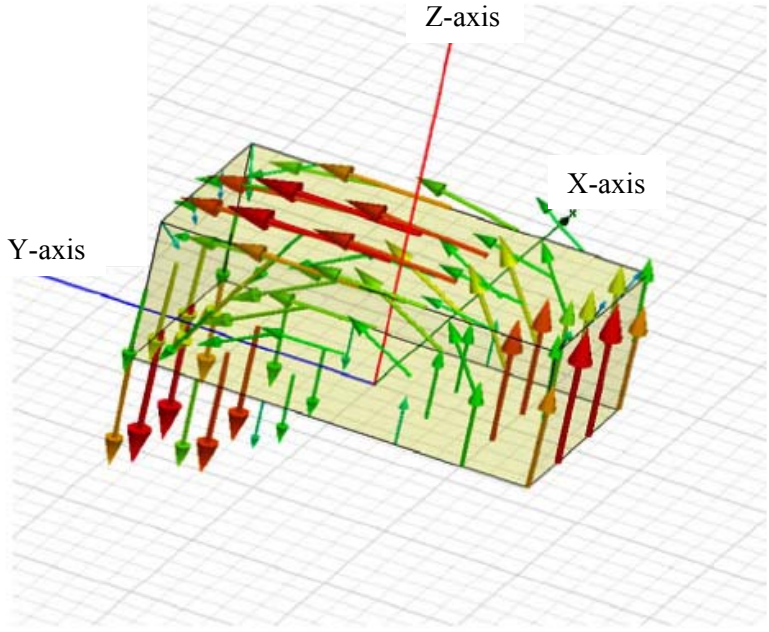

(a)

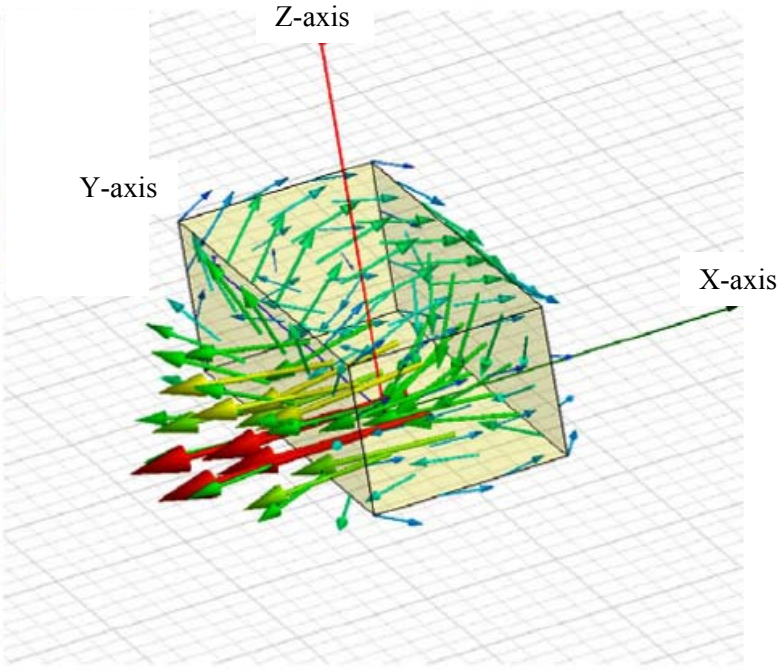

(b)

Figure 3.2 The vector field distribution plots of the isolated RDRA TE_{111} fundamental mode [164] (ε_{rd}*=10.20,* a_{RDRA}*=3.0 mm,* d_{RDRA}*=1.50 mm, and* h_{sd}*=1.270 mm),* the RDRA resides on an infinite ground plane, (a) Electric field vector plot (V/m). **(**b) Magnetic field vector plot (A/m).

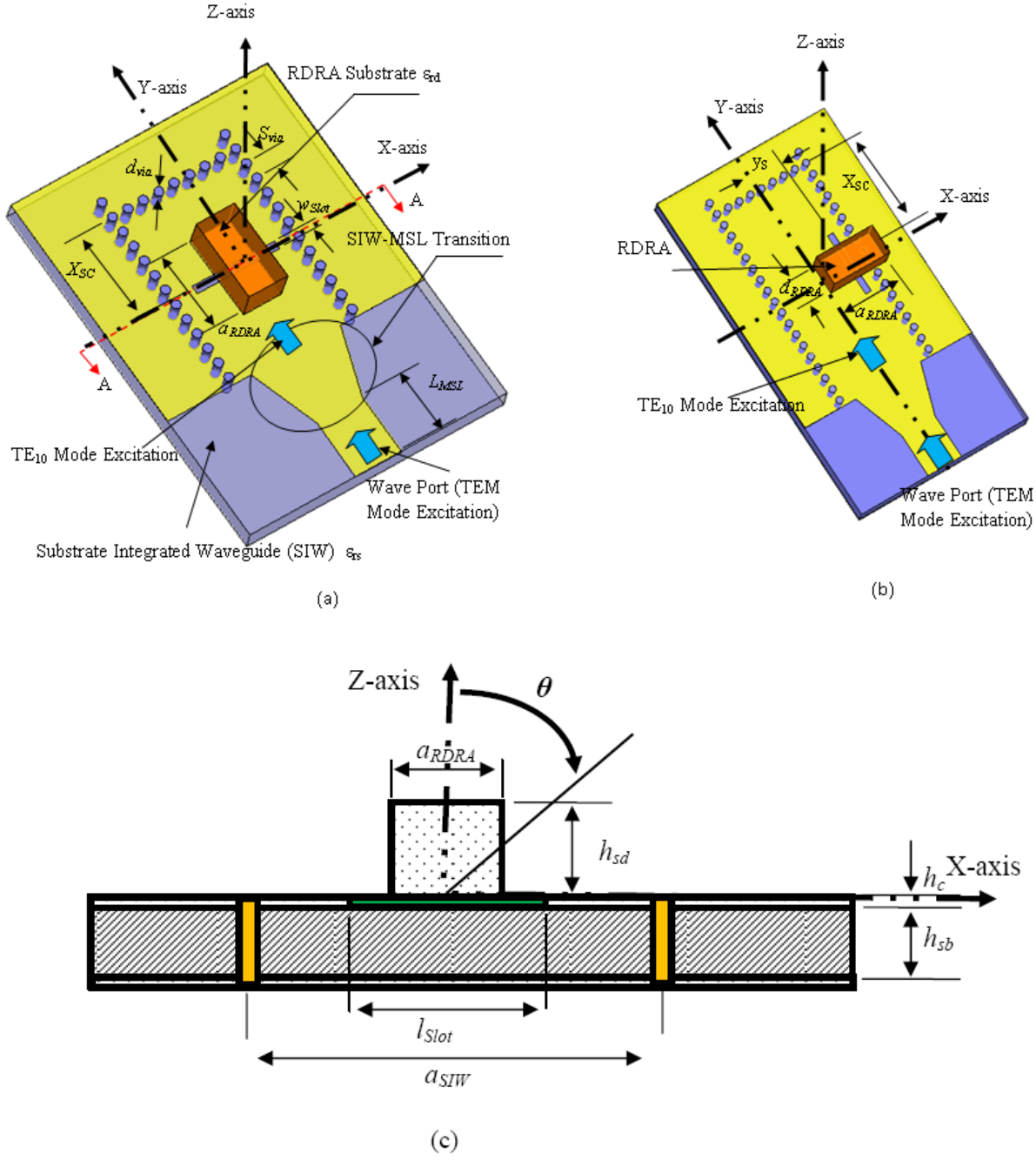

Figure 3.3 (a) The Substrate Integrated Waveguide (SIW)-fed dielectric resonator antenna (RDRA) driven model [164], (a) using horizontal polarized (transverse) slot, (b) using vertical polarized (longitudinal) slot, (c) Cross-section plane A-A.

3.3.1 The impact of slot position X_{SC}

In Figure 3.3a, the position of the transverse slot on a SIW board wall controls the amount of power coupled to the RDRA. The center position (along Y-axis) on the SIW broad wall, and at $X_{SC} = \frac{\lambda_g (inside\ \ SIW)}{2}$ from the Short Circuited (SC) end, guarantees a maximum excitation to the RDRA's fundamental mode (maximum coupled power) [135]. Since the effective dielectric constant seen by the slot ε_{eff} is not accurately known, the guided wavelength was calculated based on the average dielectric constant $\varepsilon_{eff} = \frac{\varepsilon_{rd} + \varepsilon_{rs}}{2}$ [27], to be X_{SC}=*2.60 mm*. The slot position from the short circuit was varied with an initial slot width w_{Slot}= *0.25 mm*, slot length l_{Slot}=*2.60 mm*, and a zero relative offset between the RDRA and the slot. Figure 3.4 shows the effect of changing the X_{SC} on the antenna reflection coefficient (coupling) S_{11}*(dB)* over the frequency band *28-40 GHz*. It was found that the position X_{SC} changes the amount of power coupled to the RDRA, where the maximum coupling occurs at X_{SC} =*3.50 mm*. This means that the RDRA resonates (with minimum reflection coefficient, S_{11}*(dB)*, at *f =36.73 GHz*.

As shown in Figure 3.4, the RDRA's resonance frequency differs from the designed frequency. This frequency shift can be accounted for as follows: The DWG model, which was used in the RDRA analysis, assumes that the RDRA resides on an infinite ground plane, and its height is halved. The DWG model does not take the slot effect into consideration. In other words, due to the slot effect, the assumption of using half of the RDRA's height is not accurate, and it shifts the RDRA designed resonance frequency f_o to another frequency rather than the designed one (the RDRA resonance frequency is height dependent).

3.3.2 The impact of slot length l_{Slot}

Also, the effect of the slot length was investigated by varying the length in the vicinity of $\frac{\lambda_g}{2}$, while keeping w_{Slot}=*0.25 mm*, X_{SC}=*3.50 mm* , and with a zero offset between the RDRA and the slot. As the slot length was shortened, the resonance frequency of the RDRA, f_o increased. The effect of the placing RDRA on the top of the slot was to change the input impedance so that it is matched at the frequency rather than the RDRA's natural resonance frequency as shown in Figure 3.5. Although the resonance is noticeable for each slot length, the best antenna matching is achieved when the slot length l_{Slot}=*2mm*. Furthermore, it is observed that a significant portion of energy is coupled into the RDRA at different frequencies, which gives a good indication of the TE_{111} mode broadband behavior and the slot length tuning property. As the slot length changes from *2.0 mm* to *3.50 mm*, f_o shifts from *38.30 GHz* to *36.0 GHz* keeping almost the same impedance bandwidth (S_{11}< *-10 dB*) of *2.80 GHz*.

3.3.3 The impact of slot width w_{Slot}

Figure 3.6 shows the effect of varying the slot width on the antenna reflection coefficient S_{11}*(dB)*,while the slot length is kept constant at l_{Slot}=*3.20 mm*. As shown in Figure. 3.6, increasing the slot width has the effect of increasing both the resonance f_o of the RDRA and the input bandwidth.

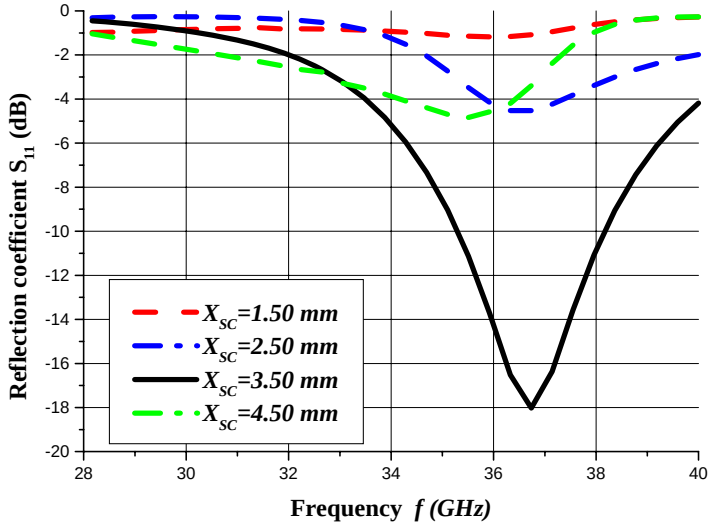

Figure 3.4 The impact of the slot position X_{SC} (mm) variation on $S_{11}(dB)$[164], *SIW parameters:* a_{SIW}*=4.80 mm,* d_{via}*=0.3302 mm,* S_{via} *=0.60 mm, RDRA parameters:* a_{RDRA}*=3.0mm,* d_{RDRA}*=1.50mm, and Slot parameters:* l_{Slot}*=2 mm,* w_{Slot} *= 0.40 mm, and* zero offset between RDRA and the Slot(*without MSL transition*).

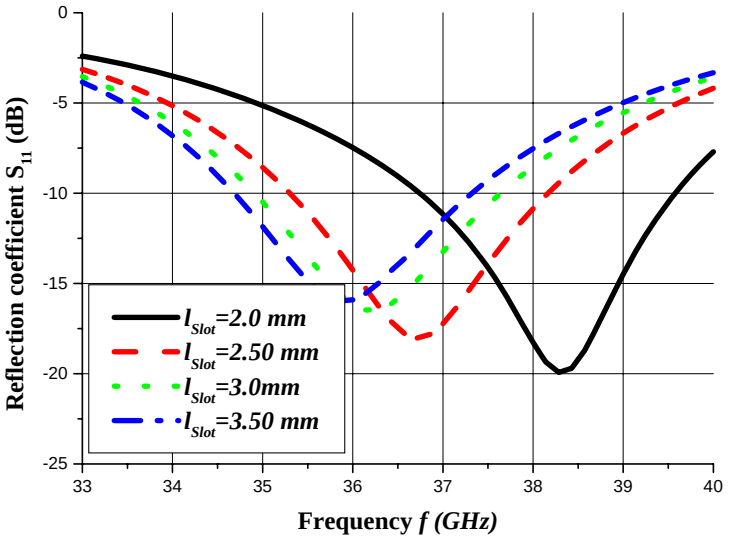

Figure 3.5 The impact of the slot length l_{Slot} *(mm)* variation on $S_{11}(dB)$[164], *SIW parameters are:* a_{SIW}*=4.80 mm,* d_{via}*=0.3302 mm,* S_{via} *=0.60 mm, RDRA parameters:* a_{RDRA}*=3.0mm,* d_{RDRA}*=1.50mm, and slot parameters:* w_{Slot} *= 0.40 mm, and* zero offset between RDRA and the Slot (*without MSL transition*).

Namely, the RDRA resonance frequency changes from a low frequency of *36.64 GHz* when the slot width is 0.20mm to a high frequency of *37.43 GHz* when the slot width is *0.40 mm*. However, the impedance bandwidth increases from *5%* at *35.64 GHz* to *11.5% at 37.43 GHz*.

3.3.4 The impact of RDRA-slot relative position (offset)

Finally, the RDRA's relative offset to the slot was studied using l_{Slot} *=3.20*, and w_{Slot}*=0.40* mm to determine the optimum placement of the RDRA above the slot. The results are presented in Figure 3.7. Offsetting the RDRA from the center of the slot not only shifts the resonance frequency f_o of the antenna, but also increases the impedance bandwidth. When the RDRA deviates by *0.50 mm* in either direction, f_o increases to approximately *38.14 GHz*, which corresponds to a reflection coefficient of *-22.50 dB* and a bandwidth of *12.50 %*. This means that for any potential error introduced by not perfectly centering the RDRA, the antenna is still matched. Further offset to *1mm*, the impedance bandwidth and the reflection coefficient are degraded due to the inefficient coupling between the RDRA and the slot. However, a very good coupling and impedance matching is obtained at no offset (as expected).

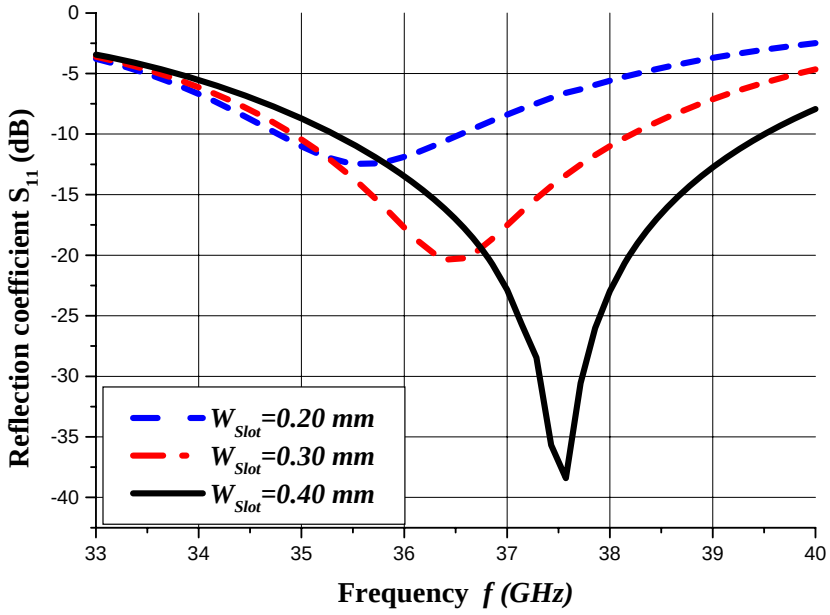

Figure 3.6 The impact of the slot width w_{Slot} *(mm)* variation on S_{11}*(dB)*[164]*, the SIW parameters are:* a_{SIW}*=4.80 mm,* d_{via}*=0.3302 mm,* S_{via} *=0.60 mm, RDRA parameters:* a_{RDRA}*=3.0 mm,* d_{RDRA}*=1.50 mm, and slot parameters:* l_{Slot}*= 3.20 mm, and* zero offset between RDRA and the Slot(*without MSL transition*).

Similarly, the proposed antenna parameters in Figure 3.3b were studied and its reflection coefficient (dB) was numerically calculated (simulated). It was found that a matching circuit is needed to minimize the reflection from the antenna and enhance the coupling between the longitudinal slot and the RDRA, as shown in Figure 3.8a.

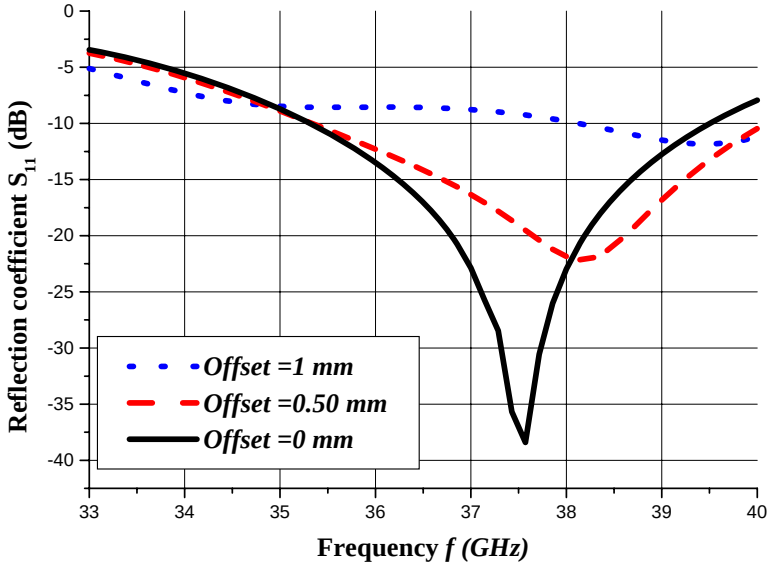

Figure 3.7 The impact of the RDRA-slot relative position (offset) *(mm)* variation on S_{11}*(dB)*[164]*, the SIW parameters are:* a_{SIW}*=4.80 mm,* d_{via}*=0.3302 mm,* S_{via} *=0.60 mm, RDRA parameters:* a_{RDRA}*=3.0mm,* d_{RDRA}*=1.50mm, and slot parameters:* l_{Slot} *= 3.20 mm,* w_{Slot} *= 3.20 mm*(*without MSL transition*).

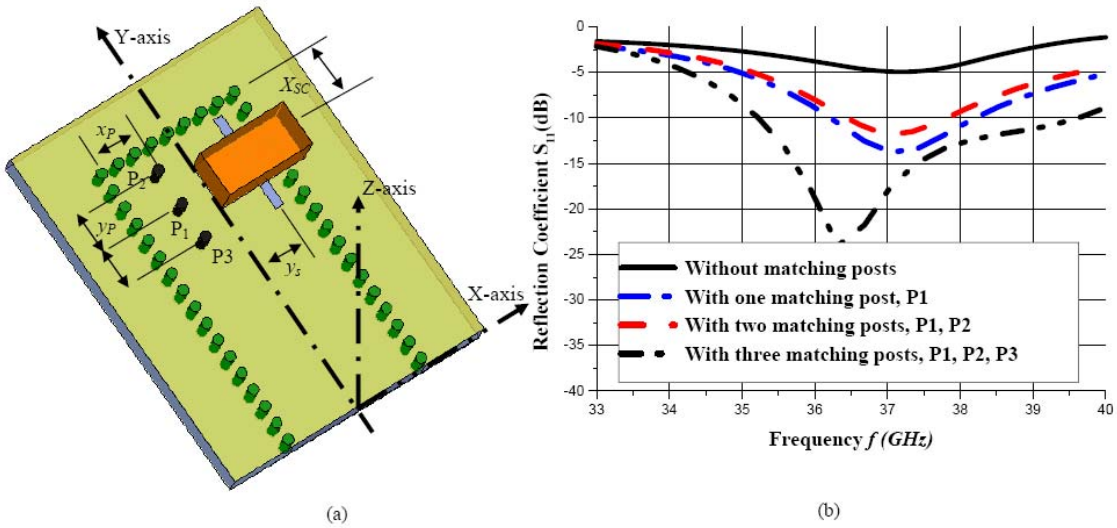

Figure 3.8 (a) The modified(matched) SIW fed RDRA using longitudinal slot orientation (*without MSL transition*), (b) The impact of using the matching circuit (metallic posts) on the reflection coefficient, S_{11}*(dB), the antenna parameters:* a_{SIW}*=4.80 mm,* d_{via}*=0.3302 mm,* S_{via} *=0.60 mm, the antenna parameters:* a_{RDRA}*=3.0mm,* d_{RDRA}*=1.50mm,* l_{Slot} *= 3.20 mm,* w_{Slot} *= 3.20 mm,* y_s*=1.50mm,* X_{SC}*=2.0mm,* x_p*=0.80mm, and* y_p*=1.20mm.*

The metallic posts, P1, P2 and P3 are positioned inside the SIW to minimize the reflections caused by the short circuit termination. The number of matching posts and their locations affect both the coupling (matching) and the impedance bandwidth ($S_{11} \leq$ *-10 dB*) as shown in Figure 3.8b. A very good coupling to the RDRA, which is less than *-20 dB* at *36.50 GHz*, and a wide impedance bandwidth of *4 GHz* are obtained when the three metallic posts are inserted inside the SIW at the positions described by x_P*= 0.80 mm*, and y_P*=1.20 mm*.

3.4 Internal Field Distribution and Radiation Pattern

Since both the internal field distribution and the radiation pattern at resonance are related, understanding of the internal field distribution leads to a good insight about the far field radiation pattern. The RDRA radiates in a manner similar to a magnetic dipole when excited in its fundamental mode [35]. The broadside radiation comes from the leakage of the internal field through the top and end of the RDRA. Therefore, examining the internal field and the far field radiation, one can confirm that the RDRA operates on its fundamental mode.

Based on the coordinate system and the RDRA structure in Figure 3.3a, the EM full-wave solver is used to study the internal and far radiated fields at the resonant frequency f_o. The RDRA used in the simulation setup has dimensions: a_{RDRA}*=3.0 mm*, d_{RDRA}*=1.50 mm*, and it is excited by a narrow slot with length of l_{Slot}*=3.20 mm* and a width of *wSlot=0.30 mm* cut onto the SIW broad wall of width a_{SIW}*=4.80 mm*, S_{via} *=0.60 mm*, and d_{via}*=0.3302mm*.Figure 3.9a, and Figure 3.9b shows the RDRA internal field distribution (vector plots) for the components, E_x and H_y, respectively for the antenna configuration in Figure 3.3b. The radiation pattern (gain) of the antenna in Figure 3.3 is shown in Figure 3.10 in two different planes *E* (XZ-plane) and *H* (YZ-plane) at the frequency *35.50 GHz*, respectively. It verifies that the RDRA radiates like a magnetic dipole oriented in X-direction (antenna in Figure 3.3a) and Y-direction (antenna in Figure 3.3b). Both antenna arrangements in Figure 3.3 almost shows the same radiation pattern (gain), especially in the co-polarized components and the boresight direction ($\theta=0^o$) which show a simulated boresight gains of *5.70 dB* and *5.51dB* for the antenna in Figure 3.3a and 3.3b, respectively. However, the antenna in Figure 3.3b shows a lower back radiation ($\theta=180^o$), of less than *-10 dB* compared to the antenna in Figure 3.3a. The latter presents a very low level of cross-polarized, with less than *-40 dB* close to the boresight direction compared to the former antenna in Figure 3.3b, which shows a cross-polarized radiated field level of less than *-20 dB*. Therefore, the proposed antenna designs in Figure 3.3 are suitable for linear polarized antenna applications.

The usefulness of the SIW as a low loss feeding structure that minimizes the conduction loss, which dominates at mm-wave band, was investigated by calculating the overall radiation efficiency over the operating frequency band. It was found that the simulated radiation efficiency is more than *97%* (the reflection loss at the port is ignored) as will discuss later in Section 3.5, which is quite high compared to the other planar feeding schemes described in Chapter 2. Also, the gain is almost stable over the same operating frequency band with a small variation of ± *0.50 dB* and maximum broadside gain of *5.19 dB*.

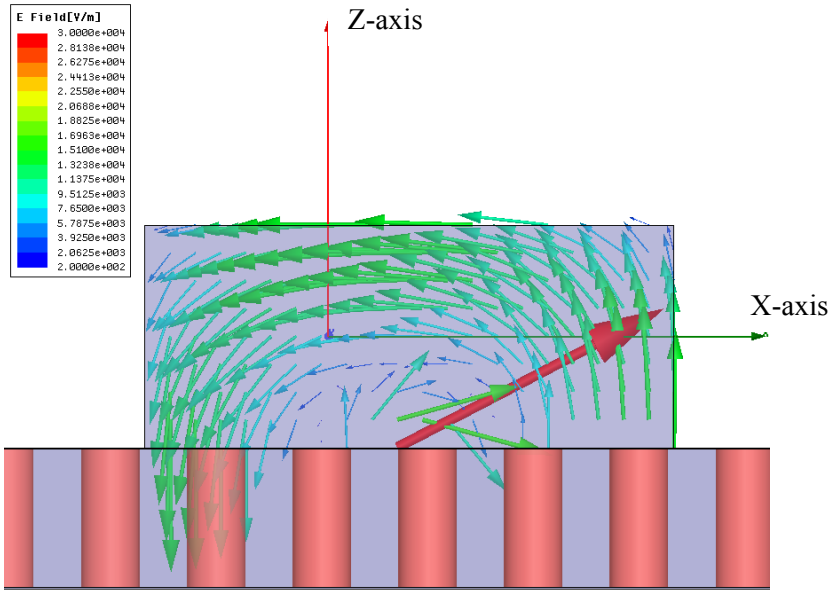

(a)

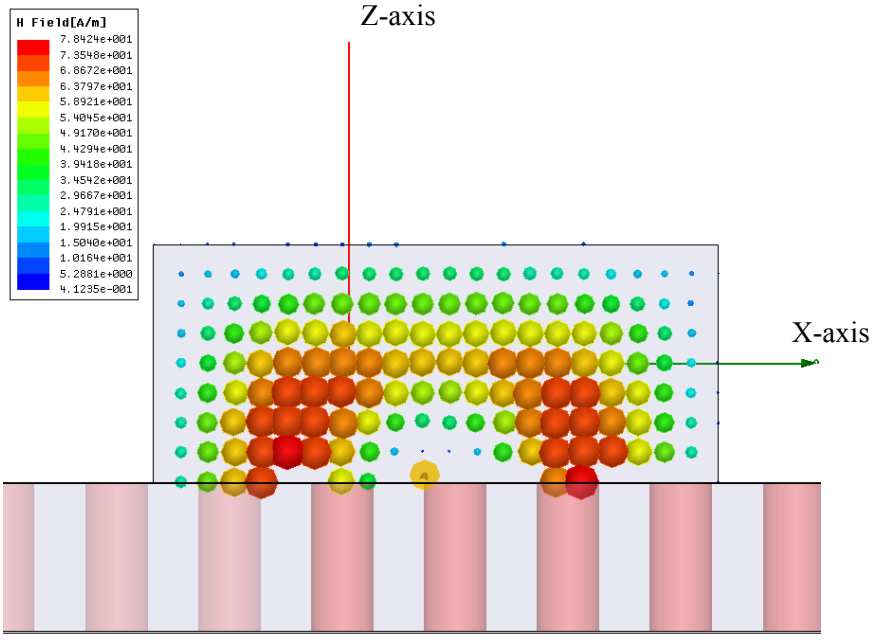

(b)

Figure 3.9 The internal field distributions of RDRA fundamental mode (vector plots) for the antenna in Figure 3.3b, (a) Electric field E_x (v/m), (b) Magnetic field H_y (A/m).

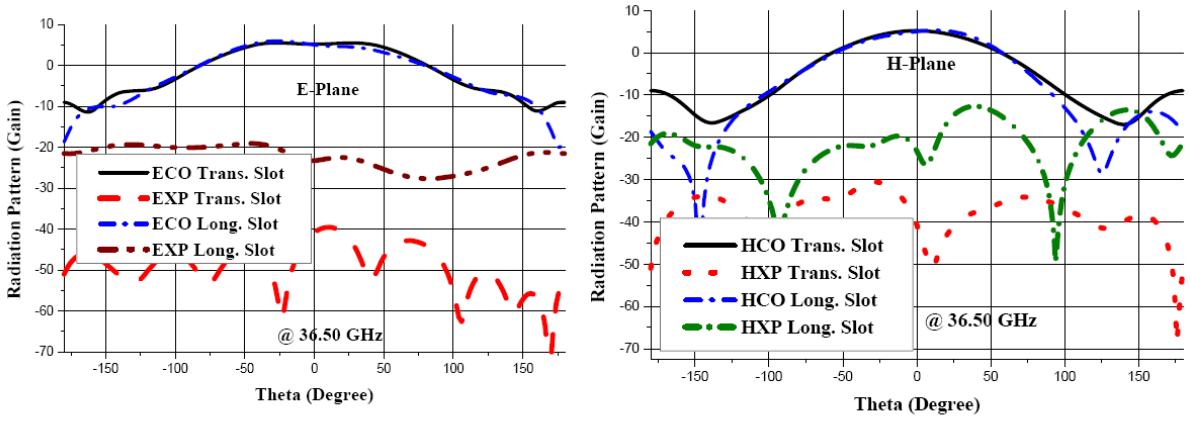

(a) (b)

Figure 3.10 The radiation pattern (gain) of SIW based-RDRA for the two slot configurations (*without MSL transition*) in Figure 3.3, (a) *E*-plane (co-polarized ECO, and cross-polarized EXP), (b) *H*-plane (co-polarized HCO, and cross-polarized HXP) at *35.50 GHz*. The *antenna parameters are:* a_{SIW}*=4.80 mm,* d_{via}*=0.3302 mm,* S_{via} *=0.60 mm,* a_{RDRA}*=3.0mm,* d_{RDRA}*=1.50mm,* l_{Slot} *= 3.20 mm,* w_{Slot} *= 3.20 mm,* y_s*=1.50mm,* X_{SC}*=2.0mm,* x_p*=0.80mm and* y_p*=1.20mm.*

3.5 Antenna Fabrication and Experimental Results

The fabrication and experimental measurements of the prototypes in Figure 3.3 is the culmination of the theoretical study of the SIW-DRA model and the extensive parameter characterization. The measured results also will confirm the validity of the theoretical model, and the accuracy of the design criteria presented in Sction 3.2. The fabrication tolerances and the experimental measurements at mm-wave frequency band may present unexpected results that require further investigations.

3.5.1 Antenna Fabrication Process

In this technology, the SIW-RDRA are fabricated using a simple fabrication technique, all of which are part of the same PCB assembly line/manufacturing process which will reduce the complexity and cost.The manufacturing of the RDRA antenna is done using a multi-step, multi-layer PCB manufacturing process. The fabricated structure consists of a three-layer PCB, with two dielectric layers comprising the SIW-fed layer, and DRA element(s), respectively. The following steps summarize the general fabrication process used:

1. The antenna performance and electrical requirements for the feeding SIW and the RDRA element(s) are identified by using the design model described in Section 3.2.
2. The SIW and RDRA element(s) are iteratively re-designed to match the electrical parameters of very low-cost dielectric substrates (bare PCBs) which are available from manufacturers such as Rogers, Arlon, Taconic, etc.

3. The result of (2) will be physical sizes, the metal layer requirements, the dielectric constant, and the loss tangent for at least two substrates (one for the SIW, one for RDRA), as shown in Figure 3.11a.
4. The SIW layer is manufactured by etching specific patterns, drilling the "via" holes between the two metal layers (through the dielectric), and plating them in a PCB standard process, as shown in Figure 3.11b.
5. A chemical bath which is available in the PCB industry is used to remove metal layer of the DR dielectric, as shown in Figure 3.11c.
6. The second layer is added to one side of the SIW and bonded with a low-loss thin bonding film. This is a standard process in the PCB fabrication, which is used when making multi-layer boards, as shown in Figure 3.11d.
7. A routing mechanism (involving a milling machine used by PCB manufacturers to cut slots or other 3D features in the substrates) is used to remove the material on the DRA layer, leaving only the areas that are needed for the antenna elements, as shown in Figure 3.11e.
8. Note that (1)–(3) are result of a particular software model that has already been developed and (4)–(7) are part of a new fabrication process. Each of the sets of steps (1)–(3) and (4)–(7), respectively, can be taken multiple numbers of times to create more complex circuitry.

The primary objective of the above process is to decrease the complexity and avoid the misalignment problem between the slot(s) and the RDRA element(s). Reducing the fabrication complexity will result in improvement in yields as well as a decrease in end-user cost. The designed antennas, SIW fed-RDRA, proposed in Section 3.2 were fabricated using the process described in Figure 3.11, and tested to validate the RDRA models and the newly proposed fabrication technique. The following Sections introduce the fabricated antenna prototypes along with the measurement results compared to the simulated ones. The designed SIW-fed RDRA were fabricated from standard low loss and low cost material substrates. First, the bottom layer which will contain the SIW feed is fabricated from a double-sided *31-mil* Roger / 5870 Duroid material $\varepsilon_{rs} = 2.33$. The copper plating is *0.5 oz (17μm)* which is the minimal necessary to allow thin metallization and allow for good slot coupling.

The planar features are etched and the substrate is drilled through and plated to create the SIW feed. Next, a one–sided *50 mil* Roger *RT/6010* substrate $\varepsilon_{rd} = 10.2$, with a *0.5 oz* copper metallization is bonded using *2-mil* thermally stabilized bonding film $\varepsilon_r = 2.34$. This is an irradiated polyolefin co-polymer developed to achieve excellent bond strength with low- flow characteristics and low temperature bonding. The top metal layer is etched away leaving a complete sheet of dielectric material. The majority of the area is milled away and what is left, is the RDRA block which remains bonded to the underlying layer. The only downside of this process is that there is a *2-mil* substrate between the top metal layer of the SIW feed and bottom of the RDRA which can affect the performance. The optimized and final designed physical parameters are listed in Table 3.2.

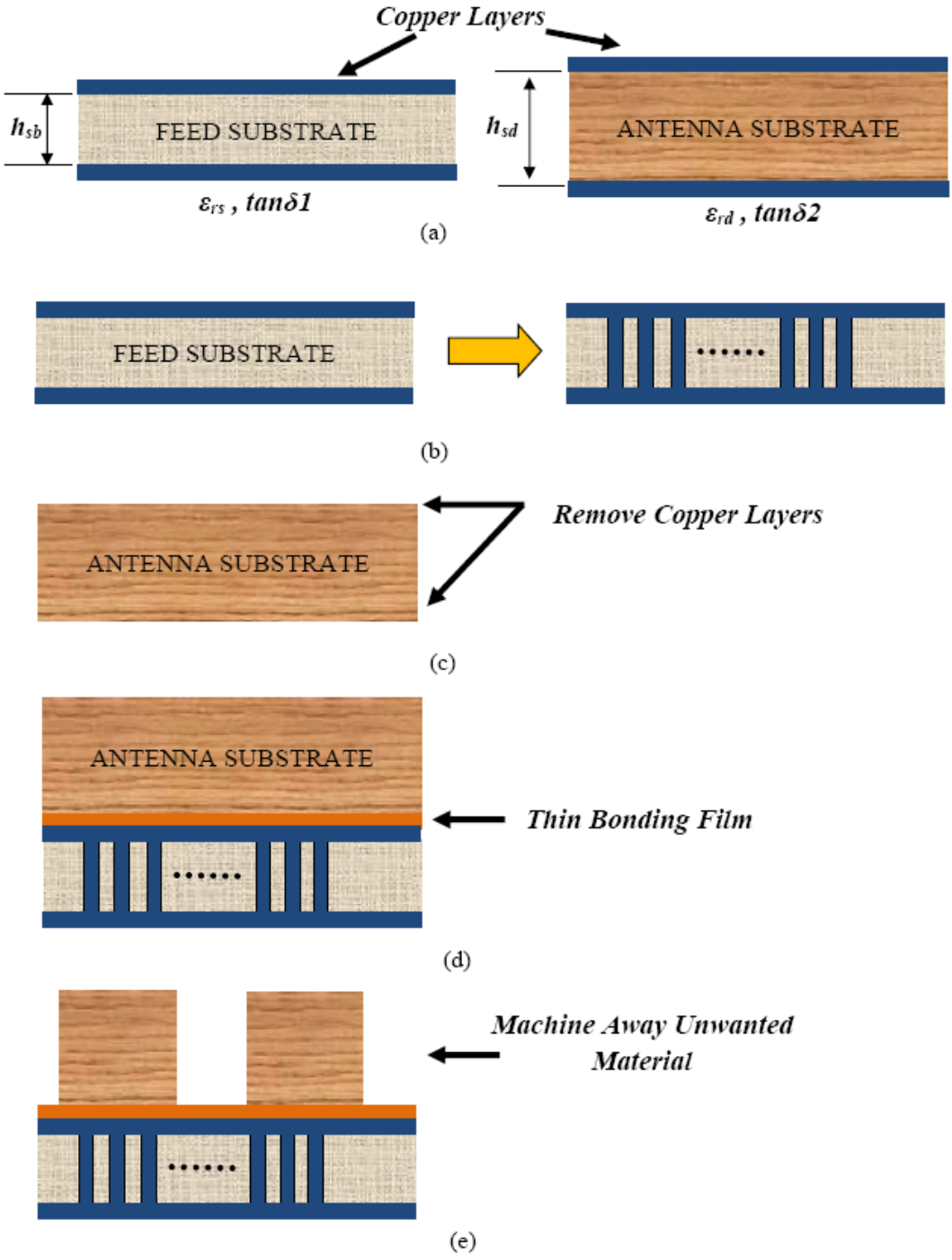

Figure 3.11 The fabrication process of SIW based-RDRA.

Table 3.2 Physical designed SIW-DRA single element parameters (*dim. in mm*) [164].

Rectangular Dielectric resonator antenna (RDRA) substrate $\varepsilon_{rd}=10.20$		
a_{RDRA}	3.0	
d_{RDRA}	1.50	
h_{sd}	1.27 mm	
Substrate integrated waveguide (SIW) $\varepsilon_{rs}=2.33$		
h_{sb}	0.7874	
a_{SIW}	4.80	
s_{via}	0.60	
d_{via}	0.3302	
SIW-based RDRA		
	Transverse slot	Longitudinal slot
l_{slot}	3.20	
w_{slot}	0.30	
x_{SC}	3.50	4.50
y_s	0	1.50

3.5.2 Antenna Measurements

Measurements were performed to determine the antenna reflection coefficient $S_{11}(dB)$ and the radiation pattern (gain) in both the *E*-plane and *H*-plane of the antenna. The obtained results show a good agreement between the simulated and the measured result taking into account the manufacturing tolerances as well as the edge connector (power launcher) misalignment and inaccurate contact to the MSL. The fabricated antenna prototypes are shown in Figure 3.12 and Figure 3.13 for both antenna configurations, respectively.

a. Antenna Reflection coefficient

The antenna reflection coefficient $S_{11}(dB)$ of the fabricated SIW- fed RDRA prototypes in Figures 3.12 and 3.13 were obtained experimentally and compared with the simulated results over the frequency range of *30-40 GHz* as provided in Figure 3.14 for both slot orientations. Figure 3.14a (for the antenna prototype in Figure 3.12) shows a good agreement between the measured and simulated results

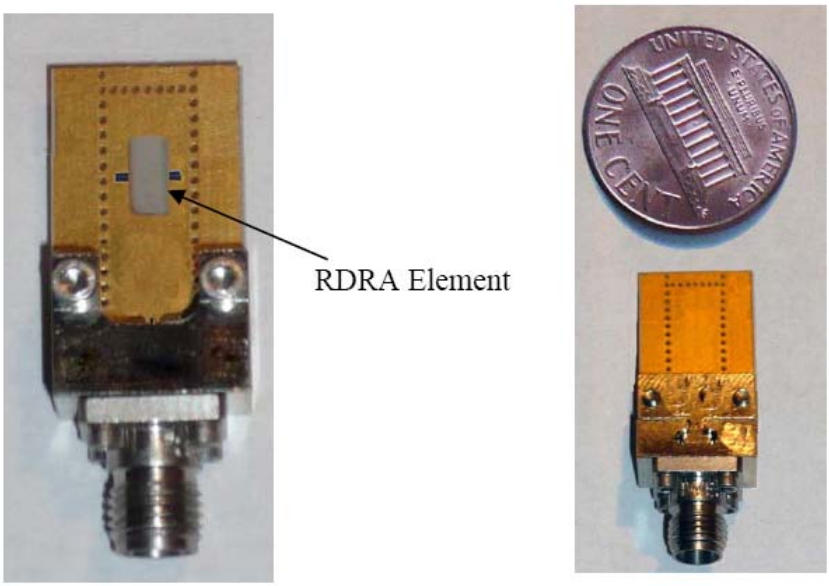

(a) Front view (b) Rear view

Figure 3.12 The fabricated prototype of SIW based- RDRA using vertical polarized (transverse) slot configuration [164].

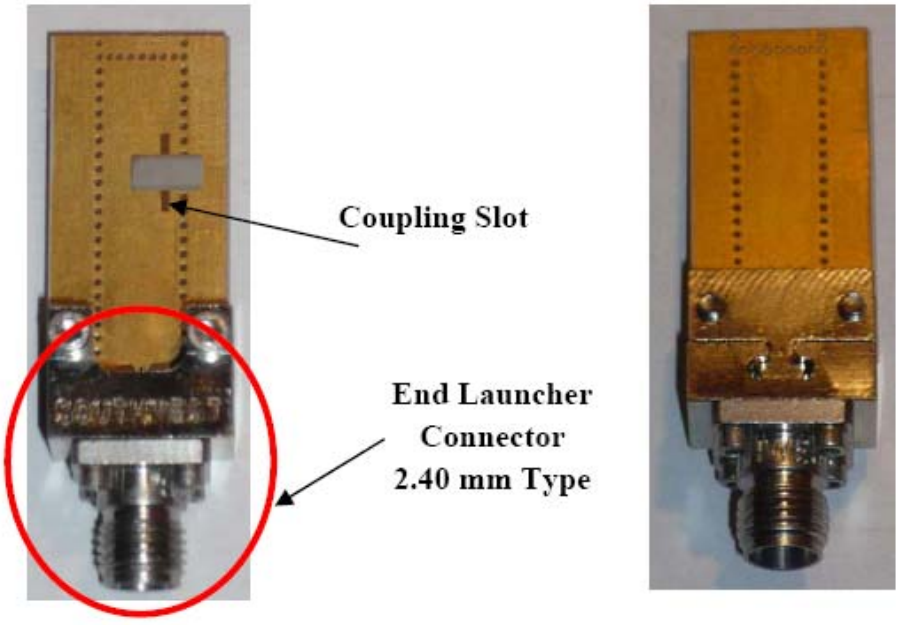

(a) Front view (b) Rear view

Figure 3.13 The fabricated prototype of SIW based-RDRA using horizontal polarized (longitudinal) slot configuration [164].

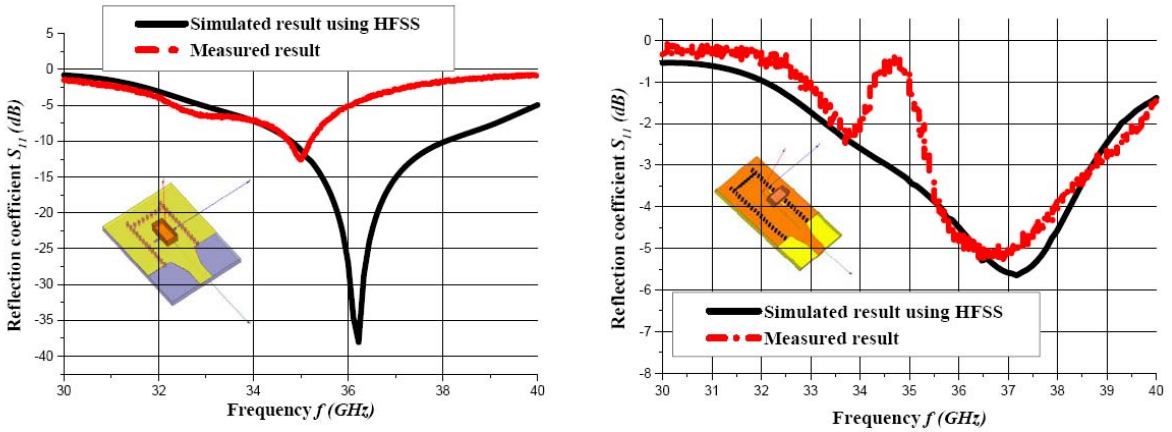

Figure 3.14 The simulated and measured reflection coefficient S_{11}(dB) of SIW-based RDRA[164] (a) Antenna prototype in Figure 3.12, (b) Antenna prototype in Figure 3.13.

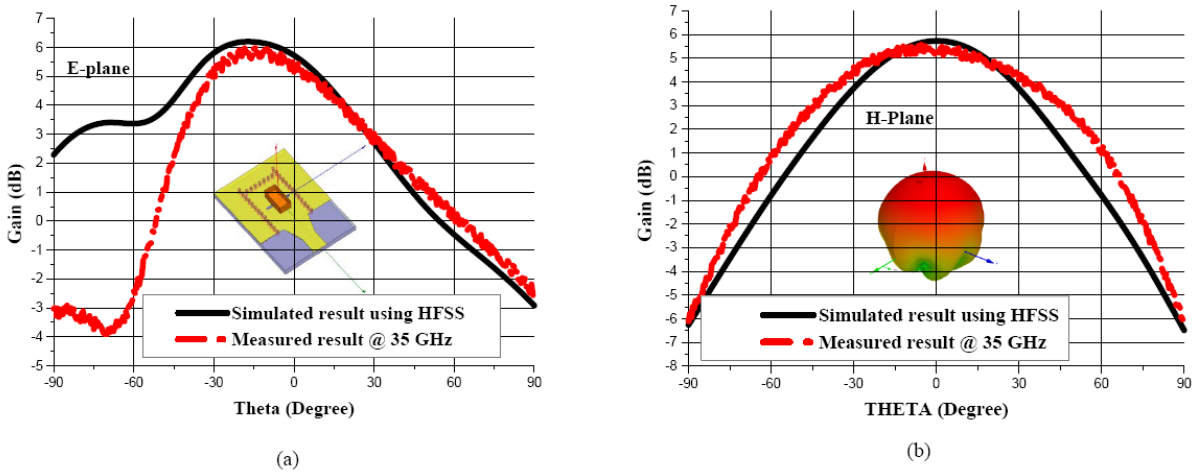

Figure 3.15 The simulated and measured radiation pattern of SIW based-RDRA (antenna prototype in Figure 3.12) *@ f= 35 GHz* [164] (a) *E*-plane (YZ plane). (b) *H*- plane (XZ-plane).

The simulated resonance frequency, which occurs at *>36 GHz,* is shifted to *~35 GHz* primarily due to the fabrication tolerances and the addition of bonding material between the feed and the DRA layers. This novel multi-layer fabrication method affects the coupling to the RDRA. Furthermore, the reduction in bandwidth is attributable to the connector contact and the alignment issues.

The measured minimum reflection coefficient, which is *-12.61 dB*, occurs at *35 GHz*. On the other hand, the measured reflection coefficient S_{11}*(dB)* (for the antenna prototype in Figure 3.13) in Figure 3.14b agrees well with the simulated result. It resonates at *37.28 GHz*, where input resistance seen at the antenna input is $14\,\Omega$ (referenced to the MSL). Therefore, a matching circuit is needed for the antenna in Figure 3.13 to enhance the coupling between the coupling slot and the RDRA element. Table 3.3 summarizes the antennas reflection coefficient main characteristics.

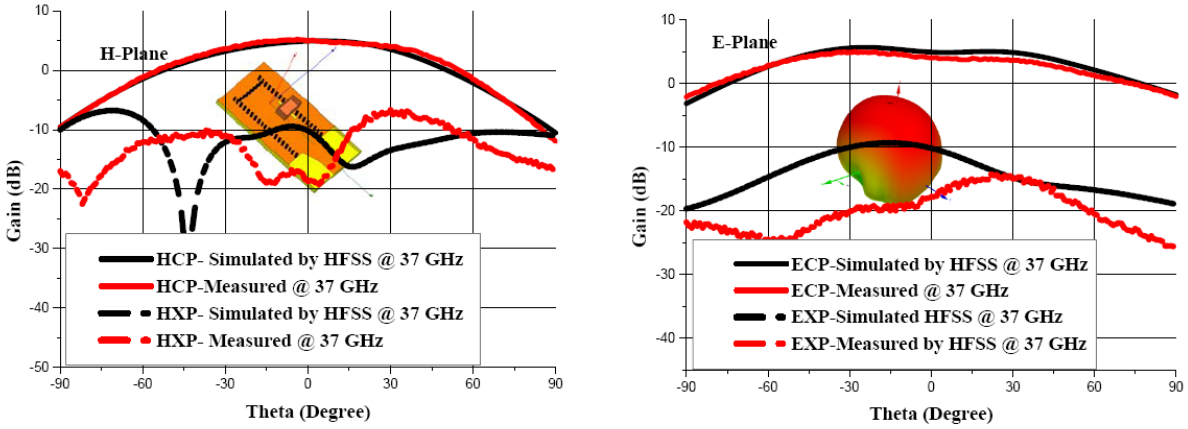

(a) (b)

Figure 3.16 The simulated and measured radiation pattern of SIW based-RDRA (antenna prototype in Figure 3.13) *@ f= 35 GHz* [164] (a) *H*-plane (YZ-plane), *(b) E*- plane (XZ-plane).

b. Antenna Radiation pattern (gain) and efficiency

The radiation pattern (gain) measurements for the two antenna prototypes in Figures 3.12 and 3.13 were carried out in an anechoic chamber at frequencies *35 GHz and 37 GHz* within scanning angle range of $-90^{\circ} \leq \theta \leq 90^{\circ}$ in two orthogonal planes.

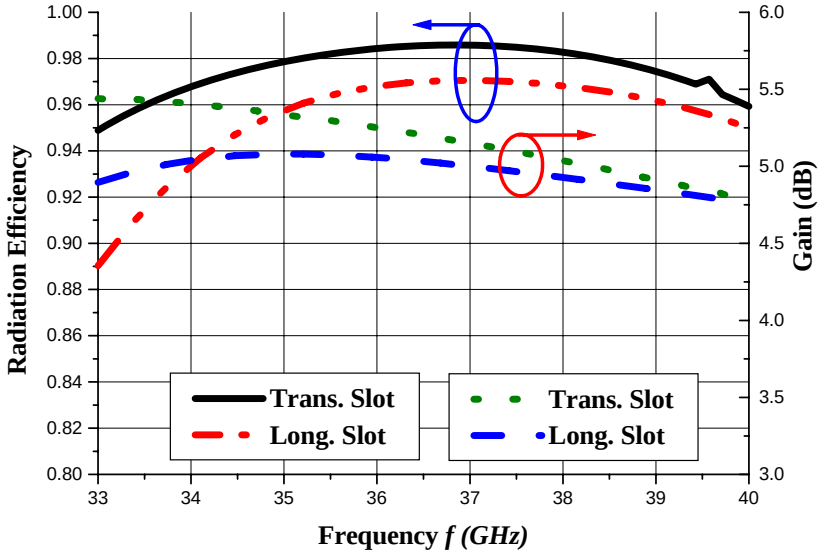

Figure 3.17 The radiation efficiency/gain (dB) variation against the frequency of SIW based-RDRA (*with MSL transition*) in Figure. 3.3, (The *antenna parameters are:* a_{SIW}*=4.80 mm,* d_{via}*=0.3302 mm,* S_{via} *=0.60 mm,* a_{RDRA}*=3.0 mm,* d_{RDRA}*=1.50 mm,* l_{Slot} *= 3.20 mm,* w_{Slot} *= 3.20 mm,* y_s*=1.50 mm,* X_{SC}*=2.0 mm,* x_p*=0.80 mm and* y_p*=1.20 mm.*

Figures 3.15, and 3.16 show the measured and simulated radiation patterns (gain) for the proposed antenna prototypes, respectively. Both the simulated and the measured results are in a very good agreement, showing a boresight ($\theta=0^{\circ}$) gain of *5.26 dB* (antenna prototype in Figure 3.12) and *4.75 dB* (antenna prototype in Figure 3.13). Also, the co-polarized *(ECP, HCP)* and the cross polarized *(EXP, HXP)* radiated fields of the proposed prototype in Figure 3.13 at *37 GHz* in the two planes, *E (*XZ-plane*)* and *H (*YZ-plane*)*, were measured as shown in Figure 3.16. It shows a very low level cross-polarized radiation of less than *-19 dB* in the boresight direction. Thanks to the SIW guiding structure, the proposed SIW fed RDRA prototypes in Figures 3.12, and 3.13 present very high overall efficiencies which are more than *95%* (simulated), and a flat gain (simulated), as shown in Figure 3.17, over the operating frequency bandwidth. Furthermore, the SIW-DRA antenna is compact and small in size which makes it quite suitable for portable applications. Table 3.3 summarizes the main antenna radiation pattern (gain) and efficiency characteristics. The difference between the simulated and measured gain is caused by the edge connector (power launcher) used for experimental verification, which add more loss to the antenna structure (~ 0.9 dB) in addition to the dielectric loss. These issues are not included in the simulated results.

Table 3.3 SIW- based RDRA basic characteristics [164].

Antenna Characteristics		Simulation using HFSS	Measurement
Horizontal polarized (Transverse) slot	f_o @ minimum reflection coefficient) (GHz)	*36.22*	*35*
	Δ% (-10 dB reflection coefficient bandwidth) (GHz)	*8.60*	
	S_{11} *(dB)@* f_o	*-38.06*	*-12.61*
	G_{max} *(dB)* @ f_o	*5.70*	*5.26*
	Antenna Size (mm^2)	*10×13.60*	
Vertical polarized (Longitudinal) slot	f_o @ minimum reflection coefficient (GHz)	*37.0*	*37.10*
	Δ% (-10 dB reflection coefficient bandwidth)	A matching circuit is required	
	S_{11} *(dB)@* f_o	*-5.65*	*-5.26*
	G_{max} *(dB)* @ f_o	*5.51*	*4.75*
	Antenna size (mm^2)	9×17	

Chapter 4

Substrate Integrated Waveguide (SIW) Based Dielectric Resonator Antennas (DRAs) Arrays: Modeling, Design and Fabrication

4.1 Introduction

Antenna arrays are needed for many applications that require high gain and a narrow directive beam. The array antenna's ability to perform beam scanning is required as well. A number of RDRA elements similar to the one described in Section 3.2 can be arranged to form arrays for boresight radiation, where the SIW is used as a low-loss feeding scheme. There are three different antenna array arrangements that can be formed, the SIW series-fed RDRA, the SIW-corporate (parallel) fed RDRA, and the hybrid-fed RDRA arrays. In the SIW series-fed array, the RDRA elements are fed sequentially by the same power magnitude and in-phase via a single SIW-transmission line, whereas, the SIW-power splitter is needed to split the power equally and phase among the RDRA elements in the SIW-corporate fed array. The SIW-hybrid feed arrangement, which is formed by combining both the series-fed and corporate-fed configurations, is used to form two-dimensional (2D) planar antenna arrays.

In this chapter, different antenna topologies, the SIW series-fed DRA, the SIW corporate (parallel)-fed DRA, and the SIW hybrid-fed DRA will be presented, and their performance will be investigated. Moreover, a simple analysis that uses a developed Transmission Line (T.L.) circuit model and basic antenna array theory will be introduced to simplify, accelerate the design process and provide more physical insight into the proposed antenna arrays. This approach is quite simple, efficient and faster than EM full-wave solvers, such as HFSS.

4.2 Substrate Integrated Waveguide (SIW) Series-Fed Rectangular Dielectric Resonator Antenna (RDRA) Array

Figures 4.1a and 4.1b show a general layout of the SIW series fed-RDRA linear array. The SIW-DRA single element designed in Section 3.2 is used as a building block for the N-element array in two different slot configurations, the horizontal polarized (transverse) slot, and the vertical polarized (longitudinal) slot, respectively.

The slots are excited by the SIW's fundamental mode, TE_{10}, to couple the energy to the DRA elements. The primary antenna array parameter is the RDRA position, which is defined by: (1) the distance between the centers of the neighboring elements, D, and (2) the distance between the last element and the SIW short circuited end, X_S. The distance, D, between any two neighboring elements, is a vital parameter that defines the phase difference between the two successive elements, which in turn affects all the radiation characteristics of the antenna. The distance from the last element to the SIW short circuited end, X_S, not only affects the phase difference, but also, changes the antenna input impedance. In other words, by using the appropriate values for both D and X_S, the antenna elements can be placed in certain positions to give a prescribed phase distribution, such as a co-phase or linear

phase excitation. For example, choosing the distances, D and X_S, in Figure 4.1a is equal to λ_g and $\frac{\lambda_g}{2}$, respectively, and provides a co-phase SIW-fed DRA array excitation.

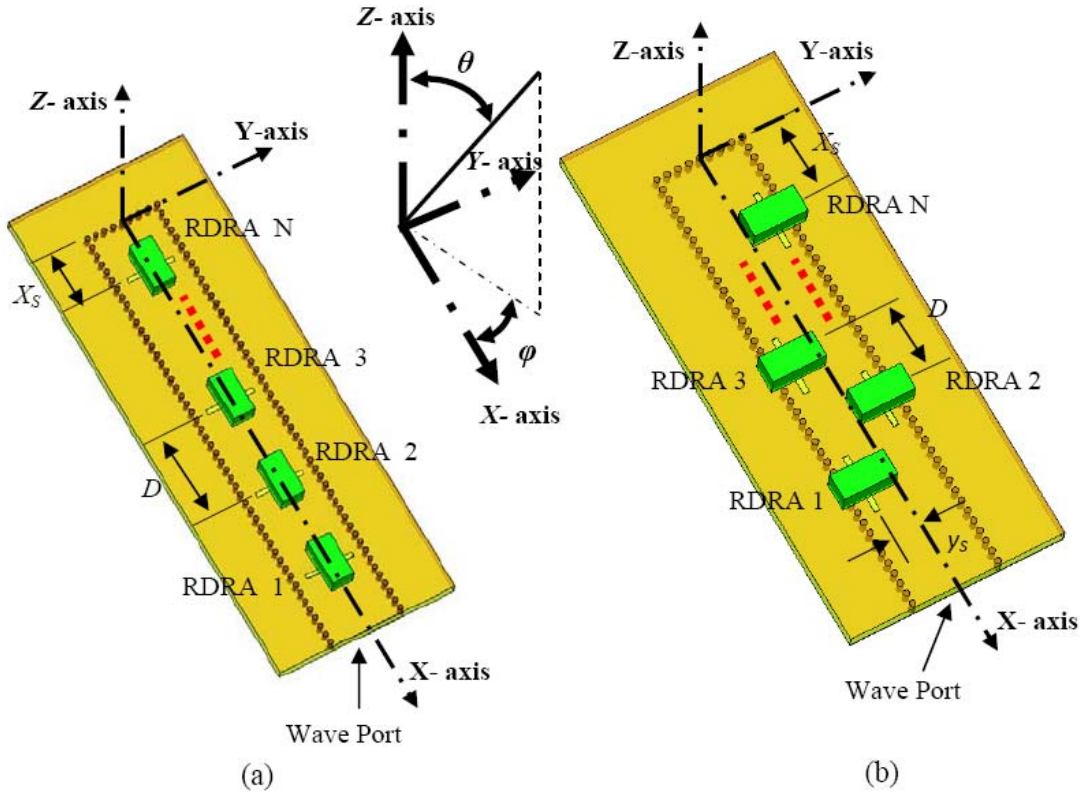

Figure 4.1 The schematic layout of the SIW series-fed DRA linear arrays[168] (without SIW-MSL transition) (a) a horizontal polarized (transverse) slot, and (b) a vertical polarized (longitudinal) slot.

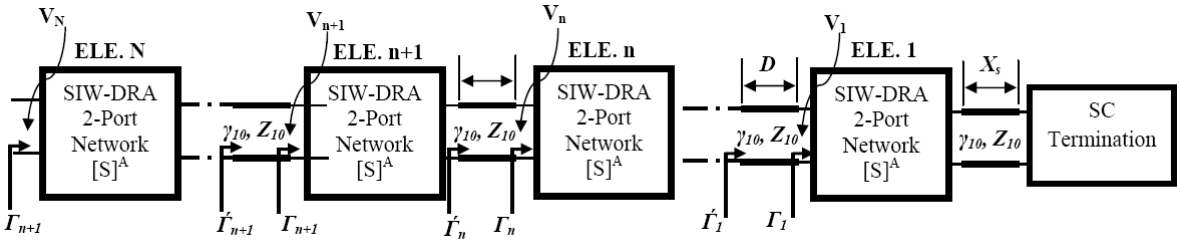

Figure 4.2 The SIW-DRA T.L. circuit model of N-elements SIW-DRA array [168].

The structure in Figure 4.1 is a Standing Wave (SW) linear array. The slots are positioned, where the maximum axial (parallel to the X-axis) SW currents occur. Therefore, the excitation slot fields are set in phase $(\Delta\phi = k_x D = \frac{2\pi}{\lambda_g}\lambda_g = 2\pi)$. On the other hand, for the antenna in Figure 4.1b, the RDRA elements are excited by longitudinal slots, cut on the broad wall of the SIW. The slots are mutually

positioned at the opposite sides of the waveguide centerline, providing an additional phase shift of π between any two neighboring slot fields. The spacing between two the successive slots and the short circuit position are $D = \frac{\lambda_g}{2}$ and $X_S = \frac{\lambda_g}{4}$, respectively. In this case, the slots are positioned such that the maximum standing-wave currents are parallel to the Y-axis. The RDRA elements are co-phased, because the excitation phase difference is $\Delta\phi = k_x D + \pi = 2\pi$.

4.2.1 SIW-RDRA Array Transmission Line (T.L.) Circuit Model and Parametric Study

To simplify the design and optimization of the antenna arrays in Figure 4.1, and to gain more physical insight, a simple T.L. circuit is developed. The proposed T.L. circuit model does not take the inter-element mutual coupling into account (the coupling effect will be studied in Section 4.2.2). Afterwards, the circuit model is used to optimize the antenna parameters, D and X_S, (by a parametric study) for the optimum overall antenna reflection coefficient $S_{11}(dB)$ and the radiation pattern (gain).

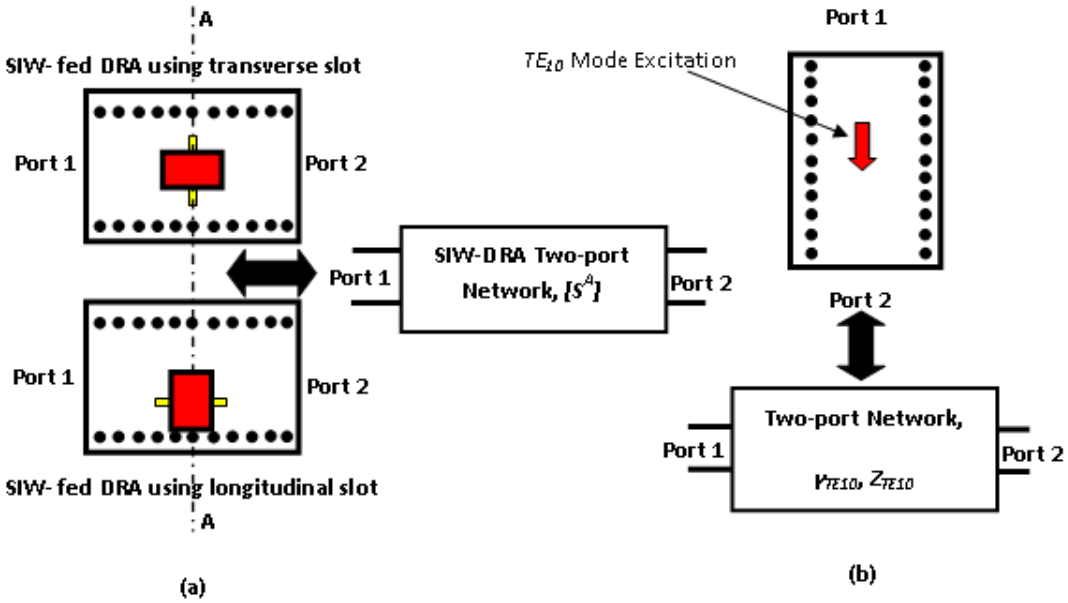

Figure 4.3 The SIW-DRA 2-port network model of both transverse slot arrangement and longitudinal slot arrangements [168] (b) T.L. circuit model of an SIW segment excited by the waveguide fundamental mode TE_{10} mode.

The proposed T.L. model in Figure 4.2 consists of the SIW-DRA 2 port-network blocks connected by a T.L. model of the interconnecting SIW segments to model N-element cascaded linear array. The SIW-DRA physical structure in Figure 4.3a is modeled by its S-parameters matrix $[S]^A$ in Figure 4.3b, and the SIW physical segment excited by the TE_{10} mode is modeled by the mode propagation characteristics in a straight T.L. with a length L_{SIW}, which is the same as the physical length of the SIW. The mode propagation characteristics are defined by the wave impedance, $Z_{10}(ohms)$, and the

propagation constant $\gamma_{10}(\omega)=\alpha_{TE10}+j\beta_{TE10}$, as shown in Figure 4.3b, where $\alpha_{TE10}(Np/m)$ and $\beta_{TE10}(rad/m)$ are the SIW fundamental mode attenuation and phase constants, respectively.

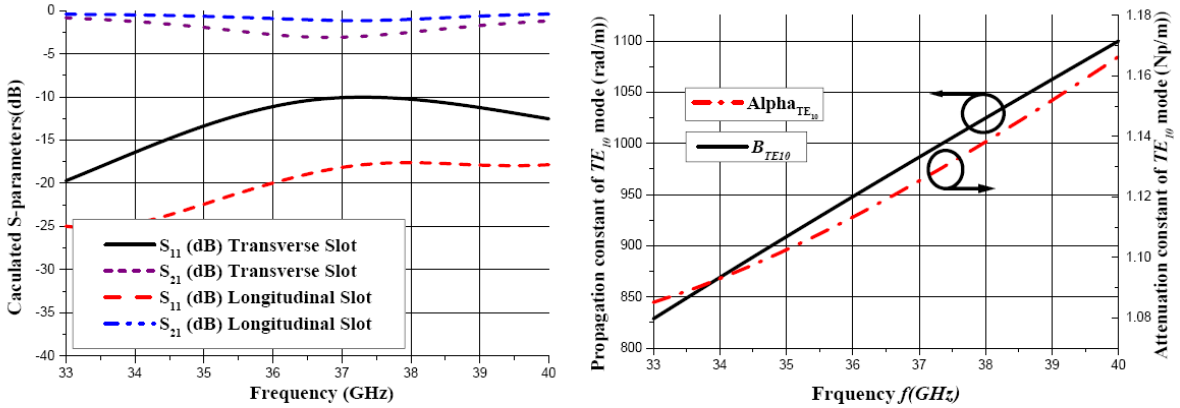

(a) (b)

Figure 4.4 (a) The calculated S-matrix of the SIW-RDRA 2 port-network, (b) The calculated propagation constant (*rad/m*), and attenuation factor (*Np/m*) of the SIW fundamental mode.

The full-wave solver used to calculate the SIW-DRA 2 port-network referred to the plane *A-A'*, $[S(\omega)]^A$ ($\omega=2f\pi$: is the radian frequency *rad/sec)*, and the phase constant and attenuation of the SIW fundamental mode, as shown in Figure 4.4a and 4.4b, respectively. The proposed T.L. model in Figure 4.2 can also be used in its simplest form, *N=1*, to model the SIW-DRA single element described in Chapter 3, whose reflection coefficient is given by:

$$\Gamma_1 = S_{11}(\omega) = S_{11}^A(\omega) + \frac{-S_{12}^A(\omega)S_{21}^A(\omega)e^{-2\gamma_{10}(\omega)X_S}}{1+S_{22}^A(\omega)e^{e^{-2\gamma_{10}(\omega)X_S}}} \tag{4.1}$$

Similarly, a *N*-element SIW-DRA array is modeled as N-cascaded SIW-DRA 2-port-network blocks, connected by a SIW-T.L of length, *D*, as shown in Figure 4.2. The overall antenna reflection coefficient is calculated as follows:

$$\Gamma_n'(\omega) = \Gamma_n(\omega)e^{-2\gamma_{10}(\omega)D} \tag{4.2}$$

$$\Gamma_{n+1}(\omega) = S_{11}^A(\omega) + \frac{\Gamma_n'(\omega)S_{12}^A(\omega)S_{21}^A(\omega)}{1-S_{22}^A(\omega)\Gamma_n'(\omega)} \tag{4.3}$$

Based on the proposed T.L. circuit model in Figure 4.2 and simple S-matrix manipulations [165], the following equation can be proved.

$$\frac{V_n}{V_{n+1}} = \left[\frac{1+\Gamma_n(\omega)}{1+\Gamma_{n+1}(\omega)}\right]\left[\frac{e^{-\gamma_{10}(\omega)D}\,S_{21}^A(\omega)}{1-S_{22}^A(\omega)\Gamma_n'}\right] \tag{4.4}$$

$n=1,2,3,....N$

The proposed T.L. circuit model is used to determine the overall antenna reflection coefficient and the antenna radiation pattern (gain). For model completeness, the overall antenna array gain is formulated by using the pattern multiplication principle with the SIW-DRA single element radiation

pattern and the excitation voltage at each antenna input circuit element. The required excitation coefficients for the array factor are calculated by the proposed T.L. circuit model. The antenna array factor (assuming the array formed along the X-axis direction) is given by:

$$AF(\theta,\phi) = V_N \sum_{n=N}^{n=1} A_n e^{j(k_o \sin(\theta))(X_n \cos(\phi)+Y_n \sin(\phi))} \quad (4.5)$$

$A_n = \frac{V_n}{V_N}$: is the antenna excitation voltage coefficient.

$k_o = 2\pi f_o$: is the free space wave number (rad/m).

V_N = is the antenna element N excitation voltage (reference voltage) (volt).

$X_n = (N-n)D$.

$Y_n = 0$: for the SIW-DRA array architecture in Figure 4.1a.

$Y_n = Sy_s$: for the SIW-DRA array architecture in Figure 4.1b.

$S=0$: when n is odd.

$S=2$: when n is even.

θ, and φ : are the coordinate system angles defined in Figure 4.1.

Due to the loading effect, caused by the antenna element(s) to the SIW T.L., the antenna array parameters, X_S and D might deviate from their assigned values as described in Section 4.2. Therefore, a detailed parametric study should be conducted to analyze the effect of these parameters on the overall antenna performance. The proposed T.L. circuit model is used to perform this study and to optimize the parameters of the SIW-DRA linear array in Figure 4.1a, and 4.1b. The circuit model is considered to be a simple and fast method, compared with the CAD software, such as the HFSS.

A parametric study is conducted on a four-element linear antenna array within the frequency range of *33-40 GHz*. Not only the phase difference among the excitation electromagnetic (EM) fields to the antenna elements are defined, but also the effect of the overall antenna reflection coefficient, S_{11} *(dB),* is described. For brevity, the impact of X_S on S_{11} *(dB)* and the impact of D on the radiation pattern (gain) are described.

a. Short circuit position : X_S

To verify the proposed T.L. circuit model, a simple example, the SIW-DRA single ($N=1$) element, was studied. The reflection coefficient is calculated and compared with that of full-wave solver result, as shown in Figure 4.5, for different values in the vicinity of $X_S = \frac{\lambda_g}{2}$ (for the transverse slot configuration, in Figure 4.1a), and $X_S = \frac{3\lambda_g}{4}$ (for the longitudinal slot configuration, in Figure 4.1b).

The proposed T.L. circuit model is in a good agreement with the full-wave solver, HFSS, at $X_S = 3.5$ *mm* (Figure 4.5a), and $X_S = 4.5$ *mm* (Figure 4.5b). A similar study was performed on the array in Figure 4.1for four elements ($N=4$). This study was conducted by the proposed T.L. circuit model for different short circuit positions, X_S, at the same inter-element distance, D, as shown in Figure 4.6. The short circuit position, X_S, acts as a matching stub (first degree of freedom) for the antenna input impedance, and it shifts the RDRA resonance frequency (frequency tuning).

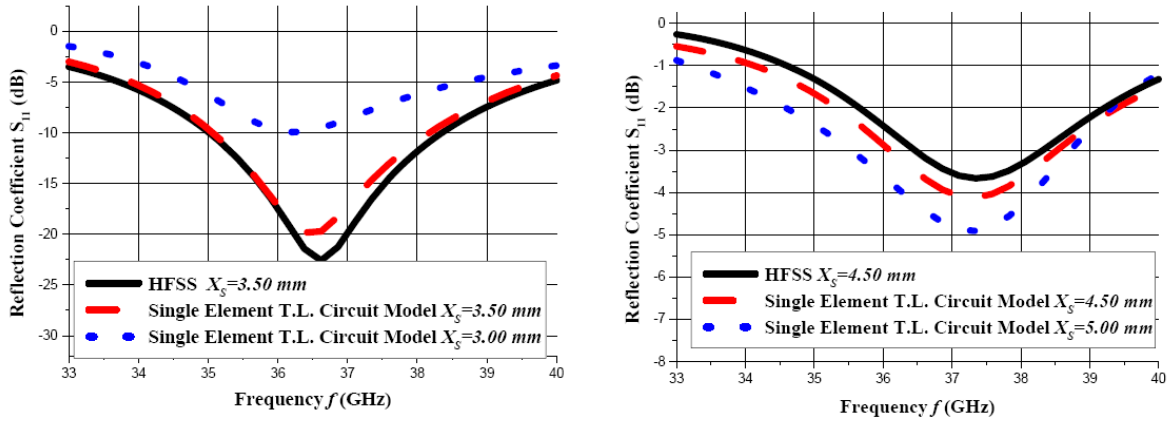

Figure 4.5 The calculated reflection coefficient S_{11} *(dB)* of the SIW fed RDRA single element in Figure 3.3 by using the proposed T.L. circuit model in Figure 4.2 for $N=1$, and full-wave solver for different short circuit positions, X_S, (a) transverse slot and (b) longitudinal slot.

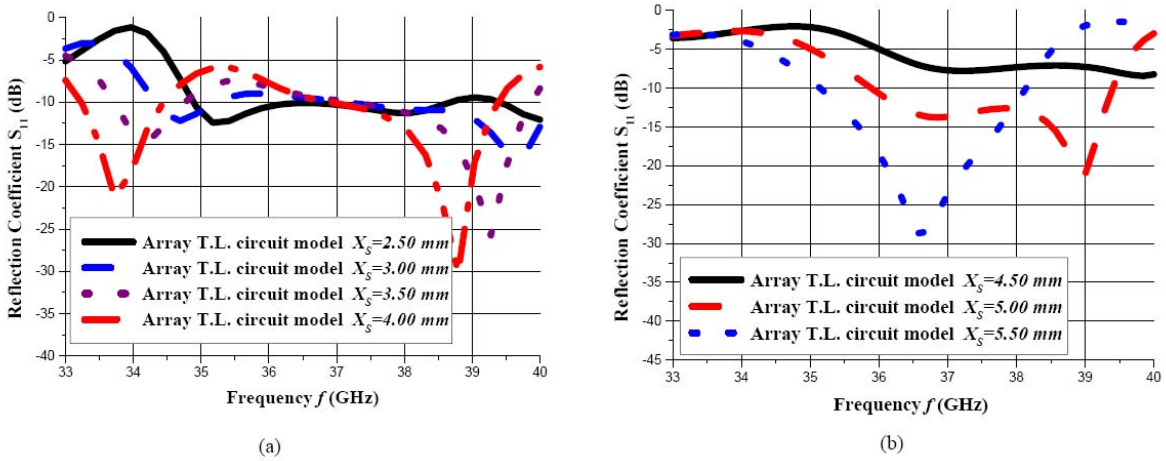

Figure 4.6 The calculated reflection coefficient (by using the proposed T.L. circuit model), S_{11} *(dB)*, of the SIW series-fed RDRA array (Four elements) [168], for different short circuit positions X_S (a) the transverse in Figure. 4.1a, for $D=7.60$ *mm*, and (b) longitudinal slot in Figure. 4.1b, for $D=3.50$ *mm.*

b. Array inter-element distance: D

The antenna inter-element distance, D (second degree of freedom), affects both the antenna input impedance as well as the amplitude and the phase differences for the antenna array element excitation voltages, as illustrated by Table 4.1. As indicated by equation (4.5), the excitation voltage coefficients, A_n, controls the antenna array radiation pattern (gain). Therefore, the proposed circuit model is used to study the impact of changing the inter-element distance, D, of a SIW-DRA array, comprised of four elements on the total gain (dB).

Table 4.1 Voltage excitation coefficients A_n of $N=4$ elements SIW series-fed DRA array [168].

D(mm)	Excitation Voltages Coefficients A_n					
	A_3		A_2		A_1	
	Mag.	Phase (Degree)	Mag.	Phase (Degree)	Mag.	Phase (Degree)
	Transverse Slot , X_s=3.50 mm and f_o =34 GHz					
6.50	0.49	49	0.62	150	0.82	171
7.00	1.04	59	1.42	86	1.48	92
7.50	0.98	-1	0.96	-5	0.95	-11
8.0	0.94	-30	1.01	-53	1.12	-86
	Longitudinal Slot, X_s=4.50 mm and f_o = 38 GHz					
3.0	0.46	152	0.53	129	1.01	36
3.50	1.001	10	1.01	7	1.02	3
4.0	1.06	-36	1.01	-31	0.81	-20
4.50	0.69	-92	1.20	-135	0.98	-146

Table 4.1 summarizes this study for both slot configurations in Figure 4.1a, 4.1b at the frequencies of *34 GHz* and *38 GHz*, respectively. As the distance *D* approaches a specific value that corresponds approximately to λ_g=*7.60* mm, and $\frac{\lambda_g}{2} \approx 3.50\ mm$, respectively, the antenna elements are almost co-phased and excited equally. Consequently, their radiated far field is added constructively to form a broadside radiation of maximum gains, *12.80 dB and 12.62 dB*, as demonstrated in Figure 4.7. Conversely, as the distance *D* deviates from these critical values, the antenna array elements become out of phase and are not excited equally. Therefore, the antenna array radiation pattern (maximum gain) deteriorates. To study the radiation bandwidth of the antenna arrays in Figure 4.1 and their frequency-scanning characteristics, the radiation pattern is simulated over the frequency range of *33-40 GHz*, as shown in Figure 4.8. It is noticed that as the frequency changes from *35.21 GHz to 40.0 GHz* and the main beam of the antenna in Figure 4.1a is steered by *15*$^\circ$ with a maximum gain variation of *0.66 dB* as shown in Figure 4.8a. Alternatively, the main beam of the antenna array in Figure 4.1b is steered by *12*$^\circ$ with a maximum gain variation of *2.6 dB* over the frequency band *34.47-40 GHz.*

4.2.2 SIW Series-Fed RDRA Array Inter-elements Mutual Coupling

The single (fundamental) mode T.L. circuit model in Figure 4.2 is valid, as long as the discontinuities (antenna, short circuit, junctions, and other types of discontinuities) are sufficiently apart, so that the higher order mode interactions are negligible. Therefore, it is pivotal to study the

mutual coupling and its effect on the proposed T.L. model validity, particularly when the antenna elements are close.

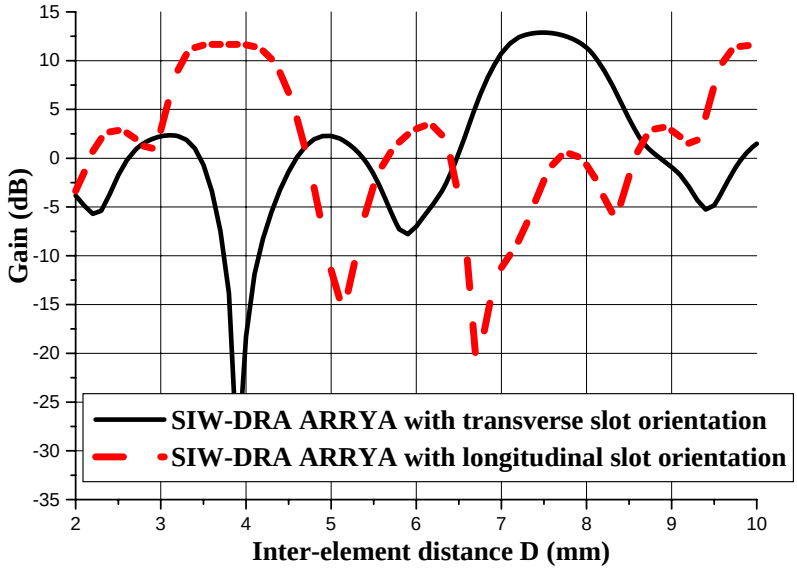

Figure 4.7 The broadside gain (dB) calculated by the proposed T.L. circuit model [168](the SIW-MSL transition is not included) of the SIW series fed-DRA array (*N=4*) for both antenna array configurations in Figure 4.12.

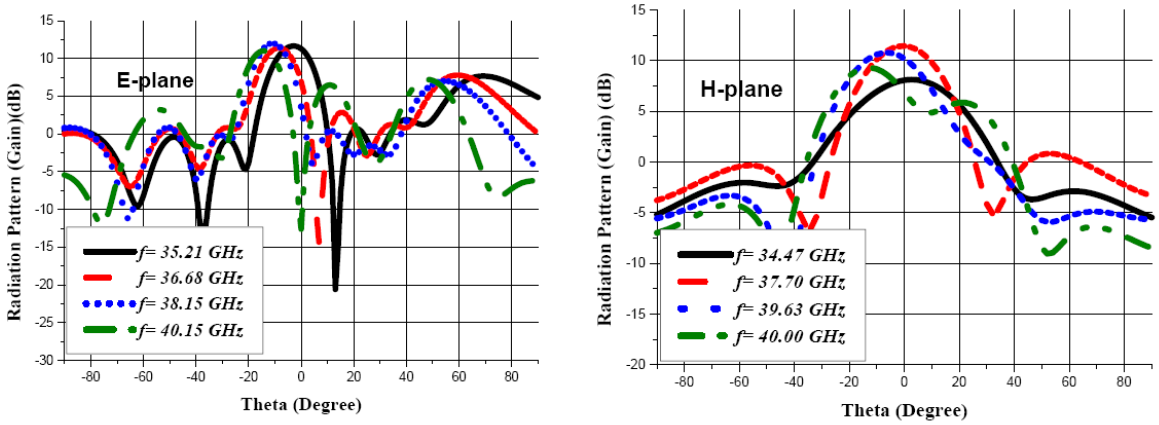

(a) (b)

Figure 4.8 The calculated radiation pattern (gain) (dB) (by the proposed T.L. circuit model) of the SIW series-fed RDRA array (four elements) studied at different frequencies[168] (SIW-MSL transition is included) (a) transverse slots array in Figure 4.1a for *D=7.60 mm* (*E*-plane) , and (b) the longitudinal slots array shown in Figure 4.1b for *D=3.50 mm* (*H*-plane).

The mutual coupling between the adjacent antenna elements is due to two mechanisms: the internal coupling (caused by the excitation of the higher order modes at the SIW-slot interface

discontinuities), and the exterior coupling (caused by the electromagnetic space wave interactions). Figure 4.8 reflects the geometries for studying the mutual coupling between a two antenna elements for both array configurations. It consists of two identical SIW-fed RDRA elements set close to each other, and then excited independently with waveguide ports, P1, and P2, to study both the *E*-coupling (Figure 4.9a) and *H*-coupling (Figure 4.9b). To study the exterior mutual coupling, a row of copper-plated vias (SIW-SC) was inserted between the two RDRA elements to block any internal coupling between the two ports. In other words, the geometries in Figure 4.9a, b, and 4.9b allow for a space wave only to be coupled between the two ports (antenna exterior mutual coupling).

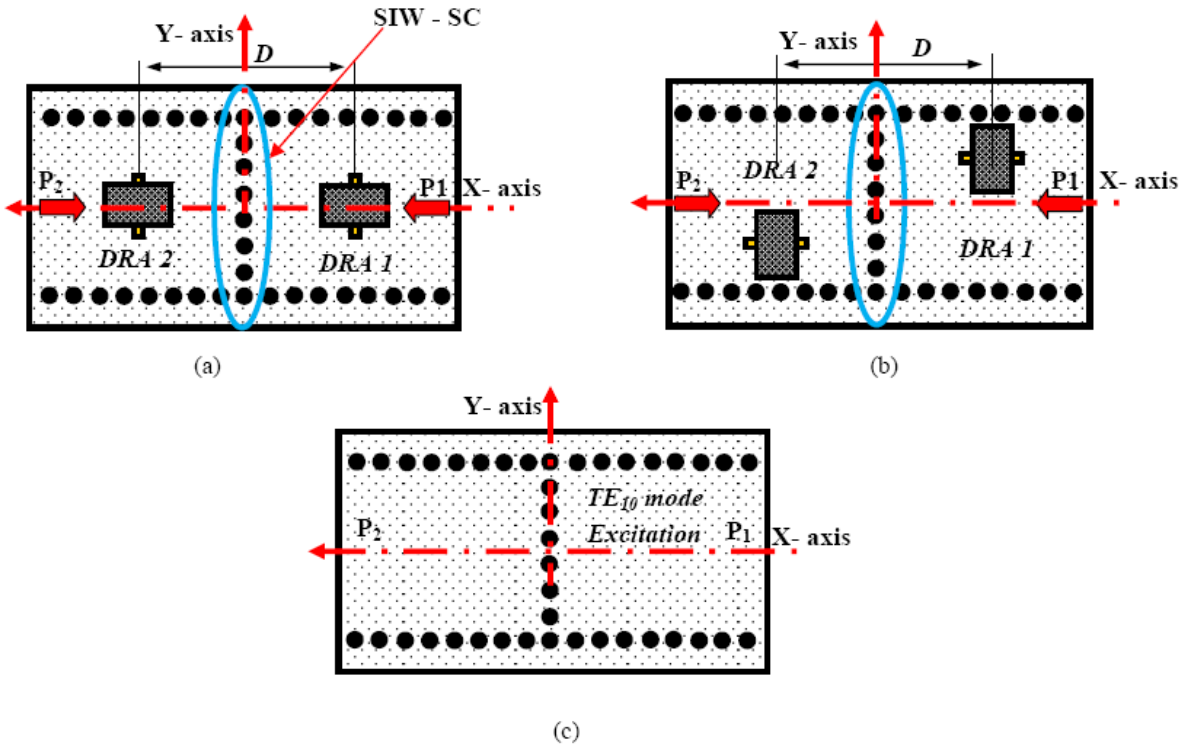

Figure 4.9 The physical model used to study the mutual coupling between RDRA elements fed by SIW in the SIW series-fed RDRA array layouts [168] (a) *E*-coupling, and (b) *H*-coupling, (c) SIW-SIW back to back.

The distance between the two RDRA elements are kept at $D = \lambda_g \approx 7.60$ *mm*, and $D = \frac{\lambda_g}{2} \approx 3.50$ *mm* to maintain the far field co-phase radiation as presented in Figure 4.1a, and 4.1b, respectively. The calculated (simulated) mutual coupling demonstrates that the mutual coupling in both the *E*-plane (E-coupling) and the *H*-plane (H-coupling) is less than *-15 dB*, and *-40 dB*, respectively over the operating frequency bandwidth, as shown in Figure 4.10a. Therefore, the mutual coupling between the array elements is considered to be weak, particularly in the *H*-plane. As a reference, the mutual coupling of the SIW-SIW back to back model in Figure 4.9c, is calculated to be less than - *40 dB* as shown in Figure 4.10a. The calculated mutual coupling verifies that the SIW structure has a negligible leakage loss.

Another study is performed to investigate the total mutual coupling between the antenna elements by using the setup in Figure 4.9a, and 4.9b, except that the SIW-SC is removed. Then, it is modeled by the T.L. circuit model shown in Figure 4.2 (for $N=2$, without the short circuited termination). The coupling (insertion loss), S_{21} *(dB)*, from P1 to P2 is calculated by the T.L. model and the full-wave solver. Figure 4.10b shows the results for this study for different D, for both antenna arrangements at the frequencies *36 GHz* and *37.50 GHz*, respectively.

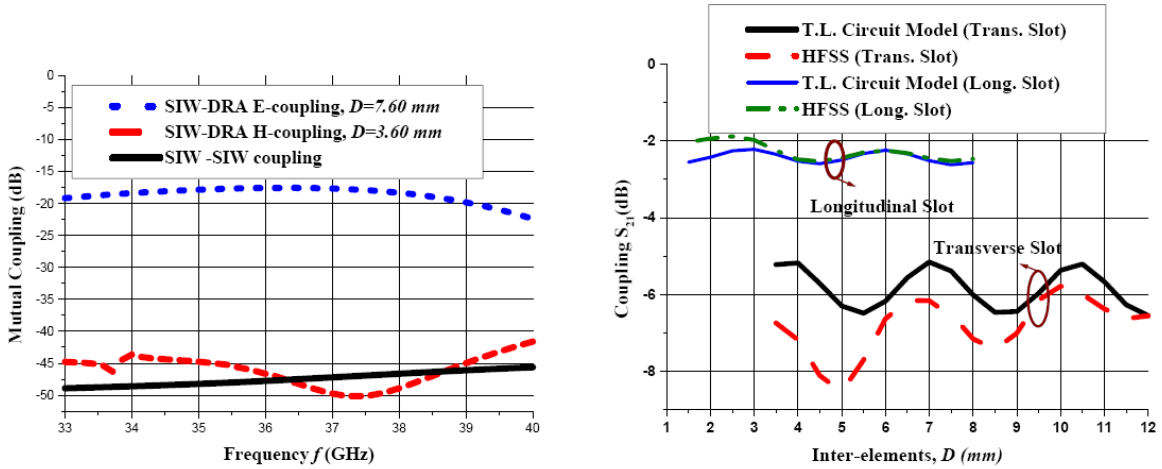

(a) (b)

Figure 4.10 The calculated mutual coupling (dB) between the RDRA elements fed by SIW in the SIW series-fed RDRA array layouts (a)Exterior coupling[168](with the SIW-SC), (b) The overall mutual coupling (exterior and internal) (without SIW-SC).

As the distance D increases, the full-wave solver result converges to that of the T.L. model, indicating that the mutual coupling, due to the higher order modes and radiation, decreases. Conversely, as the elements become closer, the two results diverge, and the aforementioned mutual coupling increases. However, the effect of internal coupling effect appears at $D=7.60$ *mm* (in transverse slot configuration), which might cause some discrepancies between the T.L. model and the measured results. Alternatively, this effect is negligible in longitudinal slot configuration. The effect of mutual coupling on the measured antenna performance will discuss in Section 4.5.

The performance of the antenna arrays are also numerically verified by the EM full-wave solver and the results are compared to these obtained using the proposed T.L. circuit model. The antenna arrays are simulated within the frequency band *33-40 GHz*. Figure 4.11 shows the reflection coefficient, and it is noticed that the T.L. model deviates from that of the EM full-wave solver, especially in Figure 4.11a, where there is a stronger mutual coupling. Alternatively, a minor deviation is noticed in Figure 4.11b. This deviation is attributed to the discrete nature of the SIW structure that affects the Short Circuit (SC) performance (magnitude and phase), T.L. lengths, and the mutual coupling between any two adjacent antenna elements, which caused by the excitation of higher order mode at the SIW-slot interfaces. All these issues are handled efficiently and are taken into account by the full-wave solver. However, the proposed T.L. circuit model is still valid, and it can easily estimate the resonance behavior of the antenna arrays.

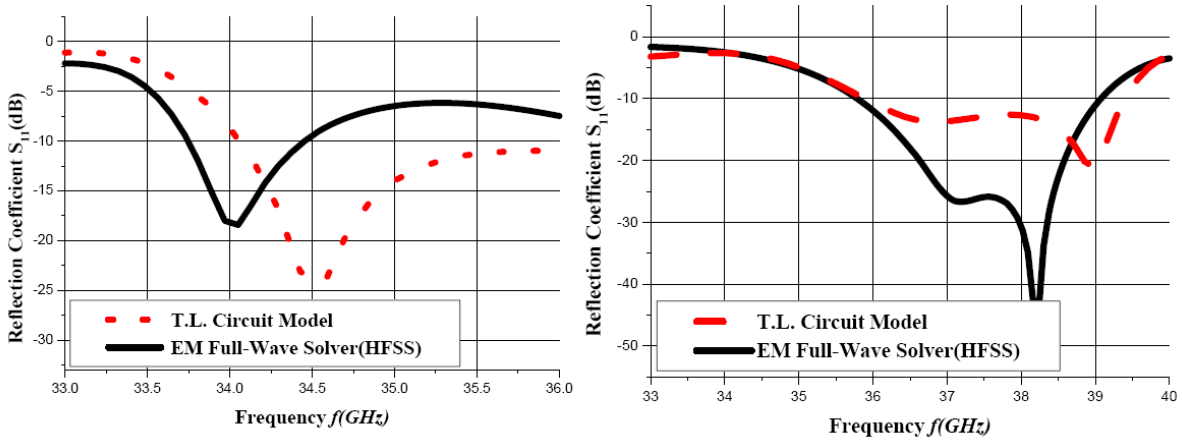

Figure 4.11 The calculated reflection coefficient $S_{11}(dB)$ of the SIW series-fed DRA($N=4$ elements) using both the proposed T.L. circuit model and EM full-wave solver (the SIW-MSL transition is not included) (a)using transverse slot, $D=7.60mm$, $X_S=2.50\ mm$, (b) using longitudinal slot, $D=3.50mm$, $X_S=4.50\ mm$, $y_S=1.50mm$.

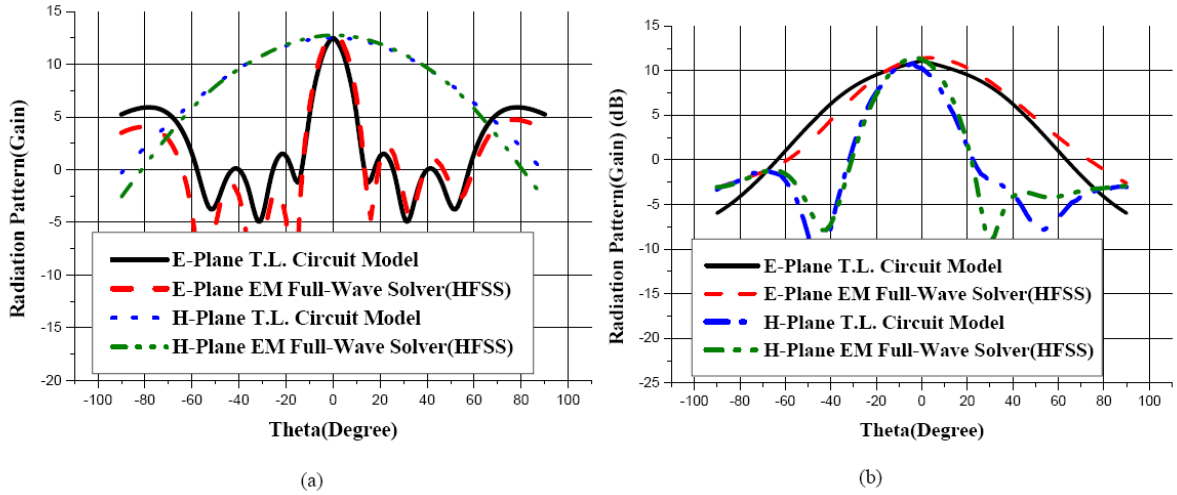

Figure 4.12 The calculated radiation pattern (gain) of the SIW series-fed DRA (4-elements) using both the proposed T.L. circuit model (the SIW-MSL transition is not included) and EM full-wave solver (the SIW-MSL transition is not included), (a) using transverse slot@ *34 GHz*, $D=7.60mm$, $X_S=2.50\ mm$, (b) using longitudinal slot@ *38 GHz*, $D=3.50mm$, $X_S=2.50\ mm$, $y_S=1.50mm$.

A very good agreement is observed in the radiation pattern (gain) between the proposed model and the full-wave solver, especially in the boresight radiation, as shown in Figure 4.12. The antenna array in Figure 4.1a shows a boresight gain of *12.80 dB* (calculated by the T.L. model) /*12.75 dB* (calculated by the full-wave solver), as shown in Figure 4.12a. However, the antenna configuration in Figure 4.1b shows a simulated gain of *11.68 dB* (calculated by the T.L. model) /*11.39 dB* (calculated by full-wave solver), as shown in Figure 4.12b. This gain difference between two simulated results is

attributed to the SIW-MSL transition loss *(~0.20 dB*), which is not included in the T.L. model in Figure 4.2.

Of all the antenna parameters that characterize the mm-wave antenna arrays, the overall radiation efficiency is highly affected by the feeding structures. Therefore, one of the primary goals of this research is to propose a novel and appropriate feeding scheme for mm-wave applications and to verify its performance. The simulated results demonstrate a stable gain of more than *11dB*, and high radiation efficiency of more than *93%*. Figure 4.13 denotes the calculated gain (*dB*) and the radiation efficiency for the proposed SIW-DRA array (*N=4*) over the operating impedance bandwidth. The antenna array shown in Figure 4.1b shows a wider gain/radiation efficiency bandwidth than the antenna in Figure 4.1a.

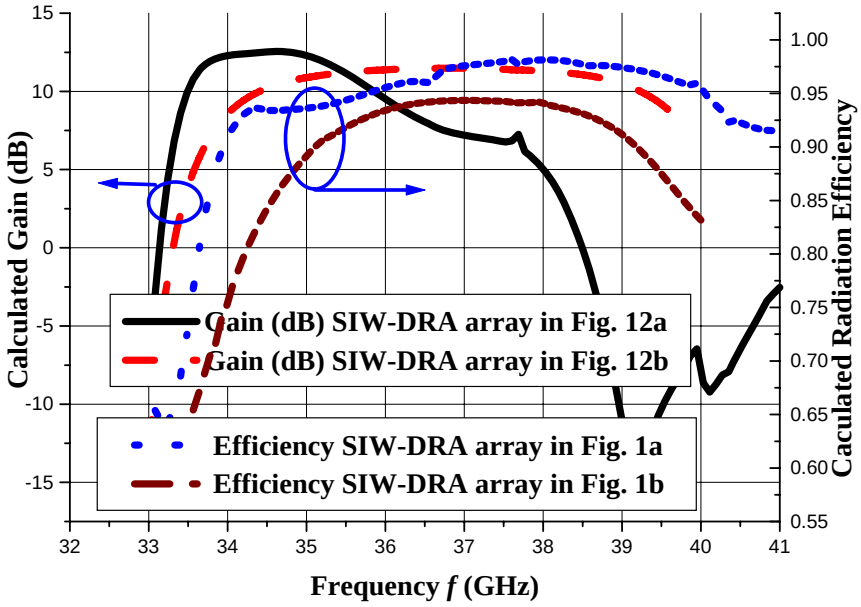

Figure 4.13 The calculated antenna gain (*dB*), and the radiation efficiency of the SIW series-fed RDRA arrays (*N=4*) [168], in Figure 4.1.

Table 4.2 Modeling and design algorithm of the SIW series-fed DRA array[168].

1. Design Specifications

- The operating frequency range is chosen.
- Substrate materials for SIW and DRA (dielectric constants, thickness…), ε_{rs}, ε_{rd}, h_{sb}, h_{sd}, f are chosen.

2. SIW-DRA Single Element Modeling and Design, Figure 3.3

- SIW parameters, a_{SIW}, s, *and* d_{via}, are modeled.
- DRA parameters, a_{DRA} *and* d_{DRA}, are modeled.
- SW-slot dimensions, L_{Slot} *and* W_{Slot}, are modeled and optimized.

3. SIW- DRA Array Modeling (by using the proposed T.L. circuit model), and Design

- S-parameters of SIW-DRA single element 2 port-network are evaluated by the EM full-wave solver (HFSS) at *A-A'* reference plane, shown in Figure 4.2.
- Constructing SIW-DRA array T.L. circuit model described in Section 4.2.1. It is based on cascading *N*-elements of the SIW-DRA 2 port network-model, and SIW T.L. model as in Figures 4.2 and 4.3. The T.L. circuit model uses equations (4.1)-(4.5), to calculate the SIW-DRA array's reflection coefficient, $S_{11}(dB)$, and radiation pattern (gain).
- The SIW array parameters, X_S and D, are optimized using the proposed T.L. circuit model, where their initial values are chosen based on the standing wave (SW) array concept presented in Section 4.2.7.

4.3 Substrate Integrated Waveguide (SIW) Corporate (Parallel)-Fed Rectangular Dielectric Resonator Antenna (RDRA) Arrays

The SIW corporate-feed network is characterized by a single input line branched into several secondary stages of transmission lines able to deliver a uniform signal to each radiating element of

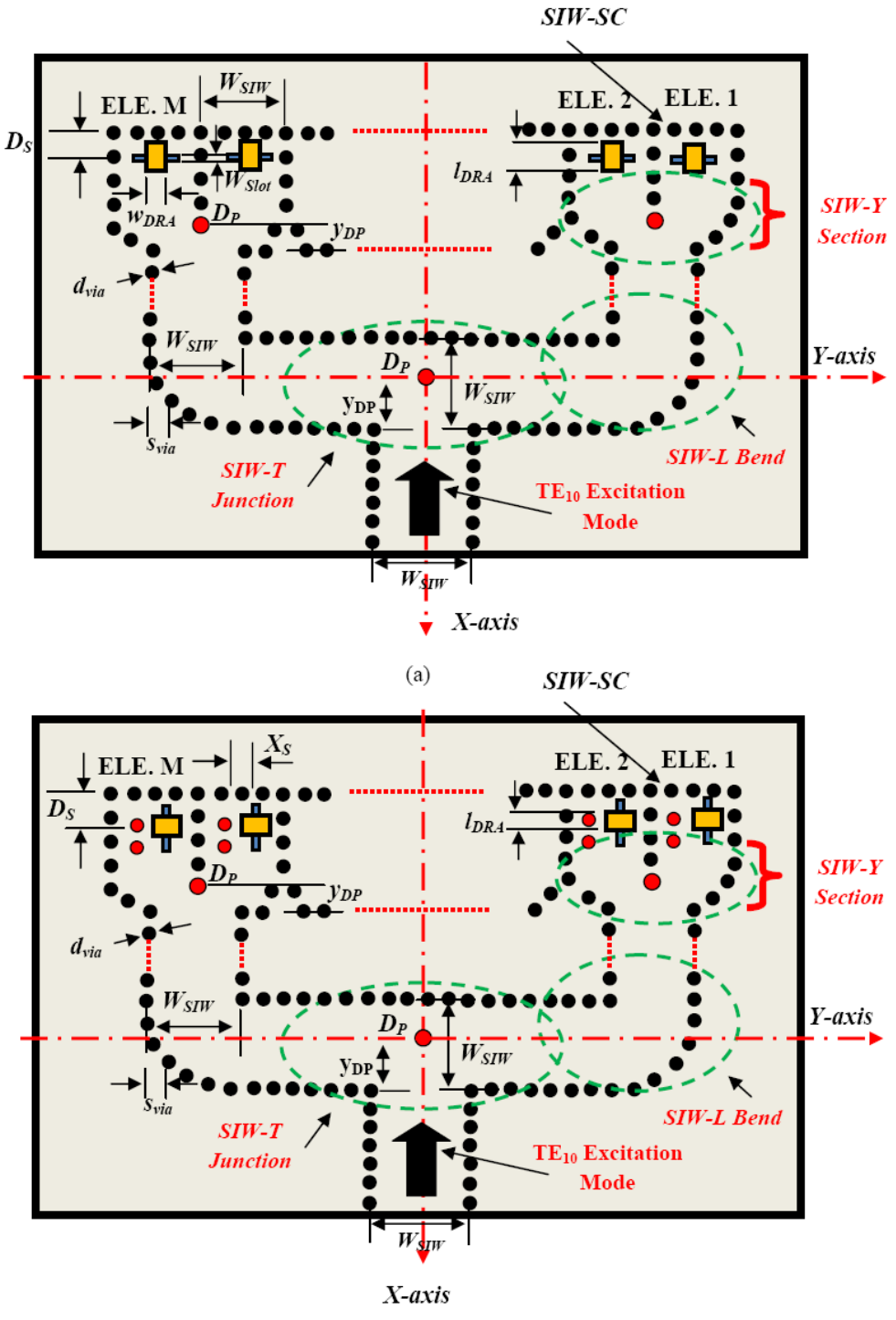

Figure 4.14 The general physical layout SIW-corporate (parallel) fed RDRA array (without SIW-MSL transition), (a) Transverse slot configuration, (b) Longitudinal slot configuration.

both magnitude and phase. It employs three types of SIW discontinuities: a 90° L-bend, a Y-junction and a power splitting T-junction. Figure 4.13a and 4.13b shows the geometry of the SIW parallel fed-RDRA array of the M-elements using two different configurations, the transverse slot (Figure 4.14a), and the longitudinal slot (Figure 4.14b). Typically, the antenna array consists of two major sections: (1) $1 \times M$ SIW-power splitter (beam forming network) used to split the power equally and in phase among the RDRA elements. It consists of the SIW T-junctions, L-Bends, and Y-junctions of width W_{SIW}. (2) The RDRA elements excited by coupling slots. All the SIW junctions forming the power splitter have the same SIW effective width W_{SIW} in order to support the TE_{10} fundamental mode over the operating frequency band. The posts D_P are used to split the power and minimize the reflections caused by the SIW discontinuities. Therefore, the D_P diameter and the location, $y_{DP,}$ have to be chosen properly.

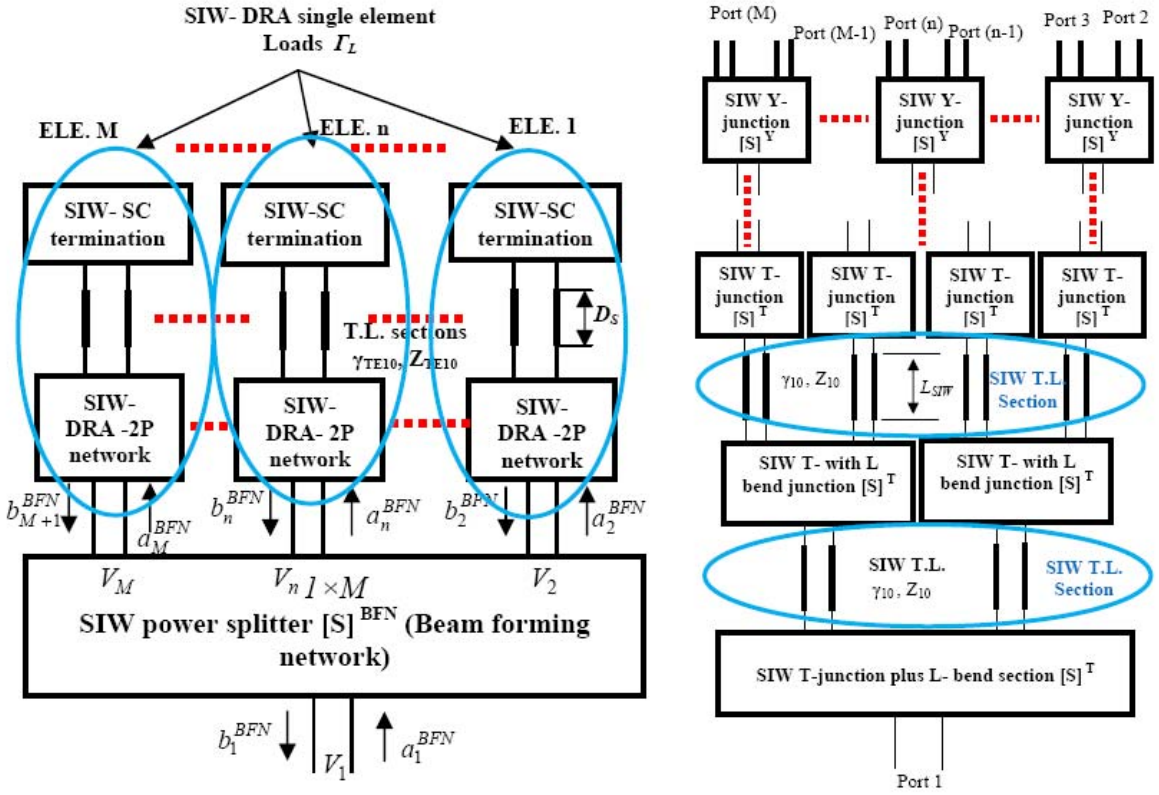

Figure 4.15 The proposed T.L. circuit model for (a) the SIW parallel (corporate) fed-RDRA linear array, (b) $1 \times M$ SIW-power splitter (beam forming network) T.L. model.

Similarly, the SIW segment of length L_{SIW}, connecting these junctions, is modeled by a 2 port-network, as discussed in Section 4.2.1 (Figure 4.2b).

The Transmission Line (T.L.) circuit model similar to the one discussed in Section 4.2.1 is presented in this chapter for the antenna array shown in Figure 4.14 to simplify and accelerate the design process. The $1 \times M$ SIW-power splitter (antenna beam forming network), is modeled by $[S]^{BFN}$,

and each RDRA element, which is excited by a narrow slot, is modeled by a 2 port-network, $[S]^A$, as discussed in Section 4.2.1. Moreover, the physical short circuit termination (SIW-SC), which is positioned at distance D_S is modeled by an ideal SC termination (magnitude of unity and phase of 180°). The proposed T.L. circuit model of the SIW parallel-fed RDRA array in Figure 4.15a does not take into account the inter-element mutual coupling, since our study showed that the mutual coupling between the elements is less than *-19 dB* (this will be studied in Section 4.3.1) over the operating frequency bandwidth.

To complete the T.L. model, the $1\times M$ SIW-power splitter (beam forming network) model part in Figure 4.15a is presented in details in Figure 4.15b. In this model, the SIW-splitter discontinuities are modeled by their multi-port network S-parameters as follows: the SIW T-junction (3 port-network) is modeled by $[S]^T$, the SIW L-bend (2 port-network) is modeled by $[S]^L$, and the SIW Y-junction (3 port-network) is modeled by $[S]^Y$.

The full-wave numerical solver was used to calculate the S-matrices $[S]^L$, $[S]^Y$, and $[S]^T$ for different D_P diameters and locations x_{DP}. For simplicity in the analysis, the two matrices $[S]^T$ and $[S]^L$ are combined(cascaded) and modeled by $[S]^T$, as shown in Figure 4.15b. Then, the SIW power splitter's overall S-matrix, $[S]^{BFN}$, was calculated by using simple S-matrix manipulations[165, 166]. For example, the *1×5 (6 dB)* SIW-power splitter, which consists of two L-band sections, two Y-junctions, and one T-junction, is considered to be the main building block in forming larger arrays. Therefore, the following formulations will focus on modeling the *1×5 (6 dB) SIW*-splitter in Figure 4.16, which its S-matrix, $[S]^{1\times 5}$ is calculated as follows:

$$[S]_{1\times 5} = [S_{PP}] + [S_{PC}]([\Gamma] - [S_{CC}])^{-1}[S_{CP}] \tag{4.6}$$

$$[S_{PP}] = \begin{bmatrix} s_{11}^T & 0 & 0 & 0 & 0 \\ 0 & s_{22}^Y & s_{23}^Y & 0 & 0 \\ 0 & s_{32}^Y & s_{33}^Y & 0 & 0 \\ 0 & 0 & 0 & s_{22}^Y & s_{23}^Y \\ 0 & 0 & 0 & s_{32}^Y & s_{33}^Y \end{bmatrix}, \qquad [S_{PC}] = \begin{bmatrix} s_{12}^T & s_{13}^T & 0 & 0 \\ 0 & 0 & s_{21}^Y & 0 \\ 0 & 0 & s_{31}^Y & 0 \\ 0 & 0 & 0 & s_{21}^Y \\ 0 & 0 & 0 & s_{31}^Y \end{bmatrix}$$

$$[S_{CP}] = \begin{bmatrix} s_{21}^T & 0 & 0 & 0 & 0 \\ s_{31}^T & 0 & 0 & 0 & 0 \\ 0 & s_{12}^Y & s_{13}^Y & 0 & 0 \\ 0 & 0 & 0 & s_{12}^Y & s_{13}^Y \end{bmatrix}, \qquad [S_{PP}] = \begin{bmatrix} s_{22}^T & s_{23}^T & 0 & 0 \\ s_{32}^T & s_{33}^T & 0 & 0 \\ 0 & 0 & s_{11}^Y & 0 \\ 0 & 0 & 0 & s_{11}^Y \end{bmatrix}, \text{ and}$$

$$[\Gamma] = \begin{bmatrix} 0 & 0 & 0 & e^{-\gamma_{10}L_{SIW}} \\ 0 & 0 & e^{-\gamma_{10}L_{SIW}} & 0 \\ 0 & e^{-\gamma_{10}L_{SIW}} & 0 & 0 \\ e^{-\gamma_{10}L_{SIW}} & 0 & 0 & 0 \end{bmatrix}$$

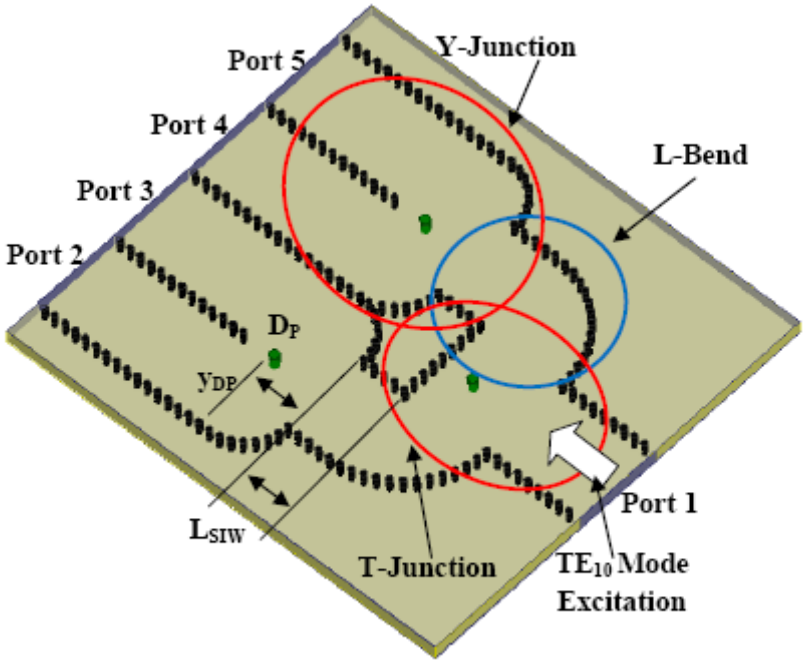

Figure 4.16 The physical structure of 1×4 (*6 dB*) SIW-power splitter.

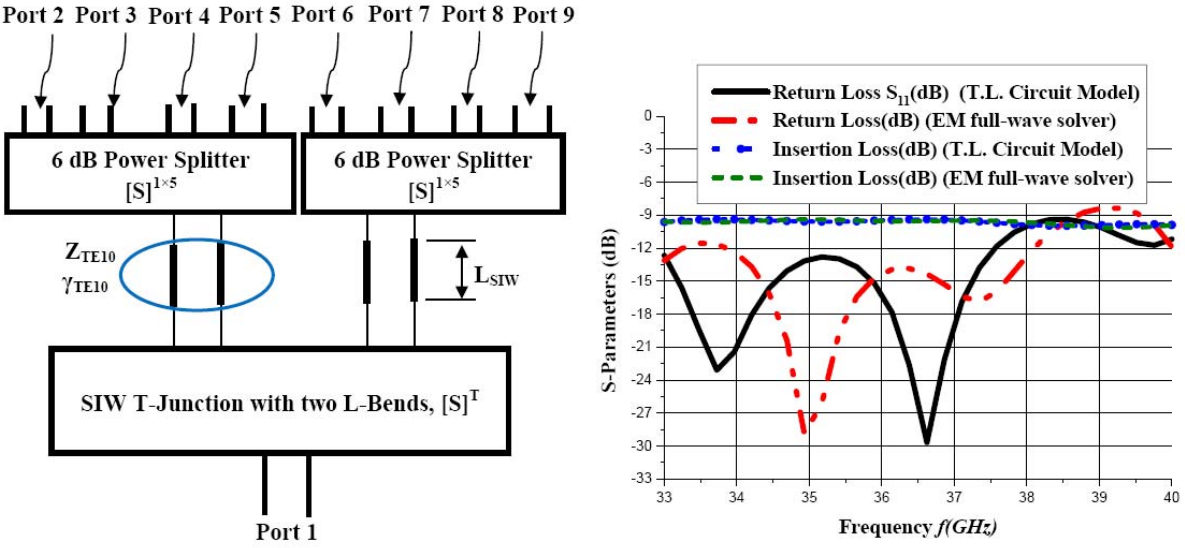

Figure 4.17 The 1× 8 (*9dB)* SIW-power splitter (beam forming network), (a) Simplified model, (b) The return/insertion loss (dB) of calculated by the T.L. circuit model and EM full-wave solver. The splitter main dimensions are: D_P=*0.50mm,* y_{DP}=*3.0 mm*, and L_{SIW}=*2.40mm.*

In order to validate the proposed T.L. circuit model shown in Figure 4.15b, the S-matrix, $[S]^{BFN}$, of the *1×8 (9 dB)* splitter which consists of one T-junction, two L-bends, and two *1×5* SIW-power

splitter, was calculated using the simplified model in Figure 4.17a, and compared to the that calculated by the EM full-wave solver over the frequency range *33-40 GHz*, as shown in Figure 5.17b. A good agreement is noticed in calculating the insertion loss, showing an insertion loss of *-9.7 dB* within the frequency band *33-38 GHz*. This loss is mainly attributed to the dielectric and the SIW-discontinuity losses. However, the SIW loss is still lower than that of the multi-conductor open structures, such as MSL and CPW, which suffer from conduction loss at the mm-wave frequency band. Meanwhile, the return loss (*dB*) calculated by the T.L. circuit model deviates from that of the full-wave solver result. This deviation is mainly attributed to the reflections caused by the excitation of the higher order modes at the SIW-discontinuities, forming the splitter, and the SIW discrete nature, which are not taken into account by the proposed T.L. circuit model. However, the proposed T.L. circuit model is still valid and able to estimate the same return loss bandwidth *($S_{11} \leq$ -12 dB)* as the full-wave solver, which is *4.5 GHz*.

The overall antenna array reflection coefficient, *S_{11}(dB)*, at the indicated reference as show in Figure 4.15a can be calculated using the proposed T.L. circuit model in Figure 4.15b, as follows[166]:

$$S_{11} = \frac{b_1^{BFN}}{a_1^{BFN}} = [S_{AA}] + [S_{AC}][\Gamma - S_{AC}]^{-1}[S_{CA}] \tag{4.7}$$

a_1^{BFN} *:* is the incident wave (*volts*) to the beam forming network at port 1.

b_1^{BFN} *:* is the reflected wave(*volts*) from the beam forming network at port 1.

$$[S_{AA}] = S_{11}^{BFN},\ [S_{AC}]_{1\times M} = \left[S_{12}^{BFN} \ \ldots \ \ldots \ S_{1(M+1)}^{BFN}\right],\ A = 1,\ C = 1,\ [S_{CA}]_{M\times 1} = \begin{bmatrix} S_{21}^{BFN} \\ \vdots \\ \vdots \\ S_{(M+1)1}^{BFN} \end{bmatrix},$$

$$[S_{CC}]_{M\times M} = \begin{bmatrix} S_{22}^{BFN} & \cdots & \cdots & S_{2(M+1)}^{BFN} \\ \vdots & \vdots & \vdots & \vdots \\ \vdots & \vdots & \vdots & \vdots \\ S_{(M+1)2}^{BFN} & \cdots & \cdots & S_{(M+1)(M+1)}^{BFN} \end{bmatrix}, \qquad [\Gamma]_{M\times M} = \begin{bmatrix} \frac{1}{\Gamma_L} & 0 & \cdots & 0 \\ 0 & \frac{1}{\Gamma_L} & \cdots & 0 \\ \vdots & \vdots & \vdots & \vdots \\ 0 & 0 & \cdots & \frac{1}{\Gamma_L} \end{bmatrix}, \quad \text{and}$$

$$\Gamma_L = S_{11}^A + \frac{-S_{12}^A S_{21}^A e^{e^{-2\gamma TE10 D_S}}}{1 + S_{22}^A e^{e^{-2\gamma TE10 D_S}}}$$

Also, the proposed T.L. circuit model of the SIW corporate-fed RDRA can be used to calculate the antenna array radiation pattern (gain) by using the product of the antenna array factor and the single element radiation pattern. The antenna array factor formulation depends on the amplitudes and the phases of $V_1, V_2 \ldots V_M$, which are calculated by the proposed T.L. circuit model. The array factor is formulated as follows (assuming the antenna linear array is formed along the Y-axis direction):

$$AF(\theta,\varphi) = V_M \sum_{n=1}^{n=M} A_n e^{j(M-n)k_o W_{SIW}\sin(\theta)\sin(\varphi)} \quad (4.8)$$

Where,
V_M : is the M^{th} antenna element excitation voltage (reference voltage).

$A_n = \frac{V_n}{V_M}$: is n^{th} the antenna element exciting voltage coefficient.

V_n : is n^{th} the antenna element voltage defined at the antenna input circuit in Figure 4.15a.

In Figure 4.15a, the relationship between the incident waves, a_n^{BFN} and reflected waves, b_n^{BFN} are described by the following equations [165] :

$$[b^{BFN}]_{(M+1)\times 1} = [S^{BFN}]_{(M+1)\times(M+1)}[a^{BFN}]_{(M+1)\times 1} \quad (4.9)$$

$$[b^{ANT}]_{M\times 1} = [\Gamma]_{M\times M}[a^{ANT}]_{M\times 1} \quad (4.10)$$

Where, the matrices $[b^{BFN}]$, $[a^{BFN}]$, $[a^{ANT}]$, and $[b^{ANT}]$ are

$$[b^{BFN}]_{(M+1)\times 1} = \begin{bmatrix} b_1^{BFN} \\ b_2^{BFN} \\ \vdots \\ b_{M+1}^{BFN} \end{bmatrix}, \qquad [a^{BFN}]_{(M+1)\times 1} = \begin{bmatrix} a_1^{BFN} \\ a_2^{BFN} \\ \vdots \\ a_{M+1}^{BFN} \end{bmatrix}$$

$$[b^{ANT}]_{M\times 1} = \begin{bmatrix} b_2^{BFN} \\ b_3^{BFN} \\ \vdots \\ b_M^{BFN} \end{bmatrix}, \qquad [a^{ANT}]_{M\times 1} = \begin{bmatrix} a_2^{BFN} \\ a_3^{BFN} \\ \vdots \\ a_M^{BFN} \end{bmatrix}$$

$$[V_n]_{M\times 1} = [b^{BFN}]_{M\times 1} + [a^{BFN}]_{M\times 1} \quad (4.11)$$

$$[V_n]_{(M+1)\times 1} = \begin{bmatrix} V_1 \\ V_2 \\ \vdots \\ V_{M+1} \end{bmatrix}$$

Equations (4.9), (4.10) becomes a system for simultaneous of *(2M+1)* linear equations in *(2M+1)* unknowns (a_n^{BFN}, and b_n^{BFN}) if the incident wave at the antenna array input in Figure 4.15a is normalized ($a_1^{BFN} = 1$ *volt*). Then, the excitation voltages at all the antenna array elements and the array factor can be defined by equation (4.11), and (4.8), respectively.

4.3.1 SIW-Parallel Fed RDRA Array Inter-Elements Mutual Coupling

The mutual inter-elements coupling among the antenna elements in the SIW corporate-fed DRA configuration Figure 4.13 and its impact on the proposed T.L. is investigated. Figure 4.18a and 4.18b

shows the physical model setup used to study the mutual coupling for both the transverse slot (*H-coupling*), and the longitudinal slot (*E-coupling*), respectively. It consists of two identical RDRA elements that are excited independently by the SIW fundamental mode, TE_{10}, via two waveguide ports, Port 1, and Port 2.

The antenna parameters; *Ds*, and the posts P_1, P_2 diameter and their locations x_p, and y_p should be selected properly to match the RDRA elements to the waveguide mode as discussed in Chapter 3. The EM full-wave solver was used to calculate the S-parameters of the two coupled antennas for the two configurations. It was found that the antenna setup in Figure 4.18b (*E-coupling*) shows a stronger coupling than the antenna setup in Figure 4.18a (*H-coupling*). The calculated *E-coupling*, $S_{21}(dB)$, is less than *-14 dB*, and the *H-coupling* shows less than *-20 dB* over the frequency band of *35-37.25 GHz* as defined by the reflection coefficient $S_{11} \leq -10\ dB$, as shown in Figure 4.19.

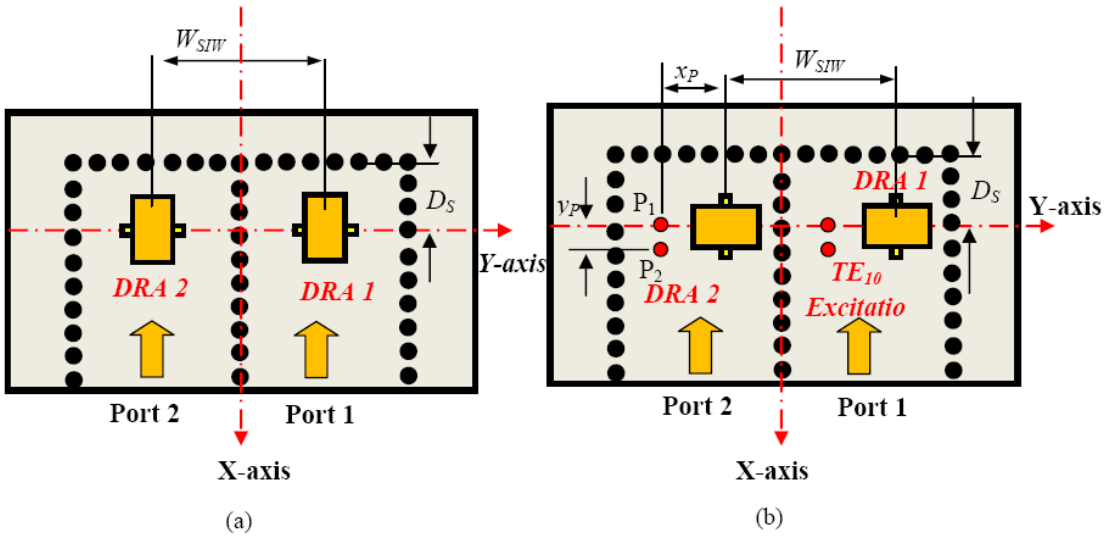

Figure 4.18 The physical model setup used to investigate the inter-element mutual coupling (*dB*) among the SIW corporate-fed RDRA elements in Figure 4.14, (a) transverse slot configuration (*H-coupling*), (b) longitudinal slot configuration (*E-coupling*).

The proposed T.L. circuit model described by the equations (4.6)-(4.11) was used to calculate the overall reflection coefficient and the radiation pattern (gain) for an *M=8* element corporate-fed antenna array (case study). Also, the EM full-wave solver was used to characterize the antenna array performance and verify the T.L. circuit model results. Figure 4.20 shows the calculated antenna array reflection coefficient (*dB*) for the antenna configurations, for the transverse slot in Figure 4.14a, and longitudinal slot in Figure 4.14b, respectively. The antenna array in Figure 4.14a shows an impedance bandwidth of *34.25-38.25 GHz*, whereas, the antenna array in Figure 4.14b shows an impedance bandwidth of *34.50-38.0 GHz.*

As expected, the T.L. circuit model results deviate from these of the full-wave solver. This deviation is caused by the power splitter discontinuities effect discussed in Section 4.3 and shown in Figure 4.17b, and the mutual coupling effect described and shown in Figure 4.19. However, the proposed T.L. circuit model in Figure 4.15a is still valid and is able to estimate the antenna array resonance behavior. On the other hand, the full-wave solver, HFSS is able to handle these issues more

efficiently, but it takes longer time during the simulation process due to the huge generated mesh for this complex structures.

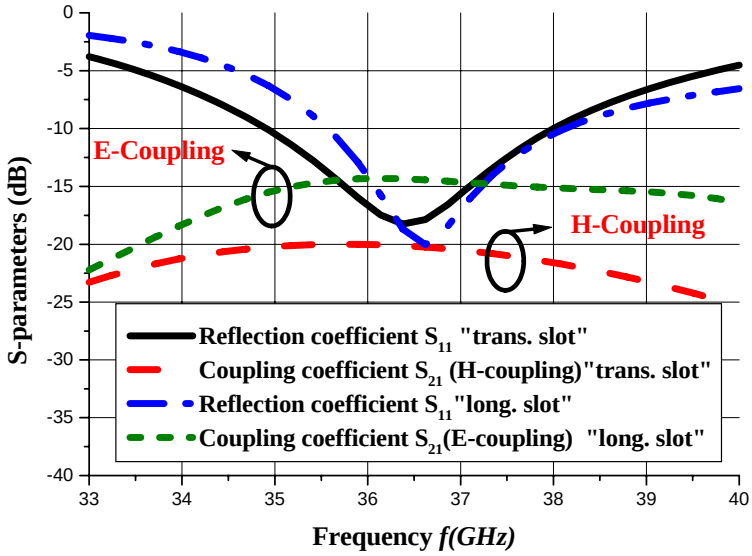

Figure 4.19The calculated S-parameters (*dB*) of the two port-network (mutual coupling set up) in Figure 4.18.

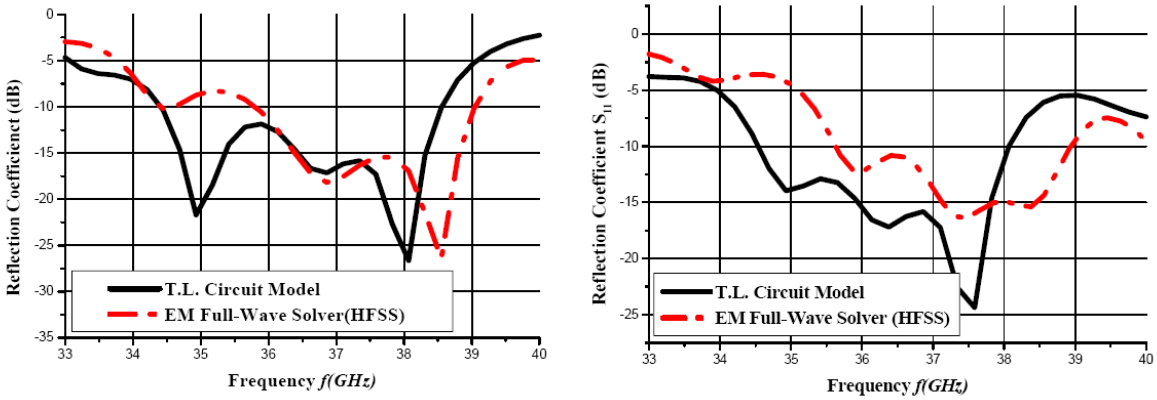

Figure 4.20 The reflection coefficient S_{11}*(dB)* of the SIW corporate-fed RDRA array(*M=8* elements) calculated by the proposed T.L. circuit model and EM full-wave solver (a)with transverse slot arrangement D_S*=3.50 mm*, D_P*=0.50mm*, y_{DP}*=3.0 mm*, and L_{SIW}*=2.40mm*, (b)with longitudinal slot arrangement, D_S*=2.0 mm,* D_P*=0.50mm*, y_{DP}*=3.0 mm*, and L_{SIW}*=2.40mm.*

For completeness, the radiation pattern (gain) of the proposed antenna arrays in Figure 4.14 was investigated by the proposed T.L. circuit and verified numerically by the full-wave solver, HFSS, in two the orthogonal planes, the *E*-plane (XZ-plane for the antenna in Figure 4.14a / YZ-plane for the antenna in Figure 4.14b) and the *H*-plane (YZ-plane for the antenna in Figure 4.14a / XZ-plane for

the antenna in Figure 4.14b), as shown in Figure 4.21a,b. They show a boresight gains (maximum) of *12.7 dB* (the antenna in Figure 4.14a), and *14.9 dB* (the antenna in Figure 4.14b) over the entire operating impedance bandwidth, as shown in Figures 4.21a, and 4.21 b, respectively. A very good agreement is observed between the T.L. model results and these of full-wave solver, especially in the H-plane in Figure 4.21a, and in the E-plane as shown in Figure 4.21b near the main beam (boresight direction). The difference between the proposed T.L. circuit model and the full-wave solver results in the E-plane/ H-planes and far off-side lobes in the E/H-plane is mainly due to the scatterings from the ground plane edges (finite ground plane effect), which is not taken into account by the proposed T.L. model. However, the proposed T.L. circuit model is still valid, and it is able to calculate the antenna radiation pattern, which correlates well with that of HFSS.

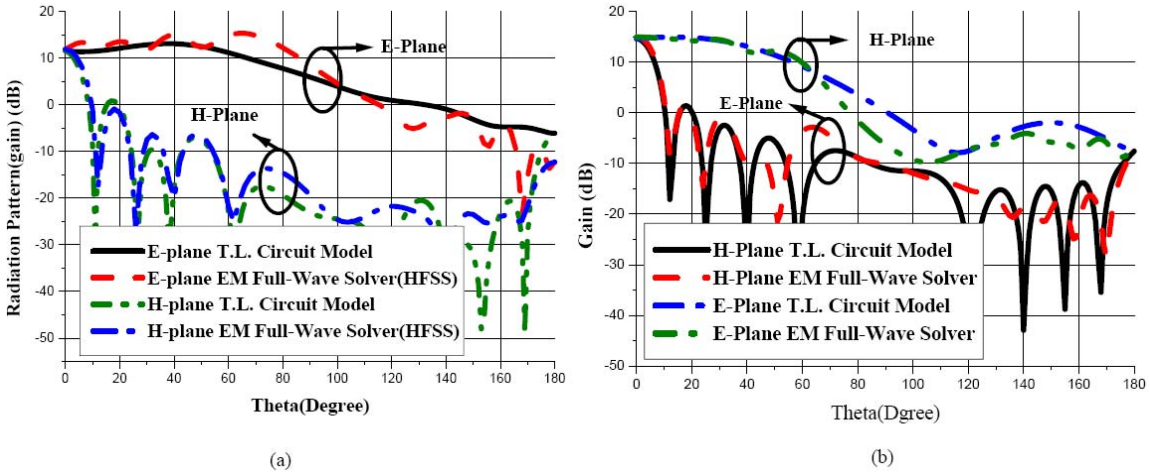

Figure 4.21 The radiation pattern (gain) (dB) of the SIW corporate-fed RDRA array(8-elements) at *36 GHz* calculated by the proposed T.L. circuit model and EM full-wave solver (a)with transverse slot arrangement in Figure 4.14a, D_S*=3.5 mm,* D_P*=0.50mm,* y_{DP}*=3.0 mm, and* L_{SIW}*=2.40mm, (*b) with longitudinal slot arrangement in Figure 4.14 b*,* D_S*=2.0 mm,* D_P*=0.50mm,* y_{DP}*=3.0 mm, and* L_{SIW}*=2.40mm.*

4.4 Substrate Integrated Waveguide (SIW) Hybrid (Series-Corporate) Fed-Rectangular Dielectric Resonator Antenna (RDRA): Two Dimensional (2D) Arrays

When the SIW-series fed RDRA linear array of the *N* elements arrangement in Figure 4.1 combined with the SIW corporate-fed array of the *M* elements in Figure 4.14, the SIW hybrid (series-corporate combination)-feed configuration can be implemented to form a two-dimensional (2D) RDRA array with dimension of *N*×*M* for mm-wave high gain applications. Figure 4.22 shows the general physical layout of the SIW hybrid fed-RDRA array implemented in longitudinal slot based configuration. The longitudinal slot is preferred to the transverse slot configuration due to its smaller overall size, which is suitable for low profile RF front-end applications. Moreover, its radiation pattern shows lower Side Lobe Level (SLL) ~ *11dB*, as discussed in Section 4.2.

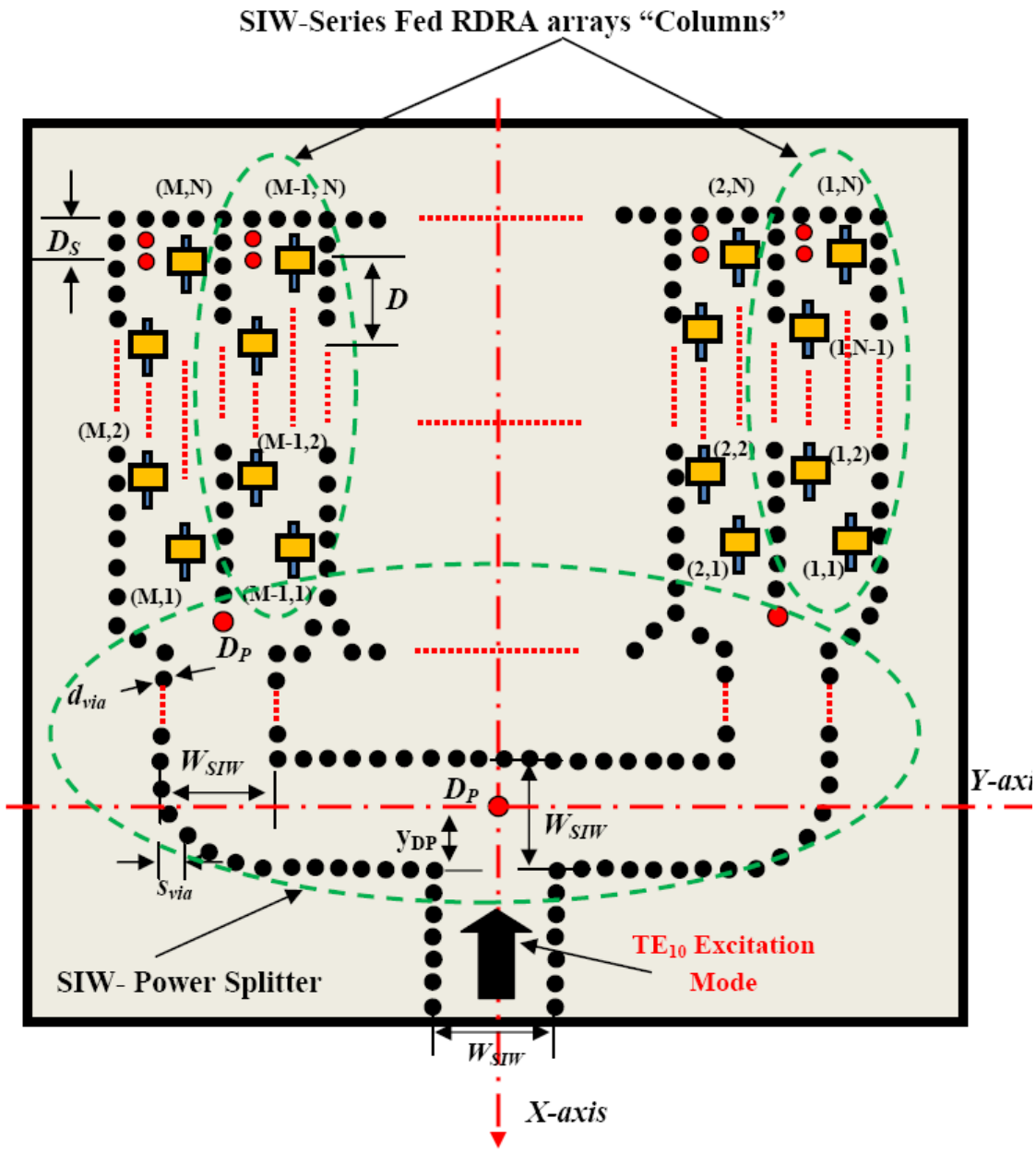

Figure 4.22 SIW-hybrid (serried-corporate combination) fed RDRA 2D array.

The $1 \times M$ SIW-power splitter is used to split the incident power equally among the M sets of the N-series fed-RDRA elements. The metallic post diameters, D_P and their locations, y_{DP} are tuned to distribute the power equally and minimize the antenna array reflection coefficient. Alternatively, the series fed-array elements are positioned properly according to the design approach disused in Section 4.2 to ensure equal amplitude and equi-phase excitations to all array elements (uniform distribution). In

the corporate-feed part, the elements are positioned a distance $W_{SIW} \cong \frac{\lambda_g}{2}$ apart to keep both the mutual coupling between elements and overall antenna size at a minimum level.

The proposed T.L. circuit models presented for the series fed- antenna array in Figure 4.2 and for the corporate fed-antenna array in Figure 4.15 can be combined to form a complete T.L. circuit model for the 2D antenna array in Figure 4.22. In this T.L. model, each series-fed array "column" is modeled as a load Γ_L in Figure 4.15a, which can be calculated by using the formulation described by equations (4.1)-(4.3). Then, the overall reflection coefficient is calculated using the equation (4.7). The antenna radiation pattern of the antenna array in Figure 4.22 can also be calculated by using the formulations described in Sections 4.2 and 4.3. A case study, $M=8\times N=8$ antenna array, is modeled and designed.

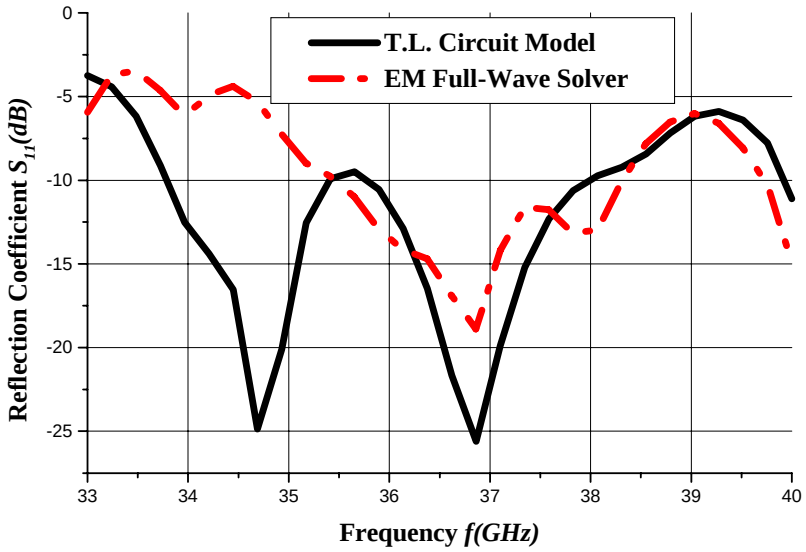

Figure 4.23 The reflection coefficient $S_{11}(dB)$ of the SIW hybrid fed-RDRA array (8×8-elements) calculated by the proposed T.L. circuit model and EM full-wave solver.

The T.L circuit model was used to calculate the reflection coefficient, $S_{11}(dB)$ and the radiation pattern (gain), and its validity was investigated by the full-wave solver, HFSS. Figure 4.23 shows the reflection coefficient, $S_{11}(dB)$,of the SIW hybrid-fed RDRA 2D array in Figure 4.22, which is calculated was by the proposed T.L. circuit model and the EM full-wave solver. The circuit model shows an impedance bandwidth, $S_{11}(dB) \leq 10$, that covers the frequency band of *33.72-37.38 GHz*.

A good agreement between the T.L. circuit model result and the full-wave solver result in calculating $S_{11}(dB)$ is only observed when close to the frequency band of *35.41-38.31 GHz*, which corresponds to an impedance bandwidth of *2.90 GHz* centered at *36.86GHz*. Alternatively, there is a noticeable difference between the two simulated results below *35.41 GHz*, as shown in Figure 4.23. This difference is mainly due to the accumulation of errors in the series and corporate-fed arrays results, which are attributed to the issues discussed in Sections 4.2 and 4.3. In other words, as the

number of elements in the array increases, the more discontinuities are added to the array structure and become closer; causing the T.L. circuit results to deviate more from these calculated by the full-wave solver, especially the reflection coefficient characteristics. Consequently, the circuit model would fail to estimate the antenna array overall performance accurately.

The radiation characteristics of the antenna array in Figure 4.22 were studied by the proposed T.L. model and the EM full-wave solver. Figure 4.24 a, and 4.24b shows the antenna array radiation pattern (gain) in the E (YZ-plane), and the H (XZ-plane) planes at *36.86 GHz,* respectively. Although the T.L. results deviates from the full-wave solver in both planes, especially off the boresight direction ($\theta=0°$), it is still able to predict the radiation pattern (gain) near the main beam. The antenna shows a maximum boresight gain of *22.5 dB* with a narrow *3dB* beam width in both planes of 8°, which is quite suitable for high gain phased array mm-wave applications. Figure 4.25a illustrates the field distribution on an auxiliary plane that coincides with the coupling slots plane. It shows a well confined (guided) wave inside the SIW structure and a uniform distribution of the excitation fields for all the RDRA elements that leads to co-phase radiation in the boresight direction, as shown in Figure 4.25b.

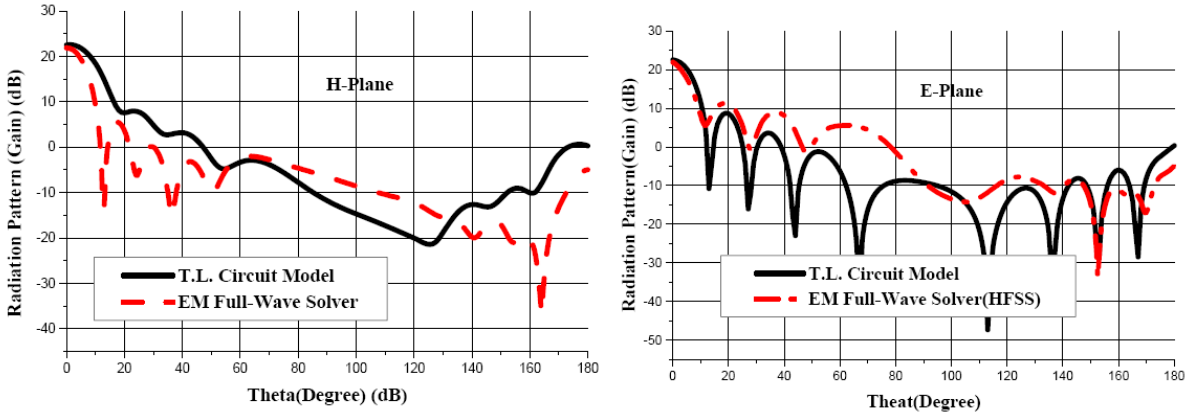

(a) (b)

Figure 4.24 The radiation pattern (gain) (dB) of the SIW-hybrid fed RDRA array in Figure 4.22 (*8×8*-elements) at *36.50 GHz* calculated by the proposed T.L. circuit model and EM full-wave solver configuration, (a) *H*-plane (YZ-plane), (b) *E*-plane (XZ-plane).

Since, the main objective of this thesis is to explore and investigate the usefulness of combining both the SIW technology (as a feeding scheme) and the DRA technology (as a radiator) for low cost and high radiation efficiency mm-wave applications. A study was conducted to investigate the losses (conduction and dielectric) variation over operating frequency of the antenna array structure in Figure 4.22.

The overall radiation efficiency of the antenna was calculated by taking into account only one of these losses at a time compared to the case where all the losses are included. The results of this study are depicted in Figure 4.26. It was found that, when all the losses were included (case 1) in the calculation, the antenna's overall simulated radiation efficiency was more than *85%* over the frequency band of *35.41-38.31 GHz*.

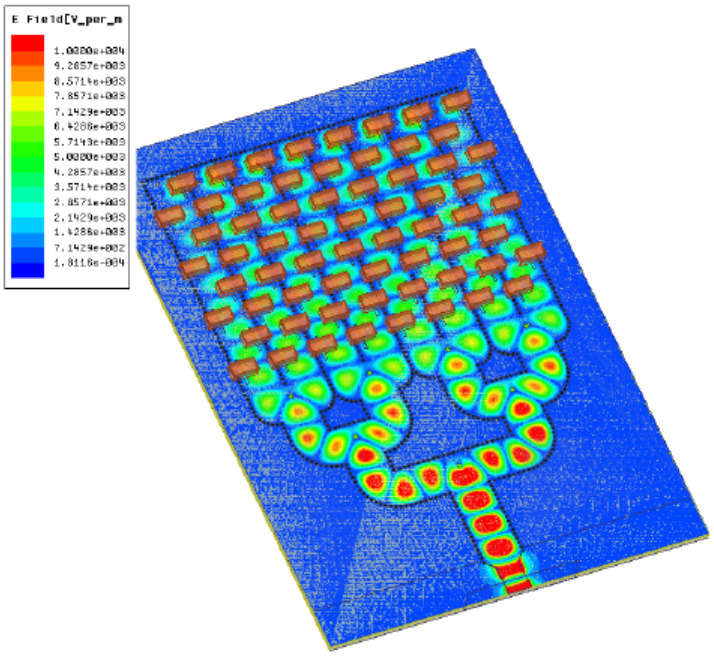

(a)

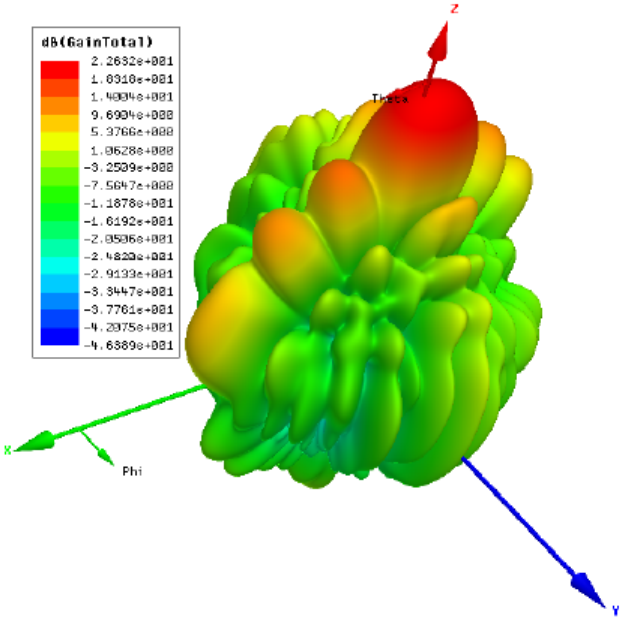

(b)

Figure 4.25 The field distribution plots of the SIW hybrid fed 2D RDRA array (*8*×*8*-elements) in Figure 4.22 at *36.50 GHz*, (a) the electric field*, E (v/m)*, (b) the far field 3D radiation pattern, *Gain (dB)*.

This high efficiency is close to measured efficiency reported in [167] for a MSL-fed DRA single element over the same operating frequency band. This efficiency enhancement is attributed to the SIW and RDRA combination that minimizes the conduction loss, which dominates at the mm-wave as described in Chapter 2.

To confirm this concept, the radiation efficiencies of the antenna in Figure 4.22 was calculated when the conduction loss is only included (case 2), and in another case only the dielectric loss is included (case 3). As shown in Figure 4.26, they are more than *96%* (*0.7%* is the numerical error provided by the full-wave solver), and *89%*, respectively. These simulations indicate that the SIW keeps the conduction loss at the minimum level (case 2). However, the radiation efficiency in case 3 is close to that of case 1, showing that the dielectric loss dominates the conduction loss at the mm-wave band when the SIW is used as a feeding scheme.

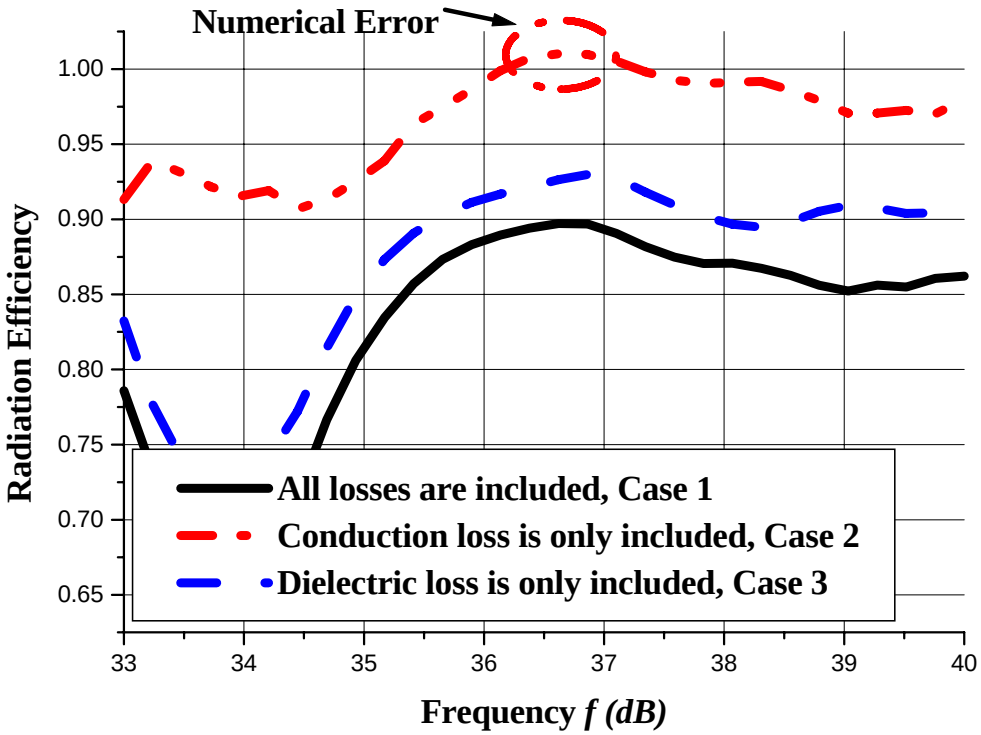

Figure 4.26 The calculated radiation efficiency (by HFSS) of SIW hybrid fed- 2D RDRA array ($M=8\times N=8$ elements) in Figure 4.22.

4.5 SIW Fed-RDRA Arrays Fabrication and Measurements

In order to validate the antenna array designs for real applications, and verify the proposed T.L. circuit models described in this chapter, the SIW series fed-RDRA arrays were fabricated using the technique outlined in Section 3.5.1, as shown in Figure 4.27, and their prototypes are tested. The

reflection coefficient and radiation characteristics of the SIW series fed-RDRA array prototypes in Figure 4.27 were measured over the operating frequency band of *33-40 GHz.*

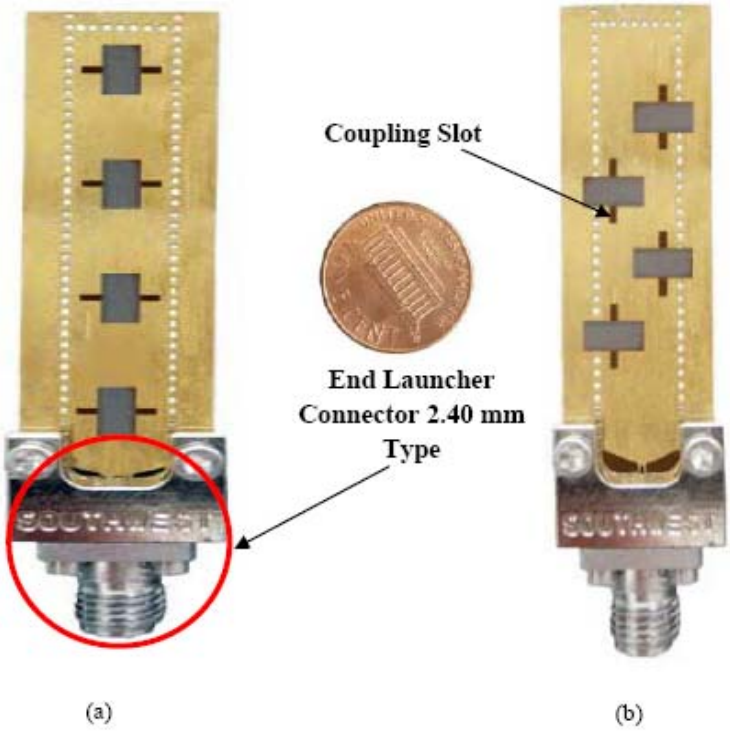

Figure 4.27 The fabricated prototypes of the SIW series-fed RDRA array [168] (a) using vertical polarized (transverse) slot configuration, (b) using horizontal polarized (longitudinal) slot configuration.

The measured reflection $S_{11}(dB)$ coefficients for both antenna array configurations are depicted in Figure 4.28. The antenna prototype in Figure 4.27a shows an impedance bandwidth of *1.60%* (around the center frequency *33.87 GHz*), as shown in Figure 4.28a, whereas, the antenna prototype in Figure 4.27b shows a *4.70%* bandwidth (around the center frequency *37.80 GHz*), as shown in Figure 4.28b. A very good agreement is observed between the measurements and the full-wave solver, HFSS, results, especially near the frequency at which the reflection coefficient is minimum (resonance). However, the proposed circuit model results deviated from that of the measured ones, especially in Figure 4.28a, where there is a stronger mutual coupling (as discussed in Section 4.2.2). In general, there are noticeable deviations between the proposed T.L. model results and the measured ones in Figure 4.28a, and 4.28b. These differences are attributed to the discrete nature of the SIW structure that affects the short circuit (SC) performance (magnitude and phase), T.L. lengths, and the mutual coupling between the adjacent antenna elements, caused by the excitation of higher order mode at the SIW-slot interfaces, as discussed in Section 4.2.

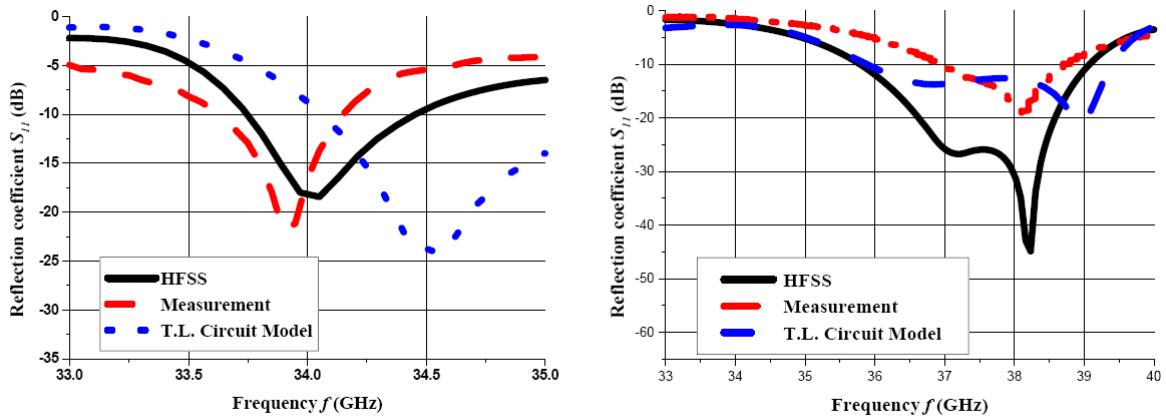

Figure 4.28 The simulated and measured reflection coefficient (dB) of the SIW series-fed DRA array [168] (*N=4*), (a) using the horizontal polarized SIW-slot arrangement prototype in Figure 4.27a, (b) using the vertical polarized SIW-slot arrangement prototype, in Figure 4.27b.

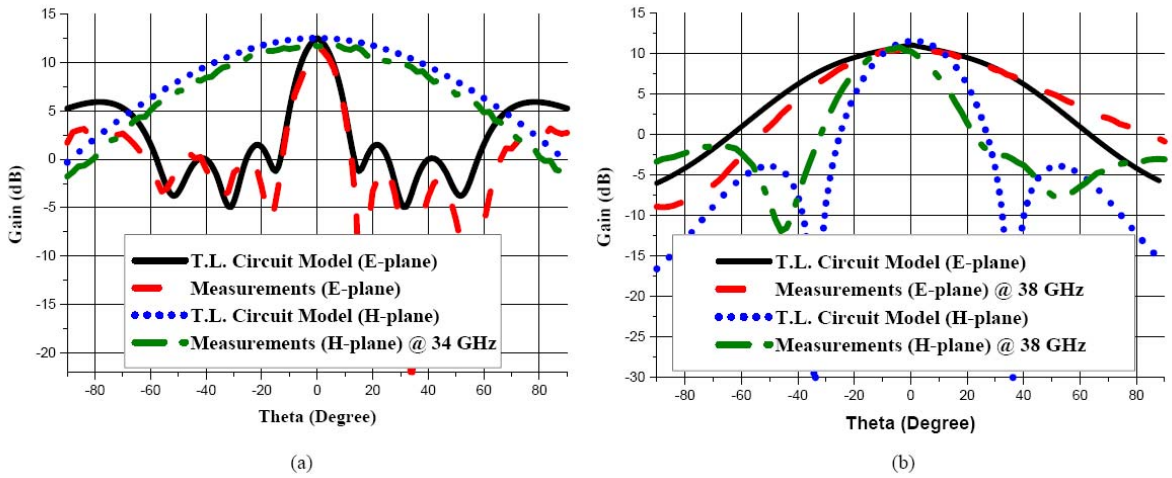

Figure 4.29 The simulated and measured results of the SIW series fed-RDRA array (*N=4)* (a) using the horizontal polarized SIW-slot arrangement prototype in Figure 4.27a [168]: *E*-plane (XZ-plane) and *H*-plane (YZ-plane), (b) using vertical polarized SIW-slot arrangement prototype in Figure 4.27b: *H*-plane (XZ-plane), *E*-plane (YZ-plane).

All these issues are handled efficiently and are taken into account by the full-wave solver. Therefore, the measured reflection coefficient agrees to that of the HFSS, except for a very small deviation, caused by the fabrication tolerances and measurement errors. However, the proposed T.L. circuit model is still valid and is able to predict and estimate the resonance behavior and the impedance bandwidth of the proposed antenna arrays in very short time compared with the full-wave solver.

Also, the radiation patterns (gains) of the fabricated antenna prototypes were experimentally verified. The measured radiation pattern (gain) of the two antennas with a scanned angle θ varied

between -90^o and $+90^o$ arranged along X-axis as indicated by the coordinate system in Figure 4.1 is described. The simulated and measured XZ- and YZ- plane radiation patterns are shown in Figure 4.29a, and 4.29b, respectively. The antenna array in Figure 4.27a, b arrays show maximum boresight ($\theta=90$) gains of *11.70 and 10.60 dB*, respectively.

Obviously, as shown in Figure 4.29, the measured radiation pattern results correlate well with the simulated results calculated by the proposed T.L. model in both the *E*-and *H*-planes, especially in the vicinity of the main beam with less than *1.10 dB* difference in the in the boresight direction. This difference is attributed to the dielectric loss (very small), the SIW-MSL transition loss (*~ 0.25 dB)*, and the launcher losses *(~0.9 dB*) which are not taken into account by the T.L. circuit model. Both the MSL-SIW transition and the edge connector (power launcher) are used in this work for experimental verification only, and their effect on the antenna overall performance have to de-embedded during the radiation efficiency calculations/measurement.

As discussed in Section 4.2, the antenna array overall radiation efficiency was investigated numerically by a full-wave solver, as shown in Figure 4.13 for 4 elements. However, the efficiency of the antenna excluding the SIW-MSL transition and the edge connector (power launcher) can be calculated based on the simulation (by full-wave solver). The SIW-MSL transition and the edge connector (power launcher) introduce *~ 1 dB* loss at *35 GHz*. The simulated directivity and gain of the antenna array in Figure 4.27 are *13.0 dB* and *12.75 dB*, receptively at *35 GHz* with an estimated efficiency *94.4%.* By taking the *1.05 dB* difference (indicated by Table 4.3) between the measured and the simulated gain into account (after excluding the launcher loss *~ 0.9 dB*), the measured efficiency estimate is be up to *91.2%.*

The previous discussion indicates that highly efficient mm-wave antenna arrays can be built when the SIW technology integrated with the DRA. This technology can replace the conventional multi-conductor planar feeding scheme technologies for other planar antennas, such as the MPA. The SIW is a high Q-feeding structure that keeps most of the excitation fields inside its structure. Accordingly, the overall antenna radiation efficiency is enhanced by the SIW, and provides a stable gain by minimizing the conduction, leakage losses, and blocks the undesirable radiation caused by other feeding structures.

Table 4.3 provides a comparison between the measured and simulated results which were calculated by using the HFSS and the proposed T.L. circuit model for the antenna characteristics. The antenna prototype in Figure 4.27b depicts a wider bandwidth (impedance and radiation) with a more compact and smaller area than the antenna prototype in Figure 4.27a. However, the latter provides a narrower beam width due to its larger physical area. Both antennas show different characteristics suitable for different high radiation efficiency applications. All these characteristics demonstrate that the proposed SIW-DRA array structures are low cost, highly efficient, and compact antenna, which are suitable for portable mm-wave applications. As compared with the full-wave electromagnetic (EM) numerical solvers,

Table 4.3 indicates that the proposed T.L circuit model is an easy and fast approach for calculating the antenna array main characteristics, such as reflection coefficient and radiation pattern compared to the full-wave solver. Besides, it can be used for optimizing the antenna array parameters to achieve the optimum performance.

Table 4.3 The SIW series-fed RDRA Array (*N=4*) reflection coefficient/radiation characteristics [168].

Antenna Characteristics		Simulation		Measurement
		HFSS	Model	
Horizontal Polarized (Transverse) Slot	Center frequency f_o (GHz)	*34.10*	*34.50*	*33.87*
	Impedance Bandwidth Δ% (-10 dB reflection coefficient)	*1.87*	*5*	*1.60*
	S_{11}*(dB)* @ f_o	*-15.70*	*-24.0*	*-22*
	G_{max}@ f_o	*12.75*	*12.80*	*11.70*
	Efficiency @ f_o	*0.95*		
	Beam width (Degree)	*16*	*16*	*16*
	Radiation bandwidth (%)	*8*		
	Antenna size	*10×37 mm²*		
Vertical Polarized (Longitudinal)Slot	Center frequency f_o *(GHz)*	*37.45*	*38*	*37.80*
	Impedance Bandwidth Δ% (-10 dB reflection coefficient)	*8.70*	*9%*	*4.70*
	f_o	*-26.45*	*-21*	*-19.70*
	G_{max}@ f_o	*11.39*	*11.68*	*10.60*
	Efficiency @ f_o	*0.93*		
	Beam width (Degree)	*34*	*34*	*34*
	Radiation bandwidth (%)	*14*		
	Antenna size	*9×28 mm²*		

Chapter 5
Discussion and Future Recommendations

5.1 Introduction

High radiation efficiency planar antennas based on the planar waveguide technology, the Substrate Integrated Waveguide (SIW), for low cost mm-wave applications were investigated. In particular, the DRA single element/arrays-fed by a novel low cost and loss feeding scheme, SIW, were investigated. The SIW-based DRA were modeled, designed, and fabricated. The design guidelines (algorithm) based on antenna theory, Transmission Line (T.L.) circuit model, and full-wave simulations were presented to accelerate the design and the optimization processes. Also, the Experimental results for fabricated antenna prototypes were presented to verify the design guidelines, and the simulated results. It was found that the SIW as feeding scheme is very well suited for many planar antennas, such as the DRAs and the MPAs. It enhances their overall radiation efficiency that normally degraded by tradition feeding schemes at the mm-wave frequency band. Moreover, the measured results were correlated well to the simulated ones.

5.2 Brief Summary of the Research

This thesis presents an investigation of the Substrate Integrated Waveguide (SIW) based Dielectric Resonator Antennas (DRA) operating at the mm-wave frequencies for high radiation efficiency applications. The information gained from a thorough review of the theoretical foundation on which the DRAs are based, and from a study of previously reported conventional planar feeding schemes at the mm-wave frequency band, was utilized as a basis for providing a novel low loss feeding scheme that can be used for planar antennas, such as the DRA, and MPAs.

In this research, the SIW based-DRA technology implemented in two different configurations was investigated. The DRA's fundamental mode, TE_{111}, was excited for radiation through a narrow slot coupled by the SIW's fundamental mode, TE_{10}. All the design and the modeling aspects involving the dielectric materials used, the physical dimensions (parameters), and the impact of these parameters on the antenna performance were studied (parametric study). Also, the full-wave simulations were included to verify the proposed designs for the mm-wave applications.

The SIW-based DRA technology was extended in this work to investigate the radiation efficiency of large arrays in high gain system applications. In this thesis, different feeding configurations, such as the SIW series-fed DRA linear arrays, the SIW corporate-fed DRA linear arrays, and the SIW hybrid fed-DRA Two Dimensional (2D) arrays were presented. The physical architectures of the antennas were also introduced with theoretical design guidelines. Furthermore, a simple approach based on a developed Transmission Line (T.L.) circuit model was proposed as a simple tool to analysis and design the proposed antenna arrays and provides more physical insight about the antenna main parameters and their impact on the antenna performance.

The antenna designs were fabricated by a novel procedure which is compatible with low loss and low cost technologies, such as PCB. Their fabricated prototypes were measured to validate the

process and the proposed T.L. circuit model, and confirm that the SIW-fed DRA operating at millimeter-wave band is feasible.

A final discussion of the subject necessitates a comparison of the results obtained here with those previously reported for similar published designs. This will give an idea of the potential of the designs here for use in the future systems, and an idea of how much work is needed before their use in commercial systems can be become a reality. Finally, recommendation for follow on work is presented in an attempt to point the way ahead for this subject.

5.3 Summary of Thesis Main Accomplishment

In this work, significant contributions to the advancement of integrated antenna and the front-end packaging were fulfilled. Therefore, the major accomplishment of this thesis was the investigation, design and fabrication of low cost/loss planar waveguide technology based-DRA single element/arrays for mm-wave high radiation efficiency application, which was more than *90 %*. The use of SIW as a feeding scheme for the DRA at the mm-wave frequency band, especially for array applications is a relatively unexplored topic. To the author's knowledge, this thesis is considered to be the first investigation of SIW-integrated RDRA for high radiation efficiency mm-wave applications. Moreover, this research work was extended to investigate the SIW-based DRA array configurations by proposing two different excitation arrangements.

Another accomplishment was proposing a novel T.L. circuit model for the arrays to expedite the design process. It is based on generic formulations to calculate both the antenna overall reflection coefficient and the radiation pattern (gain) characteristics. The proposed T.L. was simple and fast compared to the full-wave solvers, and led to a general methodology (algorithm) for the mm-wave SIW-based planar antennas. Furthermore, the SIW-based DRA designed modules were fabricated by a novel technique that is compatible with the Printed Circuit Board (PCB) low cost technology. Due to time and cost limitations, few antenna modules namely SIW-fed DRA single element and SIW-series fed DRA array, were fabricated and tested to validate the design guidelines. The measurements were in a good agreement with the simulated results done by full-wave solver and the proposed T.L. circuit model.

5.4 Future Work

Any research work that involves new emerging mm-wave technologies, such as SIW-based RF-circuits and antennas needs further investigations. Furthermore, promising avenues of research present themselves that cannot be pursued due to the lack of time and resources. The following list of recommended research topics for the future work includes both completion of this work and potential extensions to the results presented in this thesis.

1. Building and measuring the SIW-corporate fed DRA and the SIW hybrid-fed DRA designed prototypes as described in Sections 5.3 and 5.4, respectively to validate the proposed design for real high gain/efficiency mm-wave applications, and to complete the research. Also, the measured results will be used to validate the full-wave simulations and the proposed T.L circuit model formulations. Further investigation is also required in order to overcome manufacturing problems.

2. Investigations of using this developed antenna at higher frequencies such as 60 GHz, and 77 GHz. Since the DRA elements become very small, the array structures even become more difficult to fabricate. At these frequencies, a few tens of microns deviation from the actual dimensions is enough to move the resonant frequencies to undesirable region. One potential solution to overcome these problems and fabricate high precision DRAs is X-ray lithography applied to polymer-based antenna structures with different portions of ceramic contents [169].
3. The Design and development of the SIW-based phased array using different technologies and configurations, such as the multi-layer Low Temperature Co-fired Ceramics (LTCC) technology, to implement and integrate low loss and low cost phase shifters, which are responsible for the antenna array beam steering, will be investigated. Therefore, the research will also address novel ideas for the implementation of a low cost and low loss planar waveguide based on the Micro-Electro-Mechanical Systems (MEMS) integrated phase shifter in the same antenna.
4. Even though the DRAs is preferred over the MPAs for microwave/mm-wave applications, MPAs are still an attractive candidate at the mm-wave frequency band. Especially at frequencies higher than *60 GHz*, where the DRA dimensions become critical to fabricate. Therefore, an investigation of using the SIW as a feeding scheme for the MPAs for the V-band (60 GHz) to enhance the overall radiation efficiency within the allocated *7 GHz* continuous unlicensed spectrum *57-66 GHz* is required.

Appendix A

Basic Theory and Analysis of Dielectric Resonator antenna (DRA)

A.1 Dielectric Resonators (DRs), as a radiator

The DRs are made from low-loss dielectric materials of many different shapes, within which the oscillating EM energy are confined. The main advantage of the DRs over a traditional cavity resonator is their compatibility with the planar circuits and their ease of fabrications for a very high frequency operation. Using high ε_{rd}, DRs can also be made very small in their fabrications. They provide wider bandwidth than cavity resonators for many applications.

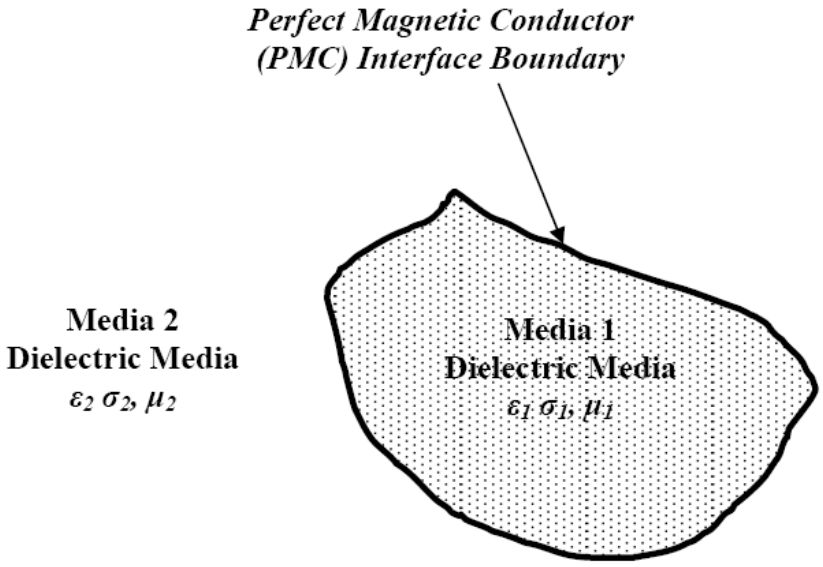

Figure A. 1 Boundary between the DR and free space.

The main sources of power dissipation in the DRs are the dielectric loss which is usually very small and the power radiates out through the walls of resonator. This power leakage from the DR can be explained briefly by considering the DR wall as the boundary between two non-conducting media (dielectric and air). Each of the two media has its own values for the basic parameters conductivity (σ), permittivity (ε_{rd}) and permeability (μ) that affects the EM wave propagation. By considering the wave behavior at the boundary between the two media the loss mechanism can be described easily. The Perfect Magnetic Wall (PMC) is assumed as a boundary condition at the boundary as shown in Figure A.1. If we consider the region inside the DR as a region 1, and the surrounding air as a region 2, then the return loss (Γ) at the boundary can be expressed in terms of the intrinsic impedances of the two media:

$$\Gamma = \frac{\eta_2 - \eta_1}{\eta_2 + \eta_1} \tag{A.1}$$

$$\eta_{1,2} = \sqrt{\frac{j\omega\mu_{1,2}}{\sigma_{1,2} + j\omega\varepsilon_o\varepsilon_{r_{1,2}}}} \qquad \text{(A.2)}$$

Since both media are non-conducting (σ =0), expression for intrinsic impedance of two media can be expressed as:

$$\eta_1 = \sqrt{\frac{\mu_o}{\varepsilon_o}} \quad \text{for air} \quad \text{and} \quad \eta_2 = \sqrt{\frac{\mu_o}{\varepsilon_o\varepsilon_{rd}}} \quad \text{for DR} \qquad \text{(A.3)}$$

$$\Gamma = \frac{1 - \sqrt{\frac{1}{\varepsilon_{rd}}}}{1 + \sqrt{\frac{1}{\varepsilon_{rd}}}} \qquad \text{(A.4)}$$

As noticed from equation (A.4), the portion of the incident wave passes through the wall or is reflected back into the DR, depending on the DR material permittivity (ε_{rd}) ,where it accounts for the energy storage in the DR. In other words, for a DR with a high permittivity, most of the energy will be stored inside the DR and little will be lost to the radiation. Conversely, a DR with a low ε_{rd} , most of its energy will be lost to radiation and very little will be reflected back to DR. In this loss mechanism, the DR can be used as a radiator if a lower value of ε_r material is used for the DR material typically $5 \leq \varepsilon_{rd} \leq 10$ where, the radiation will become the dominant feature of the lowest order resonant modes. By choosing the DR dimensions and aspect ratios such that the resonator has an unloaded quality factor (Q_U) that approximately is equal to its radiation quality factor (Q_{rad}) will result in a wide operating bandwidth for the DR. Thus, a properly designed DR excited in its lower modes can function effectively as an antenna.

A.2 Resonant Modes of DRA

The modes present inside the DRA can be classified into the E-mode and H-modes. The H-modes are characterized by the large normal H- field component at the boundaries of the DR, whereas the E-modes are modes that do not have a large normal H- field component at the DR walls. The lowest order H-modes and E-modes radiate like magnetic and electric dipole respectively. The work presented in [170] by Okaya and Barash investigated the modes within the rectangular DRA. They defined the H-modes as Transverse Magnetic (TM) modes and E-modes as Transverse Electric (TE) modes. In a subsequent work, done by [171] they used an opposite notation for these modes. He classified them as TE for the H-modes and the E-modes as TM. This is the convention that has gained acceptance as the preferred method of mode labeling. Furthermore, the numerical subscript is used to clarify a specific mode being referenced. The numbers denote field variations over the DR region in the orthogonal coordinate system being analyzed. A letter superscript is sometimes used when referring to modes in rectangular DR. This letter denotes the axis to which the specific mode is transverse.

A general classification was given by Van Bladel to the modes of an arbitrary shaped DRA of very high permittivity [172]. According to his classifications, the modes inside DRA can be either confined (supported by dielectric bodies of revolutions only, like the $TM_{01\delta}$ mode of a cylindrical

DRA) or non-confined modes. The confined modes satisfy the following two conditions at all DR surfaces:

$$\vec{E} \,.\, \hat{n} = 0 \tag{A.5a}$$

$$\hat{n} \times \vec{H} = 0 \tag{A.5b}$$

On the other hand, the non-confined modes (rectangular DRA), which satisfy the condition 3.5a. He mentioned that the lowest order confined and non-confined modes radiate like electric and magnetic dipoles, respectively. For higher order modes, the pure Transverse Electric (TE) or Transverse Magnetic (TM) cannot exist, so that both electric and magnetic field has non-vanishing, longitudinal components. Such modes are called hybrid modes. These modes exist in the DRs for which several types of modes exist at a single frequency. Cylindrical and spherical shapes DRA can support these modes. These modes are a combination of TE and TM modes. One advantage of the RDRA is the ability to avoid mode degeneracy by altering its dimensions. Since each mode has its own unique field distribution, which translates to a specific radiation pattern, the preferred mode of operation is an important factor when designing DRAs. In general, the DRAs that make use of the lowest order mode that will radiates like an electrical and magnetic dipole, as this is the most convenient DRA radiation pattern for many applications.

A.3 DRA Analysis

In order to have a better understanding of DRAs behavior, an accurate analysis representing their circuit and radiation pattern is required. The most interesting prosperities are the resonant frequency f_o, mode field distribution, the Q-factor, and the input impedance. The resonant frequency f_o of a DRA depends on its shape, dimension, aspect ratio, and ε_{rd} . There are other parameters that may affect the DRA resonance frequency f_o, namely, the coupling method, and the presence of other radiating bodies in close proximity (mutual coupling). With the Exception of closed shapes such as spheres, hemispheres, and triodes, there is no exact analytical solution for the DRA resonant frequency f_o. Approximate analytical solutions and numerical techniques are used for other shapes to provide an estimate value for the f_o. For some shapes the approximate solutions are fairly simple and yield accurate results, while for other shapes complex numerical techniques are required and the predicted f_o can be less accurate.

Non-Rectangular Dielectric Resonator Antenna (N-RDRA) Analysis

A lot of analyses of the DRAs have been presented for shapes other than the RDRAs. The CDRAs have been used for a great amount of practical applications in filters and oscillators, and they have been used in the first DRA experiments. Consequently, there are several analytical approximations to determine the characteristics of the CDRAs. Due to the axial symmetry of the cylindrical shape, most of its parameters can be estimated accurately with relative ease. The first approximate solution for a cylindrical shape was presented in [171]. Yee used a PMC boundary condition to represent the boundary of the cylinder sides, and matched the tangential field at the cylinder ends. He conducted an experimental measurements and he founded a good agreement between measured and predicted values. A simple analysis for a cylindrical DRA was carried out in [31] using a magnetic wall model

to calculate the resonant frequencies. Meanwhile, this model failed to predict the input impedance. The frequency of the fundamental (dominant) mode TM_{110}, which has the lowest resonant frequency, is given by:

$$f_{TM110} = \frac{1}{2\pi\sqrt{\mu\varepsilon}}\sqrt{X'^{2}_{11} + \left(\frac{\pi a}{2d}\right)^{2}} \qquad \text{(A.6)}$$

A simplified analysis of the cylindrical DRs has been presented in[165]. It provides basic estimates about DR parameters, but the analysis was inaccurate. Numerical methods have been also used for analyzing CDRAs. A numerical based on the surface integral equation, has been used to predict the CDRA's f_o, Q-factor, and radiation pattern is presented [173]. Another numerical method, the Finite Difference Time-Domain (FDTD), has been used to calculate the radiation pattern and input impedance of a probe feed CDRA [174]. A good agreement between the estimated and the experimental results has been found.

The hemisphere DRA offers an advantage over the RDRA and CDRA shapes in that the interface between the dielectric and the air is simple because when placed above a ground plane, the image theory allows it to be analyzed as a sphere in free space. Accordingly, it can be analyzed using simple approximate methods. The common hemisphere analysis has been presented by Leung and Luck[175]. A mode matching method analysis has been used to extract the H-field green function inside the DR. There are many other well-established analysis methods for approximating the characteristics of the DR with axial-symmetric shapes, detailed descriptions and a comparison of the different methods are beyond the scope of this work. A more detailed summery of the analysis of cylindrical, and spherical DRs have been presented by Mongia and Bhartia[176].

Rectangular Dielectric Resonator Antenna (RDRA) Analysis

The RDRAs offer practical advantages over cylindrical and spherical shapes, because it is easy to fabricate. In addition, mode degeneracy can be avoided by properly choosing the RDRA dimensions. However, the RDRA analysis is more complex as its shapes is not axial symmetric. Since no analytical solutions exist, only approximate solutions are possible. Many models have been developed for RDRA analysis, but these models are generally not accurate, because there are some approximations imposed to extract the solutions. Some of these models based on the analysis of rectangular dielectric waveguides.

The analysis of the RDRA has been presented by Okaya and Barash [170], and a solution for the field equations, the resonant frequency f_o, the mode structure, and the Q-factor have been introduced. Their calculations are based on the first and second approximations for the RDRA boundaries. In the first order approximation, the PMC boundary was assumed for all the RDRA boundaries. The second order approximation was to use the PMC conditions only on the four smallest walls and match the tangential fields at the two larger faces. The results showed that the first order approximation estimate for the resonant frequencies showed a good agreement for higher order modes, but the second order approximation was required for lower order modes. It has been shown by Van Blade [172], that the modes of the RDRA do not satisfy the magnetic wall condition even when the dielectric constant of the resonator extends to infinity.

The transmission properties of the dielectric waveguides with a rectangular cross section, which have been presented by Marcatili[177], provide the basis for many of the rectangular DR models that followed. He developed a Dielectric Waveguide Model (DWM). Marcatili assumed there was continuous E and H fields at the waveguide boundaries with exponential decaying fields outside. Afterwards, He matched the tangential fields at the boundary to complete the model. Extensive theoretical and experimental investigations has been made by Mongia to determine the resonant frequency f_o [178]. He used the DWM to discuss both the CDRAs and the RDRAs in terms of f_o and the mode structure. A good agreement between theoretical and experimental results is observed. A closed form expression for the RDRA Q-factor has been derived by Mongia and Ittipibon[35]. It is based on replacing the RDRA with electric current source. A fairly good agreement has been observed between the theoretical and measured results.

A.4 Dielectric Waveguide mixed with Magnetic wall (DWG-MW) model

This model has been outlined by Mongia and Bhartia[176, 178], and applied by Ittipiboon[179]. It is based on the Magnetic Wall (MW) model [170] and Marcatilli's DWG model [177]. In the DWG-MW approach, the isolated RDR is first considered as a truncated version of the infinite dielectric waveguide with the same cross section a_{RDRA} and b, and the truncated length d_{RDRA} , as shown in Figure A.2, with shown boundary conditions. Second, the dominant transverse components at the end of the waveguide are matched with the external exponentially decaying fields using Marcatili's approach. In other words, with these assumptions, the fields of the DRA are expanded in the TE and the TM modes using the modal expansion method. The fields inside and outside the RDRA are expressed in terms of sinusoidal and exponential decaying functions, respectively. The wave propagation and numbers and attenuation constants are then found by matching the boundary conditions.

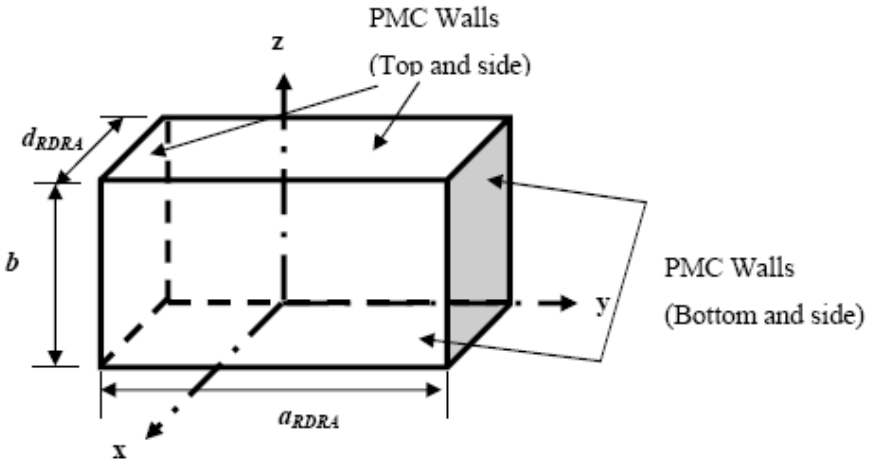

Figure A. 2 Isolated Rectangular Dielectric Resonator (RDRA).

Most of the RDRA applications are interested in the fundamental mode radiation characteristics, and the following analysis will focus on TE_{111} modes. Therefore, by properly selecting the RDRA

dimensions as $a_{RDRA} > b > d_{RDRA}$, the lowest order mode will be TE^{x}_{111}. Based on the aforementioned DWG-MW approach, the fields of the TE^{x}_{m11} modes with an odd m can be written as [35]:

$$E_{oz} = -k_y A \cos(k_z z)\cos(k_x x)\sin(k_y y)$$
$$E_{ox} = 0$$
$$E_{oy} = k_z A \sin(k_z z)\cos(k_x x)\cos(k_y y)$$
$$H_{oz} = \frac{k_z k_x}{j\omega\mu} A \sin(k_z z)\sin(k_x x)\cos(k_y y) \quad \text{(A.7)}$$
$$H_{ox} = \frac{k_z^2 + k_y^2}{j\omega\mu} A \cos(k_z z)\cos(k_x x)\cos(k_y y)$$
$$H_{oy} = \frac{k_y k_x}{j\omega\mu} A \cos(k_z z)\sin(k_x x)\sin(k_y y)$$

Where A is an arbitrary constant, $k_z = \frac{\pi}{b}$, $k_y = \frac{\pi}{a_{RDRA}}$ and k_x is determined from[17]:

$$\frac{k_x d_{RDRA}}{2} = \tan^{-1}\left(\frac{\sqrt{k_z^2 + k_y^2}}{k_x}\right) \quad \text{(A.8)}$$

The wave numbers also satisfies the equation

$$k_x^2 + k_y^2 + k_z^2 = \varepsilon_{rd} k_o^2 \quad \text{(A.9)}$$

Where k_o denotes the free-space wave number corresponding to the resonant frequency

The resonant frequency can be thus be calculated as

$$f_o = \frac{c}{\sqrt{\varepsilon_r}} \sqrt{k_x^2 + k_y^2 + k_z^2} \quad \text{(A.10)}$$

The field expressions of the TE^{x}_{n11} modes with even n are [13]:

$$E_{oz} = -k_y B \cos(k_z z)\cos(k_x x)\cos(k_y y)$$
$$E_{ox} = 0$$
$$E_{oy} = k_z B \sin(k_z z)\cos(k_x x)\sin(k_y y)$$
$$H_{oz} = \frac{k_z k_x}{j\omega\mu} B \sin(k_z z)\sin(k_x x)\sin(k_y y) \quad \text{(A.11)}$$
$$H_{ox} = \frac{k_z^2 + k_y^2}{j\omega\mu} A \cos(k_z z)\cos(k_x x)\sin(k_y y)$$

$$H_{oy} = \frac{k_y k_x}{j\omega\mu} A\cos(k_z z)\sin(k_x x)\cos(k_y y),$$

Where, B is an arbitrary constant, and the resonant frequency can be calculated from (A.8)-(A.10). The RDRA of dimensions $a_{RDRA} \times d_{RDRA} \times h = b/2$ resides on an infinite ground plane can be viewed as a single block of RDRA with a height b as in Figure A.2. Thus, the RDRA made of dielectric material with permittivity of ε_{rd}, and dimensions a_{RDRA} , b, and d_{RDRA}, the above equations can be used in an iterative manner to determine the RDRA resonance frequencies.

For the lowest order mode *(m, n=1)*, a sketch of the field configuration is shown in Figure A.3. The H_x component of the magnetic field is dominant along the center of the DRA, while the E-fields (predominantly E_y and E_x) circulates around the H_x component. These fields are similar to those produced by a short magnetic dipole. The knowledge of the relative amplitude of these fields as a function of the location within the RDRA is important for determining where to place the feed source to efficiently excite the RDRA.

Higher-order modes within the RDRA can also be excited for a certain aspect ratio. Figure A.3 shows the sketches of the fields for some of these modes. The TE^x_{131} and TE^x_{113} modes will produce a radiation pattern similar to the TE^x_{111} mode, having a peak in the broadside radiation direction (along the Z-direction). While the TE^x_{112} mode cannot exist for the case of the RDRA mounted on the ground plane. By properly combining one or more of the higher-order modes with the fundamental mode, a wider bandwidth or dual-band operation can be achieved [13, 180].

A.5 Radiation Q-Factor of RDRA

The Q_{rad} -factor is an important factor for the RDRA characterization. It describes how much energy is stored against how much power is radiated per cycle in the resonator. Also, it has a direct impact on the RDRA bandwidth. Q_{rad} of the RDRA as it has been presented in [129,134], and its closed form for is found in[181]. This formulation is based on replacing the RDRA by magnetic current source.

A verified result of the Q_{rad} in [178] is obtained by comparing it to the experimental investigations. A good agreement is noticed. In the TE^x_{111} mode analyzed above, the RDRA radiates like a magnetic dipole of moment ρ_m given by [171]:

$$\vec{\rho}_m = \frac{1}{2}\int_V \vec{R} \times \vec{J}_p \, dV \qquad \text{(A.12)}$$

Where $\vec{R}$ is the position vector from the origin, V is the volume of the RDRA, and $\vec{J}_p$ denotes the volume polarization current:

$$\vec{J}_p = j\omega\varepsilon_o(\varepsilon_{rd} - 1)\vec{E} \qquad \text{(A.13)}$$

The E in the equation (A.7) represents the electric field intensity inside the RDRA. Inserting these equations in (A.12) and (A.13) will give:

$$\vec{\rho}_m = -\frac{j8A\omega\varepsilon_o(\varepsilon_{rd}-1)}{k_x k_y k_z}\sin(\frac{k_z d}{2})\hat{a}_z \tag{A.14}$$

The power radiated by a magnetic dipole is given by [181]:

$$P_{rad} = 10k_o^4\left|\rho_m\right|^2 \tag{A.15}$$

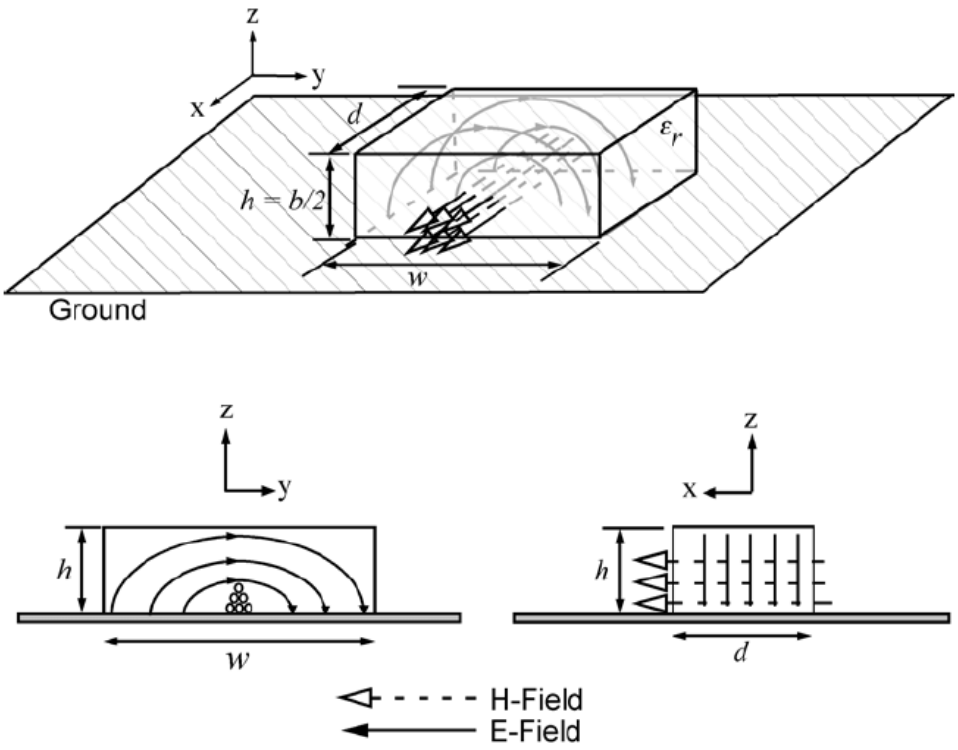

Figure A. 3 Sketch of the fields for the TE_{111}^{x} mode Of RDRA.

The stored energy inside the DR can be derived using the above field equations for TE_{111}^{x} mode

$$W_e = \frac{\varepsilon_o\varepsilon_{rd}abdA^2}{32}(1+\frac{\sin(k_z d)}{k_z d})(k_x^2+k_y^2) \tag{A.16}$$

Then, $Q_{rad} = \frac{2\omega_o W_e}{P_{rad}}$ (A.17)

Where, ω_o is the radian f_o of the RDRA. From equation (A.9), we can see that the resonance frequency is $f_o\alpha(\varepsilon_{rd})^{-\frac{1}{2}}$. Then together with the help of equation (A.16), we can also notice that RDRA radiation quality factor is:

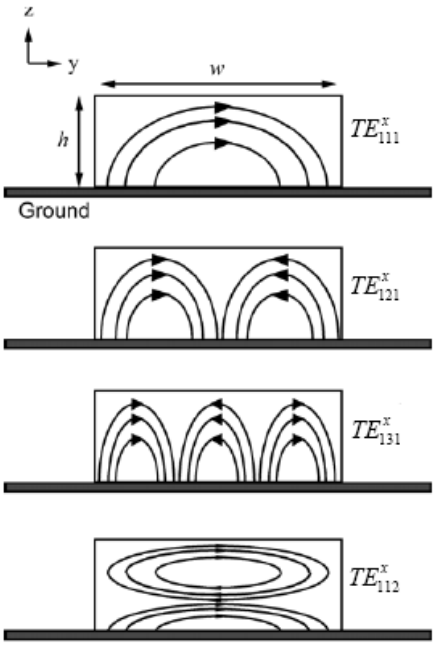

Figure A. 4 Sketches for the *E* -fields for the selected higher order modes within RDRA.

$$Q_{rad}\alpha(\varepsilon_{rd})^{\frac{3}{2}} \tag{A.18}$$

In other words, most of the stored energy lies within the resonator if the ε_{rd} of the RDRA is high, and less will be radiated. For a RDRA to be an effective antenna, the Q factor must be low. This has a direct impact on the choice of RDRA material permittivity ε_{rd}, which is recommended to be less than 20 for an effective radiation. On the other hand, the more the RDRA radiates, the wider the bandwidth will it have.

Bibliography

[1] T. S. Rapport, *Wirless Communication and Practice*: Upper Saddle River,New Jersy: Prentice Hall Inc., 1996.

[2] "Radio spectrum allocations in Canada " *Industry Canada Std,* 2005.

[3] T. T. a. E. T. Yoneyama, *Modern millimeter-wave technologies*: Tokyo, Japan: Ohmasha, Ltd., 2001.

[4] L. Yujiri, M. Shoucri, and P. Moffa, "Passive millimeter wave imaging," *Microwave Magazine, IEEE,* vol. 4, pp. 39-50, 2003.

[5] J. Wenger, "Automotive radar - status and perspectives," in *IEEE Compound Semiconductor Integrated Circuit Symposium (CSIC)*, p. 4 pp, 2005.

[6] D. J. Roscoe, J. Carrie, M. Cuhaci, A. Ittipiboon, L. Shafai, and A. Sebak, "A 30 GHz transmit array for portable communications terminals," in *Antennas and Propagation Society International Symposium(AP-S)*, pp. 1116-1119 vol.2, 1996.

[7] M. G. Keller, D. Roscoe, Y. M. M. Antar, and A. Ittipiboon, "Active millimetre-wave aperture-coupled microstrip patch antenna array," *Electronics Letters,* vol. 31, pp. 2-4, 1995.

[8] R. K. Mongia, A. Ittipiboon, and M. Cuhaci, "Measurement of radiation efficiency of dielectric resonator antennas," *IEEE Microwave and Guided Wave Letters,* vol. 4, pp. 80-82, 1994.

[9] T. B. J. Oh, D. Shin, J. Rhee, and S. Nam, "60- GHz CPW-fed dielectric -resonator above patch (DRAP) antenna for broadband WLAN Application using micromachining technology," *Microwave and optical technology letters,* vol. 49, August 2007.

[10] G. Keller, D. J. Roscoe, R. K. Mogia, Y. M. M. Antar, and A. Ittipiboon, "EHF Dielectric Resonator Antenna Array," *Microwave and optical technology letters,* vol. 17, pp. 345-349, 20 April 1998.

[11] M. T. Birand and R. V. Gelsthorpe, "Experimental millimetric array using dielectric radiators fed by means of dielectric waveguide," *Electronics Letters,* vol. 17, pp. 633-635, 1981.

[12] C. S. De Young and S. A. Long, "Wideband Cylindrical and Rectangular Dielectric Resonator Antennas," *IEEE Antennas and Wireless Propagation Letters,* vol. 5, pp. 426-429, 2006.

[13] C. Tze-Hsuan and K. Jean-Fu, "Dualband Split Dielectric Resonator Antenna," *IEEE Transactions on Antennas and Propagation,* vol. 55, pp. 3155-3162, 2007.

[14] A. Buerkle and K. Sarabandi, "A wide-band, circularly polarized, magnetodielectric resonator antenna," *IEEE Transactions on* Antennas *and Propagation,* vol. 53, pp. 3436-3442, 2005.

[15] C. Tze-Hsuan and K. Jeau-Fu, "Bandwidth enhancement by merging resonant modes of dielectric resonator antenna," in *IEEE Antennas and Propagation Society International Symposium,* pp. 2733-2736, 2007.

[16] L. Bin and L. Kwok Wa, "On the Differentially Fed Rectangular Dielectric Resonator Antenna," *IEEE Transactions on Antennas and Propagation,* vol. 56, pp. 353-359, 2008.

[17] L. Eng Hock and L. Kwok Wa, "Novel application of the hollow dielectric resonator antenna as a packaging cover," *IEEE Transactions on Antennas and Propagation,* vol. 54, pp. 484-487, 2006.

[18] I. A. Eshrah, A. A. Kishk, A. B. Yakovlev, and A. W. Glisson, "Theory and implementation of dielectric resonator antenna excited by a waveguide slot," *IEEE Transactions on Antennas and Propagation,* vol. 53, pp. 483-494, 2005.

[19] D. Deslandes and W. Ke, "Accurate modeling, wave mechanisms, and design considerations of a substrate integrated waveguide," *IEEE Transactions on Microwave Theory and Techniques,* vol. 54, pp. 2516-2526, 2006.
[20] L. Yan, W. Hong, K. Wu, and T. J. Cui, "Investigations on the propagation characteristics of the substrate integrated waveguide based on the method of lines," *IEE Microwaves, Antennas and Propagation Proceedings,* vol. 152, pp. 35-42, 2005.
[21] X. Feng, Z. Yulin, H. Wei, W. Ke, and C. Tie Jun, "Finite-difference frequency-domain algorithm for modeling guided-wave properties of substrate integrated waveguide," *IEEE Transactions on Microwave Theory and Techniques,* vol. 51, pp. 2221-2227, 2003.
[22] G. Q. Luo, W. Hong, H. J. Tang, J. X. Chen, and K. Wu, "Dualband frequency-selective surfaces using substrate-integrated waveguide technology," *IET Microwaves, Antennas & Propagation,* vol. 1, pp. 408-413, 2007.
[23] Z. Qiao-Li, Y. Wen-Yan, H. Sailing, and W. Lin-Sheng, "Compact Substrate Integrated Waveguide (SIW) Band pass Filter With Complementary Split-Ring Resonators (CSRRs)," *IEEE Microwave and Wireless Components Letters,* vol. 20, pp. 426-428, 2010.
[24] V. Sekar, M. Armendariz, and K. Entesari, "A 1.2-1.6-GHz Substrate-Integrated-Waveguide RF MEMS Tunable Filter," *IEEE Transactions on Microwave Theory and Techniques,* vol. 59, pp. 866-876, 2011.
[25] Y. J. Cheng, H. Wei, W. Ke, Z. Q. Kuai, Y. Chen, J. X. Chen, J. Y. Zhou, and H. J. Tang, "Substrate Integrated Waveguide (SIW) Rotman Lens and Its Ka-Band Multi-band Array Antenna Applications," *IEEE Transactions on Antennas and Propagation,* vol. 56, pp. 2504-2513, 2008.
[26] A. Petosa, A. Ittipiboon, Y. M. M. Antar, D. Roscoe, and M. Cuhaci, "Recent advances in dielectric-resonator antenna technology," *IEEE Antennas and Propagation Magazine,* vol. 40, pp. 35-48, 1998.
[27] R. A. Kranenburg and S. A. Long, "Microstrip transmission line excitation of dielectric resonator antennas," *Electronics Letters,* vol. 24, pp. 1156-1157, 1988.
[28] R. A. Kranenburg, S. A. Long, and J. T. Williams, "Coplanar waveguide excitation of dielectric resonator antennas," *IEEE Transactions on Antennas and Propagation,* vol. 39, pp. 119-122, 1991.
[29] X. Feng and W. Ke, "Guided-wave and leakage characteristics of substrate integrated waveguide," *IEEE Transactions on Microwave Theory and Techniques,* vol. 53, pp. 66-73, 2005.
[30] Y. Winter Dong and R. R. Mansour, "Tunable Dielectric Resonator Bandpass Filter With Embedded MEMS Tuning Elements," *IEEE Transactions on Microwave Theory and Techniques,*vol. 55, pp. 154-160, 2007.
[31] S. Long, M. McAllister, and S. Liang, "The resonant cylindrical dielectric cavity antenna," *IEEE Transactions on Antennas and Propagation,* vol. 31, pp. 406-412, 1983.
[32] D. K. a. P. Guillon, *Dielectric Resonators*: Oxford, Mississipi: Vector Fields, 1990.
[33] D. Kajfez, A. W. Glisson, and J. James, "Computed Modal Field Distributions for Isolated Dielectric Resonators," *IEEE Transactions on Microwave Theory and Techniques,* vol. 32, pp. 1609-1616, 1984.
[34] A. W. Glisson, D. Kajfez, and J. James, "Evaluation of Modes in Dielectric Resonators Using a Surface Integral Equation Formulation," *IEEE Transactions on Microwave Theory and Techniques,* vol. 31, pp. 1023-1029, 1983.
[35] R. Kumar Mongia and A. Ittipiboon, "Theoretical and experimental investigations on rectangular dielectric resonator antennas," *IEEE Transactions on Antennas and Propagation,* vol. 45, pp. 1348-1356, 1997.

[36] H. Y. Lo, K. W. Leung, K. M. Luk, and E. K. N. Yung, "Low profile equilateral-triangular dielectric resonator antenna of very high permittivity," *Electronics Letters,* vol. 35, pp. 2164-2166, 1999.

[37] K. W. Leung, K. Y. A. Lai, K. M. Luk, and D. Lin, "Input impedance of aperture coupled hemispherical dielectric resonator antenna," *Electronics Letters,* vol. 29, pp. 1165-1167, 1993.

[38] K. W. Leung, K. M. Luk, K. Y. A. Lai, and D. Lin, "Theory and experiment of a coaxial probe fed hemispherical dielectric resonator antenna," *IEEE Transactions on Antennas and Propagation,* vol. 41, pp. 1390-1398, 1993.

[39] K. W. Leung, "Analysis of aperture-coupled hemispherical dielectric resonator antenna with a perpendicular feed," *IEEE Transactions on Antennas and Propagation,* vol. 48, pp. 1005-1007, 2000.

[40] A. Petosa, R. K. Mongia, A. Ittipiboon, and J. S. Wright, "Design of microstrip-fed series array of dielectric resonator antennas," *Electronics Letters,* vol. 31, pp. 1306-1307, 1995.

[41] G. P. Junker, A. A. Kishk, and A. W. Glisson, "Input impedance of aperture-coupled dielectric resonator antennas," *IEEE Transactions on Antennas and Propagation,* vol. 44, p. 600, 1996.

[42] A. A. Kishk, A. Ittipiboon, Y. M. M. Antar, and M. Cuhaci, "Slot excitation of the dielectric disk radiator," *IEEE Transactions on Antennas and Propagation,* vol. 43, pp. 198-201, 1995.

[43] L. Kwok-Wa, L. Kwai-Man, K. Y. A. Lai, and L. Deyun, "Theory and experiment of an aperture-coupled hemispherical dielectric resonator antenna," *IEEE Transactions on Antennas and Propagation,* vol. 43, pp. 1192-1198, 1995.

[44] H. Chih-Yu, W. Jian-Yi, and W. Kin-Lu, "Cross-slot-coupled microstrip antenna and dielectric resonator antenna for circular polarization," *IEEE Transactions on Antennas and Propagation,* vol. 47, pp. 605-609, 1999.

[45] G. Yong-Xin and L. Kwai-Man, "On the improving coupling between coplanar waveguide and low-permittivity dielectric resonator antenna," in *IEEEAntennas and Propagation Society International Symposium,* pp. 486-489 vol.4, 2002.

[46] B. Ghosh, Y. M. M. Antar, A. Petosa, and A. Ittipiboon, "Feed configurations of CPW fed DRA," in *IEEE Antennas and Propagation Society(AP-S) International Symposium,* pp. 1347-1350 Vol.2, 2004.

[47] S. M. Deng, C. L. Tsai, C. W. Chiu, and S. F. Chang, "CPW-fed dual rectangular ceramic dielectric resonator antennas through inductively coupled slots," in *IEEE Antennas and Propagation Society(AP-S) International Symposium,* pp. 1102-1105 Vol.1, *2004.*

[48] D. Sheng-Ming, C. Tsung-Wen, and K. Hsiao-Hsun, "A CPW-fed rectangular dielectric resonator antenna," in *Asia-Pacific Microwave Conference(APMC)*, pp. 954-957 vol.2, 2001.

[49] M. N. Suma, S. K. Menon, P. V. Bijumon, M. T. Sebastian, and P. Mohanan, "Experimental investigation on rectangular dielectric resonator antenna excited by conductor backed coplanar waveguide," in *IEEE Antennas and Propagation Society International Symposium,* pp. 238-241 vol. 4B, 2005.

[50] G. Yuan, A. P. Popov, O. Ban-Leong, and L. Mook-Seng, "Integrated Hybrid Dielectric Resonator Antenna for System-in-Package Application," in *IEEE Microwave Theory and Technique International (MTT) Symposium,* pp. 1653-1656, 2007.

[51] A. S. Al-Zoubi, A. A. Kishk, and A. W. Glisson, "A Linear Rectangular Dielectric Resonator Antenna Array Fed by Dielectric Image Guide With Low Cross Polarization," *IEEE Transactions on Antennas and Propagation,* vol. 58, pp. 697-705, 2010.

[52] M. W. Wyville, A. Petosa, and J. S. Wight, "DIG feed for DRA arrays," in *IEEE Antennas and Propagation Society (AP-S) International Symposium,* pp. 176-179 vol. 2A, *2005*.

[53] A. S. Al-Zoubi, A. A. Kishk, and A. W. Glisson, "Aperture Coupled Rectangular Dielectric Resonator Antenna Array Fed by Dielectric Image Guide," *IEEE Transactions on Antennas and Propagation,* vol. 57, pp. 2252-2259, 2009.

[54] K. W. Leung and K. K. So, "Waveguide-excited dielectric resonator antenna," in *IEEE Antennas and Propagation Society(AP-S) International Symposium*, pp. 132-135 vol.2, 2001.

[55] K. W. Leung and K. K. So, "Rectangular waveguide excitation of dielectric resonator antenna," *IEEE Transactions on Antennas and Propagation,* vol. 51, pp. 2477-2481, 2003.

[56] I. A. Eshrah, A. A. Kishk, A. B. Yakovlev, and A. W. A. G. A. W. Glisson, "Theory and implementation of dielectric resonator antenna excited by a waveguide slot," *IEEE Transactions on Antennas and Propagation,* vol. 53, pp. 483-494, 2005.

[57] I. A. Eshrah, A. A. Kishk, A. B. Yakovlev, and A. W. A. G. A. W. Glisson, "Excitation of dielectric resonator antennas by a waveguide probe: modeling technique and wide-band design," *IEEE Transactions on Antennas and Propagation,* vol. 53, pp. 1028-1037, 2005.

[58] I. A. Eshrah, A. A. Kishk, A. B. Yakovlev, and A. W. A. G. A. W. Glisson, "Design of dielectric resonator antenna array excited by waveguide probes," in *IEEE Antennas and Propagation Society(AP-S) International Symposium,* pp. 425-428 vol. 2B, 2005.

[59] I. A. Eshrah, A. A. Kishk, A. B. Yakovlev, and A. W. Glisson, "Excitation of dielectric resonator antennas by a waveguide probe: modeling technique and wide-band design," *IEEE Transactions on Antennas and Propagation,* vol. 53, pp. 1028-1037, 2005.

[60] I. A. Eshrah, A. A. Kishk, A. B. Yakovlev, and A. W. Glisson, "Design of dielectric resonator antenna array excited by waveguide probes," in *IEEE Antennas and Propagation Society(AP-S) International Symposium,*pp. 425-428 vol. 2B, 2005.

[61] W. Ke, D. Deslandes, and Y. Cassivi, "The substrate integrated circuits - a new concept for high-frequency electronics and optoelectronics," in *6th International Conference on Telecommunications in Modern Satellite, Cable and Broadcasting Service, 2003.*, pp. P-III-P-X vol.1, 2003.

[62] L. Sunho, J. Sangwoon, and L. Hai-Young, "Ultra-Wideband CPW-to-Substrate Integrated Waveguide Transition Using an Elevated-CPW Section," *IEEE Microwave and Wireless Components Letters,* vol. 18, pp. 746-748, 2008.

[63] D. Yan and W. Ke, "Substrate Integrated Waveguide-to-Microstrip Transition in Multilayer Substrate," *IEEE Transactions on Microwave Theory and Techniques,* vol. 55, pp. 2839-2844, 2007.

[64] A. Petosa and A. Ittipiboon, "Dielectric Resonator Antennas: A Historical Review and the Current State of the Art," *Antennas and Propagation Magazine, IEEE,* vol. 52, pp. 91-116.

[65] R. K. Mongia, "Reduced size metalized dielectric resonator antennas," in *IEEE Antennas and Propagation Society(AP-S) International Symposium,* pp. 2202-2205 vol.4, 1997.

[66] Q. Rao, T. A. Denidni, A. R. Sebak, and R. H. Johnston, "A dual-band compact hybrid resonator antenna," in *IEEE Antennas and Propagation Society (AP-S) International Symposium,* pp. 156-159 vol. 2A, 2005.

[67] D. Cormos, A. Laisne, R. Gillard, F. Le Bolzer, and C. Nicolas, "Compact dielectric resonator antenna for WLAN applications," *Electronics Letters,* vol. 39, pp. 588-590, 2003.

[68] K. S. Ryu and A. A. Kishk, "Ultrawideband Dielectric Resonator Antenna With Broadside Patterns Mounted on a Vertical Ground Plane Edge," *IEEE Transactions on Antennas and Propagation,* vol. 58, pp. 1047-1053.

[69] L. Huitema, M. Koubeissi, C. Decroze, and T. Monediere, "Ultrawideband Dielectric Resonator Antenna for DVB-H and GSM Applications," *IEEE Antennas and Wireless Propagation Letters,* vol. 8, pp. 1021-1027, 2009.

[70] T. A. Denidni and Z. Weng, "Hybrid ultrawideband dielectric resonator antenna and band-notched designs," *IET Microwaves, Antennas & Propagation,*vol. 5, pp. 450-458.
[71] G. Almpanis, C. Fumeaux, and R. Vahldieck, "Offset Cross-Slot-Coupled Dielectric Resonator Antenna for Circular Polarization," *IEEE Microwave and Wireless Components Letters,* vol. 16, pp. 461-463, 2006.
[72] C. L. H. C.F. Tseng, and C.H. Hsu, "A Wideband Planar Inverted- F Dielectric Resonator Antenna for RFID System" *Microwave and optical technology letters,* vol. 48, pp. 1302-1305, July 2006.
[73] K. W. Leung, W. C. Wong, K. M. Luk, and E. K. N. Yung, "Circular-polarized dielectric resonator antenna excited by dual conformal strips," *Electronics Letters,* vol. 36, pp. 484-486, 2000.
[74] Y. Shing-lung Steven, C. Ricky, A. K. Ahmed, L. Kai-Fong, and L. Kwai-Man, "Study on Sequential Feeding Networks for Sub-arrays of Circularly Polarized Elliptical Dielectric Resonator Antenna," *IEEE Transactions on Antennas and Propagation,* vol. 55, pp. 321-333, 2007.
[75] Nasimuddin and K. P. Esselle, "Antennas with dielectric resonators and surface mounted short horns for high gain and large bandwidth," *IET Microwaves Antennas & Propagation,* vol. 1, pp. 723-728, 2007.
[76] T. A. Denidni, Y. Coulibaly, and H. Boutayeb, "Hybrid Dielectric Resonator Antenna With Circular Mushroom-Like Structure for Gain Improvement," *IEEE Transactions on Antennas and Propagation,* vol. 57, pp. 1043-1049, 2009.
[77] A. Petosa, S. Thirakoune, and A. Ittipiboon, "Higher-order modes in rectangular DRAs for gain enhancement," in *13th International Symposium on Antenna Technology and Applied Electromagnetics and the Canadian Radio Science Meeting (ANTEM/URSI)*, pp. 1-4, 2009.
[78] K. W. L. K.M. Luk, and K.W. Chow, "Bandwidth and Gain Enhancement of a dielectric Resonator Antenna with Use of a Stacking Element," M*icrowave and Optical Technology letters,* vol. 14, pp. 215-217, March 1997.
[79] A. Perron, T. A. Denidni, and A. R. Sebak, "High-Gain Hybrid Dielectric Resonator Antenna for Millimeter-Wave Applications: Design and Implementation," *IEEE Transactions on Antennas and Propagation,* vol. 57, pp. 2882-2892, 2009.
[80] A. Petosa and S. Thirakoune, "Rectangular Dielectric Resonator Antennas with Enhanced Gain," *IEEE Transactions on Antennas and Propagation,* vol. 59, pp. 1385-1389.
[81] S. P. Kingsley and S. G. O'Keefe, "Beam steering and monopulse processing of probe-fed dielectric resonator antennas," *IEE Radar, Sonar and Navigation Proceedings,* vol. 146, pp. 121-125, 1999.
[82] H. Fayad and P. Record, "Experimental investigation on new steerable dielectric resonator antenna," *Electronics Letters,* vol. 43, pp. 1009-1010, 2007.
[83] S. P. K. a. S. G. O'Keef, "Steerable-Beam Multiple-Feed Dielectric Resonator Antenna ". vol. 6,452, 565 B1, U. Patent, Ed., September 2002.
[84] A. Petosa and S. Thirakoune, "Frequency tunable rectangular dielectric resonator antenna," in *IEEE Antennas and Propagation Society (AP-S) International Symposium,* pp. 1-4, 2009.
[85] S. G. O'Keefe and S. P. Kingsley, "Tunability of Liquid Dielectric Resonator Antennas," *IEEE Antennas and Wireless Propagation Letters,* vol. 6, pp. 533-536, 2007.
[86] A. Petosa, A. Ittipiboon, M. Cuhaci, and R. Larose, "Bandwidth improvement for a microstrip-fed series array of dielectric resonator antennas," *Electronics Letters,* vol. 32, pp. 608-609, 1996.

[87] A. Hongming, W. Ke, and R. G. Bosisio, "Analytical and experimental investigations of aperture coupled unidirectional dielectric radiator arrays (UDRA)," *IEEE Transactions on Antennas and Propagation,* vol. 44, pp. 1201-1207, 1996.

[88] A. Lambrecht, O. Oestreich, J. Pontes, and W. Wiesbeck, "Dielectric Resonator Antennas for Polarization Diversity in Base Station Array Applications," in *International Conference on Electromagnetics in Advanced Applications(ICEAA)*, pp. 527-530, 2007.

[89] T. Ueda, N. Michishita, M. Akiyama, and T. Itoh, "Dielectric-Resonator-Based Composite Right/Left-Handed Transmission Lines and Their Application to Leaky Wave Antenna," *IEEE Transactions on Microwave Theory and Techniques,* vol. 56, pp. 2259-2269, 2008.

[90] A. P. F. P.V. Bijumon, M. Sayer, and Y.M. M. Antar, "On Chip Silicon Integrated Cylindrical Dielectric Resonator Antennas for Millimeter-wave Applications" in *International Symposium on Signal, System and Electronics ISSSE-2007* Montreal, April 2007.

[91] C. Xiao-Ping and W. Ke, "Low-loss ultra-wideband transition between conductor-backed coplanar waveguide and substrate integrated waveguide," in *IEEE Microwave Theory and Techniques (MTT) International Symposium*, pp. 349-352, 2009.

[92] D. Deslandes and K. Wu, "Integrated microstrip and rectangular waveguide in planar form," *IEEE Microwave and Wireless Components Letters,* vol. 11, pp. 68-70, 2001.

[93] D. Deslandes, M. Bozzi, P. Arcioni, and W. Ke, "Substrate integrated slab waveguide (SISW) for wideband microwave applications," in *IEEE Microwave Theory and Techniques (MTT) International Symposium*, pp. 1103-1106 vol.2, 2003.

[94] Y. Cassivi and W. Ke, "Substrate integrated non-radiative dielectric waveguide," *IEEE Microwave and Wireless Components Letters,* vol. 14, pp. 89-91, 2004.

[95] N. Grigoropoulos and P. R. Young, "Low cost non radiative perforated dielectric waveguides," in *33rd European Microwave Conference,* pp. 439-442 Vol.1, 2003.

[96] Y. Cassivi and W. Ke, "Substrate integrated NRD (SINRD) guide in high dielectric constant substrate for millimeter wave circuits and systems," in *IEEE Microwave Theory and Techniques (MTT) International Symposium*, Vol.3, pp. 1639-1642, 2004.

[97] A. Petosa, A. Ittipiboon, and S. Thirakoune, "Perforated dielectric resonator antennas," *Electronics Letters,* vol. 38, pp. 1493-1495, 2002.

[98] F. Shigeki, "Waveguide line," in *Ed. Japan patent*. vol. 06-0530711, Feb. 25, 1994.

[99] H. Wei, L. Bing, W. Yuanqing, L. Qinghua, T. Hongjun, Y. Xiao Xin, D. Yuan Dan, Z. Yan, and W. Ke, "Half Mode Substrate Integrated Waveguide: A New Guided Wave Structure for Microwave and Millimeter Wave Application," in *14th International Conference on Infrared Millimeter Waves and Terahertz Electronics(IRMMW-THz)*, pp. 219-219, 2006.

[100] C. Yujian, H. Wei, and W. Ke, "Half Mode Substrate Integrated Waveguide (HMSIW) Directional Filter," *IEEE Microwave and Wireless Components Letters,* vol. 17, pp. 504-506, 2007.

[101] Z. Zhen-Yu and W. Ke, "Broadband half-mode substrate integrated waveguide (HMSIW) Wilkinson power divider," in *IEEE Microwave Theory and Technique(MTT) International Symposium*, pp. 879-882, 2008.

[102] L. Qinghua, C. Fumeaux, H. Wei, and R. Vahldieck, "60 GHz Aperture-Coupled Dielectric Resonator Antennas Fed by a Half-Mode Substrate Integrated Waveguide," *IEEE Transactions on Antennas and Propagation,* vol. 58, pp. 1856-1864, 2010.

[103] J. J. Simpson, A. Taflove, J. A. Mix, and H. Heck, "Substrate integrated waveguides optimized for ultrahigh-speed digital interconnects," *Transactions on Microwave Theory and Techniques, IEEE,* vol. 54, pp. 1983-1990, 2006.

[104] C. Yu Jian, W. Ke, and H. Wei, "Power Handling Capability of Substrate Integrated Waveguide Interconnects and Related Transmission Line Systems," *IEEE Transactions on Advanced Packaging,* vol. 31, pp. 900-909, 2008.
[105] A. Suntives and R. Abhari, "Design and Application of Multimode Substrate Integrated Waveguides in Parallel Multichannel Signaling Systems," *IEEE Transactions on Microwave Theory and Techniques,* vol. 57, pp. 1563-1571, 2009.
[106] A. Ali, H. Aubert, N. Fonseca, and F. Coccetti, "Wideband two-layer SIW coupler: design and experiment," *Electronics Letters,* vol. 45, pp. 687-689, 2009.
[107] V. A. Labay, J. Bornemann, and T. R. Rao, "Design of multilayered substrate-integrated waveguide cross-slot couplers," in *European Microwave Conference,* pp. 409-412, 2009.
[108] K. Sarhadi and M. Shahabadi, "Wideband substrate integrated waveguide power splitter with high isolation," *IET Microwaves, Antennas & Propagation,* vol. 4, pp. 817-821, 2009.
[109] E. Dongsik, B. Jindo, and L. Hai-Young, "Multi-layer four-way out-of-phase power divider for substrate integrated waveguide applications," in *IEEE Microwave Theory and Technique(MTT) International Symposium*, pp. 477-480, 2009.
[110] Z. Yu Lin, H. Wei, W. Ke, C. Ji Xin, and T. Hong Jun, "Novel substrate integrated waveguide cavity filter with defected ground structure," *IEEE Transactions on Microwave Theory and Techniques* vol. 53, pp. 1280-1287, 2005.
[111] Y. Cassivi, L. Perregrini, K. Wu, and G. Conciauro, "Low-Cost and High-Q Millimeter-Wave Resonator Using Substrate Integrated Waveguide Technique," in *32nd European Microwave Conference,* pp. 1-4, 2002.
[112] H. Fan Fan, W. Ke, H. Wei, H. Liang, and C. Xiaoping, "A Low Phase-Noise VCO Using an Electronically Tunable Substrate Integrated Waveguide Resonator," *IEEE Transactions on Microwave Theory and Techniques,* vol. 58, pp. 3452-3458.
[113] A. El-Tager and L. Roy, "Novel cylindrical high-Q LTCC resonators for millimeter wave applications," in *IEEE Microwave Theory and Techniques (MTT) International Symposium,* pp. 637-640 Vol.2, 2004.
[114] D. Deslandes and W. Ke, "Single-substrate integration technique of planar circuits and waveguide filters," *IEEE Transactions on Microwave Theory and Techniques,* vol. 51, pp. 593-596, 2003.
[115] C. Sung Tae, Y. Ki Seok, K. Tokuda, and K. Yong Hoon, "A V-band planar narrow band pass filter using a new type integrated waveguide transition," *IEEE Microwave and Wireless Components Letters,* vol. 14, pp. 545-547, 2004.
[116] H. J. Tang, W. Hong, Z. C. Hao, J. X. Chen, and K. Wu, "Optimal design of compact millimeter-wave SIW circular cavity filters," *Electronics Letters,* vol. 41, pp. 1068-1069, 2005.
[117] C. Xiao-Ping and W. Ke, "Substrate Integrated Waveguide Cross-Coupled Filter with Negative Coupling Structure," *IEEE Transactions on Microwave Theory and Techniques,* vol. 56, pp. 142-149, 2008.
[118] H. Zhang Cheng, H. Wei, C. Xiao Ping, C. Ji Xin, W. Ke, and C. Tie Jun, "Multilayered substrate integrated waveguide (MSIW) elliptic filter," *IEEE Microwave and Wireless Components Letters,* vol. 15, pp. 95-97, 2005.
[119] H. Zhang-Cheng, H. Wei, C. Ji-Xin, C. Xiao-Ping, and W. Ke, "Compact super-wide bandpass substrate integrated waveguide (SIW) filters," *IEEE Transactions on Microwave Theory and Techniques,* vol. 53, pp. 2968-2977, 2005.
[120] M. Bozzi, A. Georgiadis, and K. Wu, "Review of substrate-integrated waveguide circuits and antennas," *IET Microwaves, Antennas & Propagation,* vol. 5, pp. 909-920.

[121] Y. Cassivi and K. Wu, "Low cost microwave oscillator using substrate integrated waveguide cavity," *IEEE Microwave and Wireless Components Letters,* vol. 13, pp. 48-50, 2003.
[122] C. Ji-Xin, H. Wei, H. Zhang-Cheng, L. Hao, and W. Ke, "Development of a low cost microwave mixer using a broad-band substrate integrated waveguide (SIW) coupler," *IEEE Microwave and Wireless Components Letters,* vol. 16, pp. 84-86, 2006.
[123] M. Abdolhamidi and M. Shahabadi, "X-Band Substrate Integrated Waveguide Amplifier," *IEEE Microwave and Wireless Components Letters,* vol. 18, pp. 815-817, 2008.
[124] H. Fan Fan, W. Ke, H. Wei, T. Hong Jun, Z. Hong Bing, and C. Ji Xin, "Suppression of Second and Third Harmonics using lamda/4 Low-Impedance Substrate Integrated Waveguide Bias Line in Power Amplifier," *Microwave and Wireless Components Letters, IEEE,* vol. 18, pp. 479-481, 2008.
[125] Y. J. Cheng, W. Hong, and K. Wu, "Millimetre-wave monopulse antenna incorporating substrate integrated waveguide phase shifter," *IET Microwaves, Antennas & Propagation,* vol. 2, pp. 48-52, 2008.
[126] A. Ali, N. J. G. Fonseca, F. Coccetti, and H. Aubert, "Analysis and design of a compact SIW-based multi-layer wideband phase shifter for Ku-band applications," in *IEEE Antennas and Propagation Society (AP-S) International Symposium*, pp. 1-4, 2010.
[127] K. Sellal, L. Talbi, T. A. Denidni, and J. Lebel, "Design and implementation of a substrate integrated waveguide phase shifter," *IET Microwaves, Antennas & Propagation,* vol. 2, pp. 194-199, 2008.
[128] C. Wenquan, E. K. N. Yung, and W. Ke, "Millimeter-wave ferrite phase shifter in substrate integrated waveguide (SIW)," in *IEEE Antennas and Propagation Society (AP-S) International Symposium,* pp. 887-890 vol.4, 2003.
[129] C. Yu Jian, H. Wei, and W. Ke, "Broadband Self-Compensating Phase Shifter Combining Delay Line and Equal-Length Unequal-Width Phaser," *IEEE Transactions on Microwave Theory and Techniques,* vol. 58, pp. 203-210.
[130] E. Sbarra, L. Marcaccioli, R. V. Gatti, and R. Sorrentino, "Ku-band analogue phase shifter in SIW technology," in *European Microwave Conference*, pp. 264-267, 2009.
[131] X. Feng, W. Ke, and Z. Xiupu, "Periodic Leaky-Wave Antenna for Millimeter Wave Applications Based on Substrate Integrated Waveguide," *IEEE Transactions on Antennas and Propagation,* vol. 58, pp. 340-347.
[132] C. Yu Jian, H. Wei, and W. Ke, "Design of a Monopulse Antenna Using a Dual V-Type Linearly Tapered Slot Antenna (DVLTSA)," *IEEE Transactions on Antennas and Propagation,* vol. 56, pp. 2903-2909, 2008.
[133] M. H. Awida and A. E. Fathy, "Substrate-Integrated Waveguide Ku-Band Cavity-Backed 2 by 2 Microstrip Patch Array Antenna," *IEEE Antennas and Wireless Propagation Letters,* vol. 8, pp. 1054-1056, 2009.
[134] L. Guo Qing, H. Zhi Fang, D. Lin Xi, and S. Ling Ling, "Planar Slot Antenna Backed by Substrate Integrated Waveguide Cavity," *IEEE Antennas and Wireless Propagation Letters,* vol. 7, pp. 236-239, 2008.
[135] Y. Li, H. Wei, H. Guang, C. Jixin, W. Ke, and C. Tie Jun, "Simulation and experiment on SIW slot array antennas," *IEEE Microwave and Wireless Components Letters,* vol. 14, pp. 446-448, 2004.
[136] C. Yu Jian, H. Wei, and W. Ke, "Millimeter-Wave Substrate Integrated Waveguide Multibeam Antenna Based on the Parabolic Reflector Principle," *IEEE Transactions on Antennas and Propagation,* vol. 56, pp. 3055-3058, 2008.

[137] C. Chih-Jung and C. Tah-Hsiung, "Design of a 60-GHz Substrate Integrated Waveguide Butler Matrix-A Systematic Approach," *IEEE Transactions on Microwave Theory and Techniques,* vol. 58, pp. 1724-1733.
[138] D. Deslandes, "Design equations for tapered microstrip-to-Substrate Integrated Waveguide transitions," in *IEEE Microwave Theory and Techniques (MTT) International Symposium*, pp. 704-707, 2010.
[139] D. Deslandes and W. Ke, "Integrated transition of coplanar to rectangular waveguides," in *IEEE Microwave Theory and Techniques (MTT) International Symposium*, pp. 619-622 vol.2, 2001.
[140] D. Deslandes and K. Wu, "Analysis and Design of Current Probe Transition From Grounded Coplanar to Substrate Integrated Rectangular Waveguides," *IEEE Transactions on Microwave Theory and Techniques,* vol. 53, pp. 2487-2494, 2005.
[141] Y. K. Takafumi Kai, Jiro Hirokawa, Makoto Ando, Hiroshi Nakano, Yasutake Hirachi "A Coaxial Line to Post-Wall Waveguide Transition for a Cost-Effective Transformer between a RF-Device and a Planar Slot-Array Antenna in 60-GHz Band," *IEICE Commun. ,* vol. 89-B, pp. 1646-1653, May 2006.
[142] H. Zhang Cheng, H. Wei, C. AnDing, C. JiXin, and W. Ke, "SIW fed dielectric resonator antennas (SIW-DRA)," in *IEEE Microwave Theory and Techniques(MTT) International Symposium*, pp. 202-205, 2006.
[143] A. G. Williamson, "Coaxially Fed Hollow Probe in Rectangular Waveguide " in *Inst. Elec. Eng. Proc,* pp. 273-285, Aug. 1985.
[144] A. G. Williamson, "Analysis and Modeling of a Coaxial-line/ Rectangular Waveguide Junction," in *Inst. Elec. Eng. Proc, ,* OCT. 182, pp. 262-270.
[145] R. B. Keam and A. G. Williamson, "Broadband design of coaxial line/rectangular waveguide probe transition," *IEE Microwaves, Antennas and Propagation, Proceedings -,* vol. 141, pp. 53-58, 1994.
[146] J. H. Y. Kato, M. Ando, H. Nakano, and Y. Hirachi, "Coaxial-line for millimeter-wave post-wall waveguides " IEICE Technical Report ,A.P03-259 Jan. 2004.
[147] D. Busuioc, "Conformal Integarted Antenna Array Technology for Low Cost Intelligent System Applications," in *Electrical and Computer Engineering* Waterloo: Waterloo, 2055.
[148] *Agilent, Advanced Design System -Momentum* Agilent Corporation 2002.
[149] *Ansoft , High Frequency Software Simulator, Ansoft Corporation, 2033* Agilent Corporation 2002.
[150] E. Moldovan, R. G. Bosisio, and W. Ke, "W-band multiport substrate-integrated waveguide circuits," *IEEE Transactions on Microwave Theory and Techniques ,* vol. 54, pp. 625-632, 2006.
[151] C. Hung-Yi, S. Tze-Min, H. Ting-Yi, W. Wei-Hsin, and W. Ruey-Beei, "Miniaturized Bandpass Filters With Double-Folded Substrate Integrated Waveguide Resonators in LTCC," *IEEE Transactions on Microwave Theory and Techniques,* vol. 57, pp. 1774-1782, 2009.
[152] C. Shi, H. Yousef, and H. Kratz, "79 GHz Slot Antennas Based on Substrate Integrated Waveguides (SIW) in a Flexible Printed Circuit Board," *IEEE Transactions on Antennas and Propagation,* vol. 57, pp. 64-71, 2009.
[153] D. Stephens, P. R. Young, and I. D. Robertson, "Millimeter-wave substrate integrated waveguides and filters in photoimageable thick-film technology," *IEEE Transactions on Microwave Theory and Techniques,* vol. 53, pp. 3832-3838, 2005.
[154] J. Hirokawa and M. Ando, "Single-layer feed waveguide consisting of posts for plane TEM wave excitation in parallel plates," *IEEE Transactions on Antennas and Propagation,* vol. 46, pp. 625-630, 1998.

[155] D. Pissoort and F. Olyslager, "Study of eigenmodes in periodic waveguides using the Lorentz reciprocity theorem," *IEEE Transactions on Microwave Theory and Techniques,* vol. 52, pp. 542-553, 2004.
[156] Y. Cassivi, L. Perregrini, P. Arcioni, M. Bressan, K. Wu, and G. Conciauro, "Dispersion characteristics of substrate integrated rectangular waveguide," *IEEE Microwave and Wireless Components Letters,,* vol. 12, pp. 333-335, 2002.
[157] A. Zeid and H. Baudrand, "Electromagnetic scattering by metallic holes and its applications in microwave circuit design," *IEEE Transactions on Microwave Theory and Techniques,* vol. 50, pp. 1198-1206, 2002.
[158] J. R. Bray and L. Roy, "Resonant frequencies of post-wall waveguide cavities," *IEE Microwaves, Antennas and Propagation, Proceedings,* vol. 150, pp. 365-8, 2003.
[159] X. J. W. Che, and K. Wu, "Characteristics comparison of substrate integrated rectangular waveguide (SIRW) and its equivelent rectangular waveguide," *Microwave and optical tecnology letters,* vol. 46, pp. 558-592, Sep. 2005.
[160] M. Bozzi, M. Pasian, L. Perregrini, and W. Ke, "On the losses in substrate integrated waveguides," in *European Microwave Conference,* pp. 384-387, 2007.
[161] R. E. Collin, *Field Theory of Guided Waves*:: Piscataway, NJ: IEEE Press, 1990.
[162] M. Bozzi, L. Perregrini, and W. Ke, "Modeling of losses in substrate integrated waveguide by Boundary Integral-Resonant Mode Expansion method," in *IEEE Microwave Theory and Techniques (MTT) International Symposium*, pp. 515-518, 2008.
[163] D. Deslandes and K. Wu, "Design Consideration and Performance Analysis of Substrate Integrated Waveguide Components," in *European Microwave Conference,* pp. 1-4, 2002.
[164] W. O. A. Wahab, S. Safavi-Naeini, and D. Busuioc, "Low cost Planar Waveguide Technology Based Dielectric Resonator Antenna (DRA) for Millimeter-wave Applications: Analysis, Design, and Fabrication," *IEEE Transactions on Antenna and Propagation,* vol. 58, pp. 2499-2507, 2010
[165] D. M. Pozar, *Microwave Engineering*, 2nd edition ed.: John Wiely and Sons Inc., 1998.
[166] C. M. K. R.C. Cameron, and R.R. Mansour, *Microwave Filters for Communication Systems-Fundamental, Design and Applications*: Wiley, 2007.
[167] L. Qinghua, G. Almpanis, C. Fumeaux, H. Benedickter, and R. Vahldieck, "Comparison of the Radiation Efficiency for the Dielectric Resonator Antenna and the Microstrip Antenna at Ka Band," *IEEE Transactions on Antennas and Propagation, ,* vol. 56, pp. 3589-3592, 2008.
[168] W. M. Abdel-Wahab, D. Busuioc, and S. Safavi-Naeini, "Millimeter-Wave High Radiation Efficiency Planar Waveguide Series-Fed Dielectric Resonator Antenna (DRA) Array: Analysis, Design, and Measurements," *IEEE Transactions on Antennas and Propagation,* vol. 59, pp. 2834-2843.
[169] M. K. David and et al., "X-ray fabrication of SAW resonators with narrow electrodes in thick high-aspect-ratio polymer templates," *Journal of Micromechanics and Micro engineering,* vol. 20, p. 075031.
[170] A. Okaya and L. F. Barash, "The Dielectric Microwave Resonator," *Proceedings of the IRE,* vol. 50, pp. 2081-2092, 1962.
[171] Y. Hung Yuet, "Natural Resonant Frequencies of Microwave Dielectric Resonators (Correspondence)," *IEEE Transactions on Microwave Theory and Techniques,* vol. 13, pp. 256-256, 1965.
[172] J. Van Bladel, "On the Resonances of a Dielectric Resonator of Very High Permittivity," *IEEE Transactions on Microwave Theory and Techniques,* vol. 23, pp. 199-208, 1975.

[173] A. A. Kishk, M. R. Zunoubi, and D. Kajfez, "A numerical study of a dielectric disk antenna above grounded dielectric substrate," *IEEE Transactions on Antennas and Propagation,* vol. 41, pp. 813-821, 1993.
[174] H. F. L. a. W. Chen, *Advances in Microstrip and Printed Antenna*. Toronto, ON: John Wiely and Sons, 1997.
[175] K. W. L. a. K. M. Luk, "Radiation Characteristics of an Aperature- Coupled Hemispherical Dielectric Resonator antenna," *Microwave and Optical Technology Letters,* vol. 7, pp. 667-679, 1994.
[176] R. K. M. a. P. Bhartia, "Dielectric Resonator Antennas- A Review and General Design Relations for Resonant Frequency and Bandwidth," *International Journal of Microwave and Millimeter-Wave Computer- Aided Engineering,* vol. 4, pp. 230-246, 194.
[177] E. A. J. Marcartili, "Dielectric Rectangular Waveguide and Directional Coupler for Integrated Optics," *Bell Systems,* vol. 48, pp. 2071-2102, 1969.
[178] R. K. Mongia, "Theoretical and experimental resonant frequencies of rectangular dielectric resonators," *IEE Microwaves, Antennas and Propagation, Proceedings H,* vol. 139, pp. 98-104, 1992.
[179] A. Ittipiboon, R. K. Mongia, Y. M. M. Antar, P. Bhartia, and M. Cuhaci, "Aperture Fed Rectangular and Triangular Dielectric Resonators for use as Magnetic Dipole Antennas," *Electronics Letters,* vol. 29, pp. 2001-2002, 1993.
[180] G. Bit-Babik, C. Di Nallo, and A. Faraone, "Multimode Dielectric Resonator Antenna of Very High Permittivity," in *IEEE Antennas and Propagation Society (AP-S) International Symposium,* pp. 1383-1386 Vol.2, 2004.
[181] R. K. Mongia, A. Ittipiboon, M. Cuhaci, and D. Roscoe, "Radiation Q-factor of rectangular dielectric resonator antennas: theory and experiment," in *IEEE Antennas and Propagation Society(AP-S) International Symposium,* pp. 764-767 vol.2, 1994.